

Heterogeneously Catalyzed Synthesis of Propylene Carbonate Using Carbon Dioxide

A dissertation submitted to the
Swiss Federal Institute of Technology (ETH), Zurich
for the degree of Doctor of Technical Sciences

presented by

Michael Olaf Ramin

Dipl.-Chem.

born 17 September 1974

German citizen

accepted on the recommendation of
Prof. Dr. A. Baiker, examiner
Prof. Dr. G. Consiglio, co-examiner

2006

*meinen Eltern
in Liebe und Dankbarkeit*

“Gewisse Bücher scheinen geschrieben zu sein, nicht damit man daraus lernt, sondern damit man wisse, dass der Verfasser etwas gewusst hat.”

(Johann Wolfgang von Goethe)

Acknowledgement

I am very grateful to Prof. Alfons Baiker for giving me the possibility to realize this interesting project and for the scientific supervision of this work. He gave me the valuable chance to explore the path of this work on my own, which I appreciate very much.

Moreover, I would like to thank Prof. Giambattista Consiglio for accepting the duty of the co-reference and for the careful and proficient review of my thesis.

I furthermore thank Jan-Dierk Grunwaldt for constructive discussions, his valuable suggestions, and his everlasting scientific enthusiasm. He inspired me to step into the world of synchrotrons and XAS measurements, and I really enjoyed these extra adventures with all the night-shifts, improvisation, Haribo, and synthetic voices.

Special thanks also go to Fabian Jutz for valuable contributions within his diploma work, and to Sven Reimann for his input during his practical course.

Furthermore, I would like to thank for the contributions to the present work: Marek Maciejewski for thermal analysis, Davide Ferri for the introduction to IR spectroscopy and the DRIFT measurements, Niels van Vegten for the discussions, the flame-made catalysts, and BET measurements, Carsten Beck for ICP-OES and Frank Krumeich for STEM measurements, Urs Krebs and Ján Kovacic for keeping my high pressure equipment running as well as Roland Mäder for the sophisticated design of the high-pressure *in situ* cells.

I would also like to thank Mathias Hermann, Edmund Welter, Herman Emerich, Wouter van Beek, and Stefan Mangold for their support and the good

atmosphere during the XAS measurements. HASYLAB (DESY, Hamburg, Germany), the Swiss-Norwegian Beamline (ESRF, Grenoble, France), ANKA (Forschungszentrum Karlsruhe, Germany), and the SLS (PSI, Villingen, Switzerland) are to be thanked for providing beamtime, and the Bundesamt für Energie for its financial support.

A special thank is dedicated to my office mates Markus Rohr, Matteo Caravati, Simon Diezi, and Marco Burgener for sharing all these joyful moments, high-level talks, as well as profitable and philosophical discussions during regular working hours, 24-hours-and-even-more night and day shifts, conferences, and the unforgettable moments during spare time in trains, airplanes, submarines, cafeterias, night clubs, Tresors, the local area network, and elsewhere. I thank also my short-term office mates Daniel Meier and Christiane Kartusch for the good atmosphere and conversation during the last weeks of my doctoral thesis.

Especially, I would like to mention besides my office mates the following group members for introducing me into the Swiss culture and language, into the world of wine, and, in general, for sharing a lot of good times: Carsten Beck, Reto Hess, Michael Schneider, Andy Gisler, Wolf-Rüdiger Huck, Clemens Wögerbauer, Florian Eigenmann, Leo Schmid, Simon Frauchiger, Csilla Kereszegi, Ronny Wirz, Atsushi Urakawa, Stefan Hannemann, Fabian Jutz, Niels van Vegten, Fatos Hoxha, and Sven Reimann.

Finally, I would like to thank my parents and Kathrin, for their love and support throughout all these years of my education.

Table of Contents

Acknowledgement.....	v
Summary.....	xv
Zusammenfassung.....	xix
1 Introduction.....	1
1.1 The Principles of Green Chemistry	2
1.2 Carbon Dioxide	3
1.2.1 The Carbon Cycle.....	4
1.2.2 Carbon Dioxide as Solvent.....	4
1.2.3 Chemicals Synthesized from Carbon Dioxide.....	5
1.3 Organic Carbonates	7
1.3.1 Physical Properties and Applications of Propylene Carbonate.....	8
1.3.2 General Methods of Preparation of Organic Carbonates	8
1.3.3 Synthesis of Cyclic Carbonates by Carbon Dioxide Fixation	11
1.4 Heterogeneized Catalysts.....	12
1.4.1 Immobilization Strategies.....	12
1.4.2 Support Modification.....	14
1.5 Spectroscopic Techniques	15
1.5.1 Attenuated Total Reflectance Infrared Spectroscopy.....	16
1.5.2 General Aspects of X-ray Absorption Spectroscopy.....	17
1.5.3 Basics of XANES and EXAFS	18

1.6 Scope of the Thesis	21
2 Experimental	23
2.1 Carbon Dioxide Insertion Reaction.....	23
2.1.1 High-Pressure Batch Reactor.....	23
2.1.2 Procedure of the Insertion Reaction	25
2.1.3 Analysis	25
2.1.4 Evaluation	25
2.2 X-ray Absorption Spectroscopy	27
2.2.1 XAS Under Demanding Conditions	27
2.2.2 <i>In Situ</i> XAS Batch Reactor Cell.....	28
2.2.3 Beamline Setup and Data Analysis	30
2.3 Experimental Setup for Phase Behavior Studies.....	33
2.4 Catalyst Characterization Methods.....	35
2.4.1 X-ray Photoelectron Spectroscopy	35
2.4.2 Thermal Analysis.....	36
2.4.3 Further Analytical and Physicochemical Characterization.....	36
3 Chromium Salen Complexes: Bridging Homogeneous and Heterogeneous Catalysis	37
3.1 Introduction.....	38
3.2 Experimental Section	39
3.2.1 Syntheses of the Homogeneous Complexes	39
3.2.2 Syntheses of the Heterogeneous Catalysts.....	41
3.3 Results and Discussion.....	43
3.3.1 Syntheses of the Free Complexes	43
3.3.2 Catalytic Activity of the Homogeneous Catalysts	44
3.3.3 Syntheses and Characterization of the Immobilized Catalysts....	46
3.3.4 Catalytic Activity of the Heterogeneous Catalysts.....	50

3.3.5 Reuse of the Heterogeneous Catalysts	51
3.4 Conclusions	54
4 Behavior of Homogeneous and Immobilized Zinc-based Catalysts	55
4.1 Introduction.....	55
4.2 Experimental Section	56
4.2.1 Materials	56
4.2.2 Syntheses of Homogeneous Catalysts	57
4.2.3 Syntheses of the Immobilized Catalysts	58
4.2.4 Leaching Tests.....	58
4.3 Results	59
4.3.1 General Catalyst Characterization	59
4.3.2 <i>Ex Situ</i> X-ray Absorption Measurements	61
4.3.3 IR Studies for Structural Analysis	63
4.3.4 Catalytic Performance in Carbon Dioxide Fixation	67
4.4 Discussion.....	70
4.4.1 Immobilization and Structure of the Catalysts.....	70
4.4.2 Comparison of Homogeneous and Heterogeneous Catalysts.....	71
4.5 Conclusions	74
5 <i>In Situ</i> XAS Under High Pressure Conditions.....	77
5.1 Introduction.....	78
5.2 Experimental Section	78
5.2.1 Syntheses of the Nickel Complexes	79
5.3 Results	80
5.3.1 <i>In Situ</i> X-ray Absorption Measurements.....	80
5.3.2 ICP-OES Measurements Including the Bromine Content.....	83
5.3.3 Reactivation of the Catalyst by Bromide Addition.....	84

Table of Contents

5.4 Discussion.....	85
5.4.1 Behavior of the Catalyst Under Reaction Conditions	85
5.4.2 Role of Bromide.....	86
5.5 Case Study: <i>In Situ</i> Monitoring of Nickel Catalysts	86
5.5.1 Introduction.....	86
5.5.2 Results and Discussion	87
5.6 Conclusions	90
6 Phase Behavior Studies: Expanded Liquid Versus Supercritical Fluid.....	91
6.1 Introduction.....	92
6.2 Experimental Section	93
6.2.1 ATR-IR Spectroscopy	93
6.3 Results	94
6.3.1 Phase Behavior	94
6.3.2 Catalysis	98
6.3.3 <i>In Situ</i> Spectroscopy During Reaction.....	102
6.4 Discussion.....	105
6.5 Conclusion.....	107
7 Simple Preparation Routes Toward Novel Zn-based Catalysts.....	109
7.1 Introduction.....	109
7.2 Experimental Section	110
7.2.1 Sol-gel based Synthesis of Catalysts with Oxide Support	111
7.2.2 Flame-made Catalysts.....	111
7.3 Results	112
7.3.1 Catalytic Studies.....	112
7.3.2 Further Characterization of Selected Samples	117
7.4 Discussion.....	119

7.5 Conclusions	121
Final Remarks and Outlook	123
Appendix	125
A Abbreviations.....	125
B Twelve Green Chemistry Principles	129
C Additional Analytical Data.....	131
C.1 Results of NMR Analysis.....	131
C.1.1 Data of Catalyst Precursors.....	131
C.1.2 NMR Data of Catalysts	132
C.2 Results of the Elemental Analysis.....	134
References	135
List of Publications	147
Curriculum Vitae	153

Summary

The avoidance of toxic and environmentally harmful substances in the chemical industry is requested, and in accordance with the so-called green chemistry. Carbon dioxide (CO_2), undesired by-product of combustion of fossil fuels and contribution to the greenhouse effect, can be beneficially used as C_1 -building block and non-polluting solvent in chemical processes and substitute hazardous reactants such as phosgene and carbon monoxide in chemical syntheses. A typical example is the synthesis of cyclic carbonates using CO_2 . Propylene carbonate (PC) is a representative of these carbonates, and in this work its synthesis from propylene oxide (PO) and CO_2 was targeted.

Due to its special physical properties, CO_2 can be used as liquid or supercritical solvent and reactant, respectively, at rather low pressure and temperature. Separation of the excessive liquid CO_2 from the product is possible just by decompression, no distillation is necessary. Hence only reactions without additional solvents, so-called solventless reactions, were investigated. However, the high chemical stability of CO_2 requires catalytic processes, in which heterogeneous catalysis is preferred because of the easier catalyst separation.

As only homogeneous or quite complex heterogeneous catalysts for the synthesis of PC by CO_2 insertion into PO have been reported until now, the emphasis was laid on the synthesis of simple transition metal complexes, which were immobilized onto an oxidic support. Spectroscopic techniques, including nuclear magnetic resonance (NMR), infrared spectroscopy (IR) combined with diffuse reflectance (DRIFTS), X-ray photoelectron spectroscopy (XPS), X-ray absorption (XAS), optical emission spectroscopy via inductively coupled plasma

(ICP-OES), elemental analysis (EA), thermal analysis (TA), and nitrogen physisorption at surfaces (BET) gave insight into the structure and allowed evaluating, whether the immobilization process was successful or not. Attenuated total reflectance Fourier spectroscopy (ATR-IR) and transmission IR spectroscopy combined with a view cell autoclave were used for phase behavior measurements.

First, different chromium salen complexes were tested concerning their catalytic performance in the CO₂ fixation. The most active catalysts were immobilized on a silica support via different grafting methods. These heterogeneized catalysts exhibited rates up to 300 mol (mol_{Cr} h)⁻¹ at 98% selectivity in a solventless reaction. The coordinatively bound complex was not stable and a very strong deactivation occurred during reuse, whereas the corresponding covalently bound complexes hardly showed any leaching of the active compound—the chromium salen complex. No significant difference in stability was found for single and double covalently bound complexes, but the single bound catalyst was derived from a more active homogeneous complex. This stable catalyst achieved rates up to 200 mol (mol_{Cr} h)⁻¹.

Since homogeneous zinc pyridine bromide catalysts have been reported in literature to be well-performing in the synthesis of PC using CO₂, such complexes were immobilized on silica. These heterogeneized catalysts achieved rates up to 330 mol (mol_{Zn} h)⁻¹. All intermediates of the synthesis were spectroscopically analyzed and catalytically tested, to uncover possible structural changes of the active complex during the synthesis process. Differences in the catalytic activity of these intermediates could be explained by structural characterization using XAS measurements. The catalytic activity of the immobilized zinc pyridine bromide complex decreased during reuse, but this deactivation could not be traced to leaching of the zinc. In further experiments, zinc pyridine acetate complexes exhibited only a low catalytic activity.

In situ XAS measurements using a specially designed batch reactor cell confirmed the successful and stable immobilization of the zinc even under reaction

conditions, and homogeneous catalysis by dissolved zinc species could be ruled out. However, XAS measurements uncovered bromine in the fluid reaction mixture and simultaneously the absorption at the bromine K-edge of the solid catalyst decreased. ICP-OES measurements confirmed the results of the *in situ* XAS studies. It was possible to maintain the catalytic activity by addition of bromide as co-catalyst. Such measurements are challenging because the construction of a spectroscopic batch reactor cell, which exhibits only a low absorption of X-rays, is rather sophisticated. The primarily used *in situ* XAS batch reactor cell allowed measurements at the zinc K-edge (9.659 keV), and a modified second batch cell could even provide information about the structure activity relationship of homogeneous nickel catalysts (nickel K-edge, 8.333 keV). This is also interesting to give possible insight into the reaction behavior of the above-mentioned chromium salen complexes (chromium K-edge, 5.989 keV).

Already during initializing parameter studies an unexpected pressure dependence was observed during the synthesis of PC using CO₂, which has also been reported in literature. To explain this observation, phase behavior studies based on video monitoring, transmission and ATR-IR measurements were performed in a view cell autoclave. In the process, three different regions of characteristic phase behavior were found that influenced strongly the reaction rate: At a low overall density a biphasic region with small liquid phase was observed. The catalytic activity of this system was poor. A decreasing CO₂ content at the same density resulted in an expanded liquid phase, which was beneficial for the catalytic activity. However, at too low content of CO₂ the rate decreased again, which could be possibly traced to a disadvantageous influence of the resulting solvent polarity or the chemical equilibrium. In contrast to several other reactions using supercritical CO₂, higher pressure during reaction with a resulting single-phase system was not beneficial for the yield of PC. *In situ* ATR-IR measurements of the catalyst surface revealed drastic changes in the phase behavior in the first minutes and gave important insight into the solid/fluid interface under reaction conditions.

The findings concerning the stability of zinc on silica surfaces and the possibility to use bromide as co-catalyst, resulted in a simplified catalyst synthesis. Different zinc-containing mixed oxides were tested in the solventless synthesis of PC in the presence of ammonium bromide as co-catalyst. The catalysts were prepared by the sol-gel method and by flame spray pyrolysis. A significant improvement of the flame made catalysts could be achieved by application of a colloid of pre-formed silica particles instead of using tetraethoxysilane as precursor. Yields >99% at principally 100% selectivity were obtained with 200 mg catalyst and 140 mmol PO at 120 °C in six hours—this is corresponding to a rate >750 mol (mol_{Zn} h)⁻¹. Not only the test reactions, but also scanning electron microscope (STEM) and XAS measurements evidenced, that not single site zinc but rather zinc-clusters play an important role in the catalytic activity of the system.

Zusammenfassung

Eine Abkehr von giftigen und umweltschädigenden Substanzen in der chemischen Industrie liegt im Sinn einer vom Verbraucher gewünschten sogenannten grünen Chemie. Ausgerechnet Kohlendioxid (CO_2) – sonst unerwünschtes Nebenprodukt und potentiell Treibhausgas – kann als Kohlenstoffbaustein und auch als umweltneutrales Lösungsmittel bei der Chemikalienproduktion andere bedenkliche Stoffe wie Phosgen und Kohlenmonoxid ersetzen. Ein Beispiel ist die Herstellung zyklischer organischer Carbonate. Ein Vertreter dieser Stoffklasse ist Propylencarbonat (PC), dessen Darstellung aus Propylenoxid (PO) und CO_2 im Rahmen dieser Arbeit genauer betrachtet wurde.

Aufgrund seiner besonderen physikalischen Eigenschaften kann CO_2 bereits bei niedrigen Drücken als flüssiges oder gegebenenfalls überkritisches Lösungsmittel bzw. Edukt verwendet werden. Eine Abtrennung des überschüssigen flüssigen CO_2 vom Produkt ist allein durch Dekompression möglich, eine destillative Abtrennung ist nicht notwendig. Daher wurden ausschließlich Reaktionen ohne zusätzliche Lösungsmittel betrachtet. Die hohe chemische Stabilität des CO_2 hingegen erfordert katalytische Prozesse, wobei technisch wegen der einfacheren Katalysatorrückgewinnung heterogen katalysierte Reaktionen den homogenen vorzuziehen sind.

Da bis jetzt nur homogene oder sehr aufwendig zu synthetisierende heterogene Katalysatoren für die CO_2 -Fixierung an PO zu PC zur Verfügung standen, lag der Schwerpunkt dieser Arbeit auf der Darstellung einfach zu erhaltender, auf festem Träger verankerter Übergangsmetallkomplexe. Spektroskopische

Untersuchungen mit Kernresonanzspektroskopie (NMR), Infrarotspektroskopie (IR) mittels diffuser Reflexion (DRIFTS), röntgenangeregter Photoelektronenspektroskopie (XPS), Röntgenabsorption (XAS), optischer Emissionsspektrometrie mittels induktiv gekoppeltem Plasma (ICP-OES), Mikroelementanalyse (EA), Thermoanalyse (TA) und Stickstoffphysisorption an Oberflächen (BET) erlauben eine umfassende Charakterisierung der Katalysatoren und Evaluation des Immobilisierungsprozesses, während IR-Messungen mittels abgeschwächter Totalreflexion (ATR-IR) und Transmissions-IR-Messungen durch einen Sichtfensterautoklaven halfen, das Phasenverhalten dieser Reaktion zu verstehen.

Zuerst wurden verschiedene Chrom-Salen-Komplexe auf ihre katalytische Aktivität bei der CO₂-Fixierung untersucht. Die aktivsten homogenen Katalysatoren wurden auf unterschiedliche Weise auf festen Trägern verankert. Diese heterogenisierten Katalysatoren erzielten Umsatzraten von 300 mol (mol_{Cr} h)⁻¹ und Selektivitäten von 98%. Außer CO₂ wurde kein weiteres Lösungsmittel eingesetzt. Es zeigte sich, dass eine Verankerung des Chrom-Salen-Komplexes über eine rein koordinative Bindung nicht hinreichend stabil ist. Bei den herrschenden Reaktionsbedingungen trat eine starke Desaktivierung auf, als dieser Katalysator wiederverwendet wurde. Die beiden kovalent gebundenen Komplexe hingegen zeigten fast keinen Verlust an der aktiven Komponente – dem Chrom-Salen-Komplex. Ein signifikanter Unterschied zwischen einfach und zweifach kovalent gebundenen Komplexen hinsichtlich der Stabilität wurde nicht gefunden, allerdings konnte der einfach gebundene Komplex aus einem aktiveren homogenen Katalysator gewonnen werden. Mit diesem stabilen Katalysator wurden Umsatzraten von 200 mol (mol_{Cr} h)⁻¹ erzielt.

Homogene Zink-Pyridin-Bromid-Komplexe wurden auf Silica immobilisiert, da sie in der Literatur als aktive Katalysatoren für die Synthese von PC aus CO₂ beschrieben sind. Der immobilisierte Komplex erzielte Umsatzraten von 330 mol (mol_{Zn} h)⁻¹. Dabei wurden alle Synthesewschritte spek-

troskopisch und katalytisch analysiert, um eventuelle Veränderungen am aktiven Komplex untersuchen zu können. Unterschiede in der katalytischen Aktivität dieser Zwischenstufen konnten anhand von strukturellen Untersuchungen mit XAS erklärt werden. Bei erneutem Einsatz zeigte der immobilisierte Zink-Pyridin-Bromid-Komplex eine Desaktivierung, die jedoch nicht auf einen Zinkverlust zurückgeführt werden konnte. In weiteren Versuchen wiesen Zink-Pyridin-Acetat-Komplexe nur eine geringe Aktivität auf.

In-situ XAS-Messungen in einer eigens für diesen Zweck hergestellten spektroskopischen Reaktormesszelle bestätigten, dass das Zink auch unter Reaktionsbedingungen genügend immobilisiert war. Es fand keine homogene Katalyse durch lösliche Zinkspezies statt, die sich im Laufe der Reaktion gebildet hätten. Allerdings zeigten die XAS-Messungen Brom in Lösung, zudem verringerte sich die Absorption an der Brom-K-Kante im festen Katalysator während der Reaktion. ICP-OES-Messungen konnten den Abgang des Bromids aus dem katalytisch aktiven Komplex bestätigen. Weiter zeigte sich, dass die Aktivität des immobilisierten Zink-Pyridin-Komplexes durch die Zugabe eines Bromids als Co-Katalysator aufrecht erhalten werden konnte. Die Schwierigkeit solcher Messungen besteht darin, eine geeignete Reaktormesszelle zu konstruieren, die eine so geringe Absorption an Röntgenlicht erlaubt, dass solche Messungen durchzuführen sind. Ermöglichte die hier eingesetzte Reaktormesszelle Untersuchungen an der Zink-K-Kante (9.659 keV), so konnten mit einer zweiten verbesserten Version der *in-situ* Messzelle sogar Struktur und Aktivität homogener Nickelkatalysatoren (Nickel-K-Kante, 8.333 keV) miteinander in Beziehung gesetzt werden. Dies ist hinsichtlich eines möglichen Einblicks in das Reaktionsverhalten der zuvor untersuchten Chrom-Salen-Komplexe (Chrom-K-Kante, 5.989 keV) interessant.

Schon früh zeigte sich im Rahmen dieser Arbeit bei vorbereitenden Parameterstudien ein unerwartetes Verhalten der Druckabhängigkeit während der Synthese von PC aus CO₂, die auch in der Literatur Erwähnung findet. Zur

Aufklärung dieser Beobachtung waren Phasenverhaltensstudien in einem Sichtfensterautoklaven mit Transmissions- und ATR-IR-Spektroskopie notwendig. Dabei zeigten sich drei charakteristische Bereiche verschiedener Phasen: Bei niedrigen mittleren Dichten war das Reaktionsgemisch zweiphasig zusammengesetzt und ein höherer CO₂-Gehalt führte zu einem kleineren Flüssigphasenanteil und niedrigeren Umsätzen. Verringerte man den Anteil an CO₂ bei gleichbleibender mittlerer Dichte, so vervielfachte sich das Volumen der flüssigen Phase. In dieser CO₂-gestreckten Flüssigkeit („expanded liquid“) wurden höhere Umsatzraten erzielt als bei den Reaktionen mit hohem CO₂-Gehalt. Allerdings war wiederum ein zu geringer CO₂-Anteil nachteilig für die Reaktion. Die Lösungsmittelpolarität und die Lage des chemischen Gleichgewichts könnten hierfür eine Ursache sein. Im Gegensatz zu vielen anderen Reaktionen in überkritischen Fluiden wirkte sich jedoch ein hoher Druck während der Reaktion und ein daraus resultierendes Einphasensystem ungünstig auf die Ausbeute an PC aus. *In-situ* ATR-IR-Messungen der Katalysatoroberfläche deckten drastische Änderungen des Phasenverhaltens innerhalb der ersten Reaktionsminuten auf und gaben einen wichtigen Einblick in die Fest-Flüssig-Grenzschicht unter Reaktionsbedingungen.

Die Erkenntnisse bezüglich der Stabilität von Zink auf Silicaoberflächen und der Möglichkeit, Bromid als Co-Katalysator einsetzen zu können, wurden abschließend im Hinblick auf eine vereinfachte Katalysatorsynthese genutzt, indem verschiedene Zink-Mischoxide hergestellt und diese in Gegenwart von Ammoniumbromid auf ihre katalytische Aktivität getestet wurden. Diese wurden sowohl nasschemisch als auch mittels Flammenpyrolyse dargestellt. Die Verwendung eines Kolloids aus Silicapartikel als Ausgangsstoff der Katalysatorsynthese anstelle einer Tetraethoxysilanlösung führte zu einer signifikanten Verbesserung der Katalysatoraktivität. Ausbeuten von >99% bei nahezu 100% Selektivität wurden mit 200 mg Katalysator und 140 mmol PO bereits bei 120 °C in sechs Stunden erzielt – dies entspricht einer Umsatzrate >750 mol (mol_{Zn} h)⁻¹. Nicht nur die Testreaktionen, sondern auch Messungen mit

Rasterelektronenmikroskop (STEM) und XAS bekräftigten, dass nicht einzelne Zinkatome, sondern Zinkcluster wichtig für die Katalysatoraktivität sind.

Chapter 1

Introduction

“Green chemistry has set itself the goal of making chemicals technology more environmentally benign by efficiently using preferably renewable raw materials, eliminating waste and avoiding the use of toxic and/or hazardous reagents and solvents in the manufacture and application of chemical products.” (Roger Sheldon)

The main sources of anthropogenic CO₂ emission are energy production by fossil fuels like petroleum, natural gas and coal, as well as deforestation. CO₂ is also emitted by chemical processes and cement production. This is unfavorable, because the concentration of CO₂ in the atmosphere has increased in the last 200 years from 250 ppm to 367 ppm,¹ and further anthropogenic CO₂ emissions should be avoided.²⁻⁴

However, not only the emission of CO₂, but also emission of the volatile organic compounds (VOC) which are often used as solvents in industrial processes, and, in general, energy extensive production steps are environmentally harmful. The awakened public interest to protect the environment led to debates about the global climate change,⁵ that caused political measures, for e.g., the Kyoto protocol,⁶ and also influences the chemical industry. Guidelines for an environmentally benign chemistry are summarized in the so-called ‘green chemistry’.

One aspect of pollution control is the cutback of exhaust emissions. The enforcement to build low or even zero emission plants by collecting the produced CO₂, will make CO₂ a very cheap chemical. CO₂ can be used as C₁-building

block in chemical syntheses. One possible reaction of CO₂ is its insertion into epoxides. This thesis focuses on the synthesis of PC—a chemical product with various applications—under environmentally benign reaction conditions. However, the usable amount of CO₂ in the chemical production is magnitudes smaller than anthropogenic CO₂ emission.

1.1 The Principles of Green Chemistry

Paul Anastas and John C. Warner developed twelve principles of green chemistry (see Appendix B on page 129).^{7,8} The scope of this principles was widened by Winterton toward guidelines for industrial research.⁹ The principles cover such concepts as:

- to maximize the amount of raw material that ends up in the product;
- the use of safe and environmentally benign solvents and reactants;
- the design of energy efficient processes; e.g. heterogeneous catalysis.

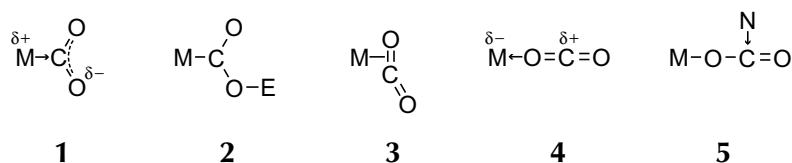
It is a great challenge to follow this concept for reactions that use CO₂ as reactant. Most chemical processes are using phosgene, carbon monoxide or isocyanates as C₁-building block. CO₂ can substitute these toxic and hazardous gases under some circumstances in CO₂ fixation reactions.^{10–13} Furthermore, the use of CO₂ can supersede additional solvents in these syntheses due to its special physical and chemical properties.¹⁴ This minimizes the risk of pollution by the application of volatile environmentally more harmful solvents. Finally, CO₂ can lead to energy efficient processes: Although CO₂ fixation reactions are endothermic, the easy separation of unconverted CO₂ (reactant and solvent) from the liquid product is carried out by depressurizing of the reaction mixture. Due to the inertness of CO₂ in reactions, the use of catalysts is required, in which the application of heterogeneous catalysts is preferred to achieve energy efficient processes.¹⁵ *In situ* spectroscopic measurements are the key for a better under-

standing of the reaction mechanism and the state of the catalyst during reaction. Such knowledge is helpful for progressive catalyst development.^{16,17}

1.2 Carbon Dioxide

The CO₂ molecule is the prototype of a linear triatomic molecule. The central carbon atom is sp-hybridized and the C–O distance of 1.16 Å is shorter than a C–O double bond involving an sp²-hybridized carbon atom.¹⁸ CO₂ is not very reactive at ordinary temperatures. The mandatory activation of CO₂ can be done by two different strategies: a) the use of highly reactive reactants like epoxides or b) the use of a reducing agent like hydrogen, amalgams, complex hydrides or an electrochemical process.

CO₂ metal complex formation on transition metal complexes can be expected to occur by electron donation from electron-rich low-valent metal centers to give oxycarbonyl-metal compounds **1** (see Scheme 1-1).¹³ The simultaneous presence of an Lewis-acid center (E) would favor this reaction by forming complexes of type **2**. The C–O π-bond may also interact with the requisite vacant metal orbital to give π-complexes of type **3**, in analogy with simple olefins. Even the oxygen atoms of CO₂ could act as weak (or potential) electron donors to electron deficient metals, e.g. **4**. A present electron donating center (N) would assist this reaction to form complex **5**.



Scheme 1-1: Possible species at the reaction of CO₂ with transition metal complexes.¹³

Although CO₂ is called non-toxic in this work, high concentrations are hazardous. Up to 0.5 vol% CO₂ is not considered harmful, but concentrations of

5 vol% CO₂ in air cause an increase in breathing rate and prolonged exposure to higher concentrations may cause unconsciousness and death.¹⁹

1.2.1 The Carbon Cycle

Atmospheric CO₂ is mainly integrated in two natural circulations (Figure 1-1): In the chemical loop,²⁰ the exchange of atmospheric CO₂ and the CO₂ of the deep oceans with the sediments is well balanced. The biological loop of CO₂ between photosynthesis and production by respiration of living creatures and mineralization of dead organic material is also in equilibrium.²¹ Approximately 200 Gt are exchanged annually between vegetation, soil and atmosphere. Human activities set free 6.5 Gt a⁻¹ of CO₂ from fossils,^{1,22} whereas only 0.1 Gt a⁻¹ of new fossils are built.²³ Another large contribution of about 2 Gt a⁻¹ is made by deforestation.

1.2.2 Carbon Dioxide as Solvent

CO₂ is nontoxic, nonflammable, environmentally benign, unregulated, and available in high purity at low costs. Because of its moderate critical parameters ($T_c = 31$ °C, $p_c = 73.8$ bar, $\delta_c = 466$ kg m⁻³),²⁴ single-phase conditions can be reached at rather low pressure and temperature (see Figure 1-2). In this work, the term ‘supercritical’ was used for single phase conditions in general although it is well-defined only for pure substances. The critical point of CO₂ allows broad variations of density and transport properties at relatively mild conditions. Thus, the physical properties can be altered drastically, from gas-like to liquid-like behavior—simply by isothermally varying the pressure around the critical pressure.^{25–28} At densities above the critical density, CO₂ has an appreciable solvent power for many organic substances.²⁹ Such preferences make CO₂ a promising solvent for chemical syntheses,^{14,30} in which it can substitute harmful organic solvents,³¹ and for applications in the food or cosmetic indus-

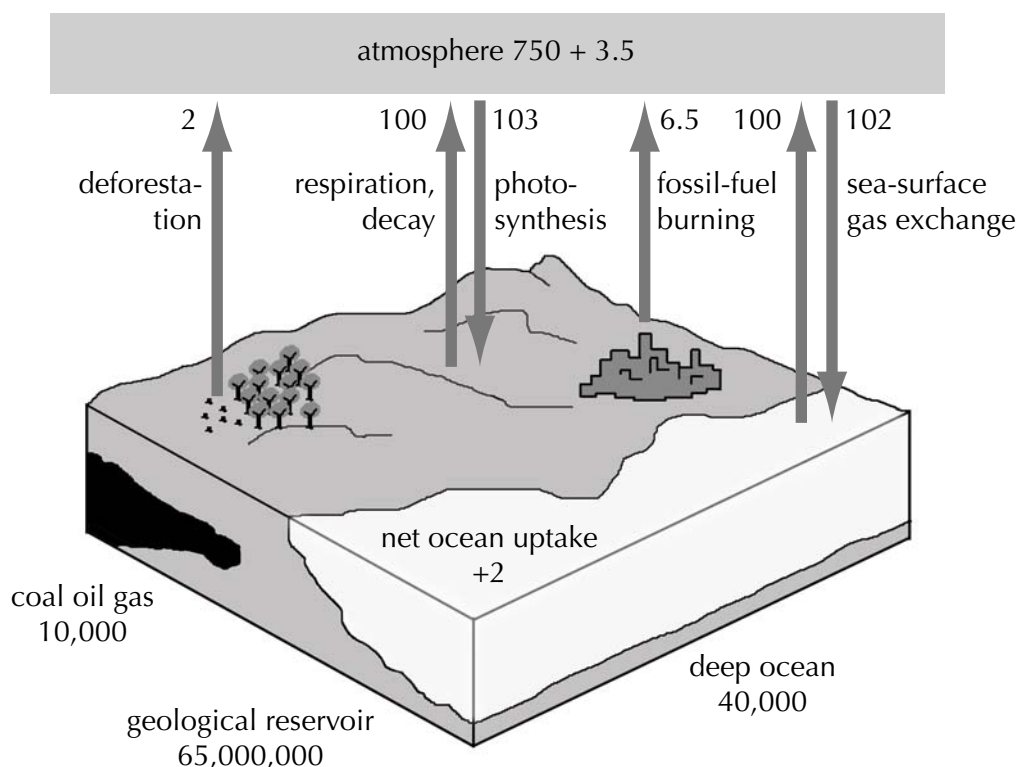


Figure 1-1: The carbon cycle. Annual changes and estimated carbon amounts of reservoirs in Gt.²³

try, in which the use of nontoxic solvents is decisive. CO_2 is used in several commercial extractions,^{32–34} its solvent power is comparable to that of hexane. The low critical temperature makes it also an ideal solvent for biologically catalyzed and thermally sensitive reactions.^{35,36}

1.2.3 Chemicals Synthesized from Carbon Dioxide

Approximately 110 Mt of CO_2 are currently used for chemical synthesis annually.³⁷ The chemicals synthesized include commercial process of urea **6**, salicylic acid **7**, cyclic carbonates **8**, and poly carbonates **9** production, as well as a number of other reactions shown in Scheme 1-2.¹⁰

Urea and urea derivative could be synthesized directly by CO_2 , which would substitute phosgene and carbon monoxide. Because CO_2 is generated and re-

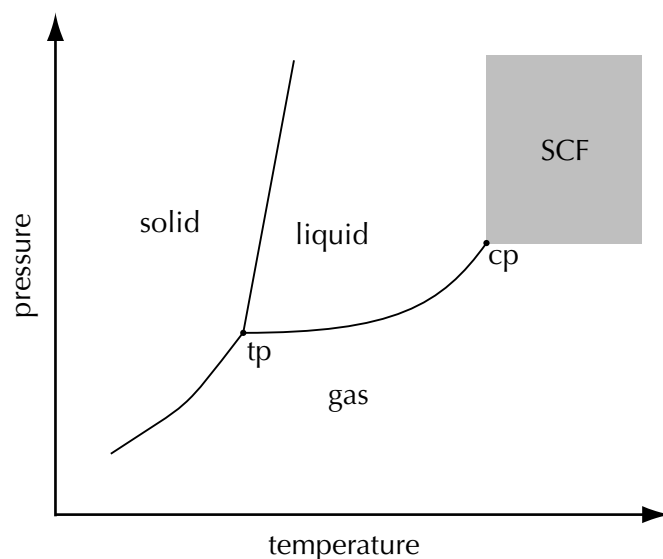
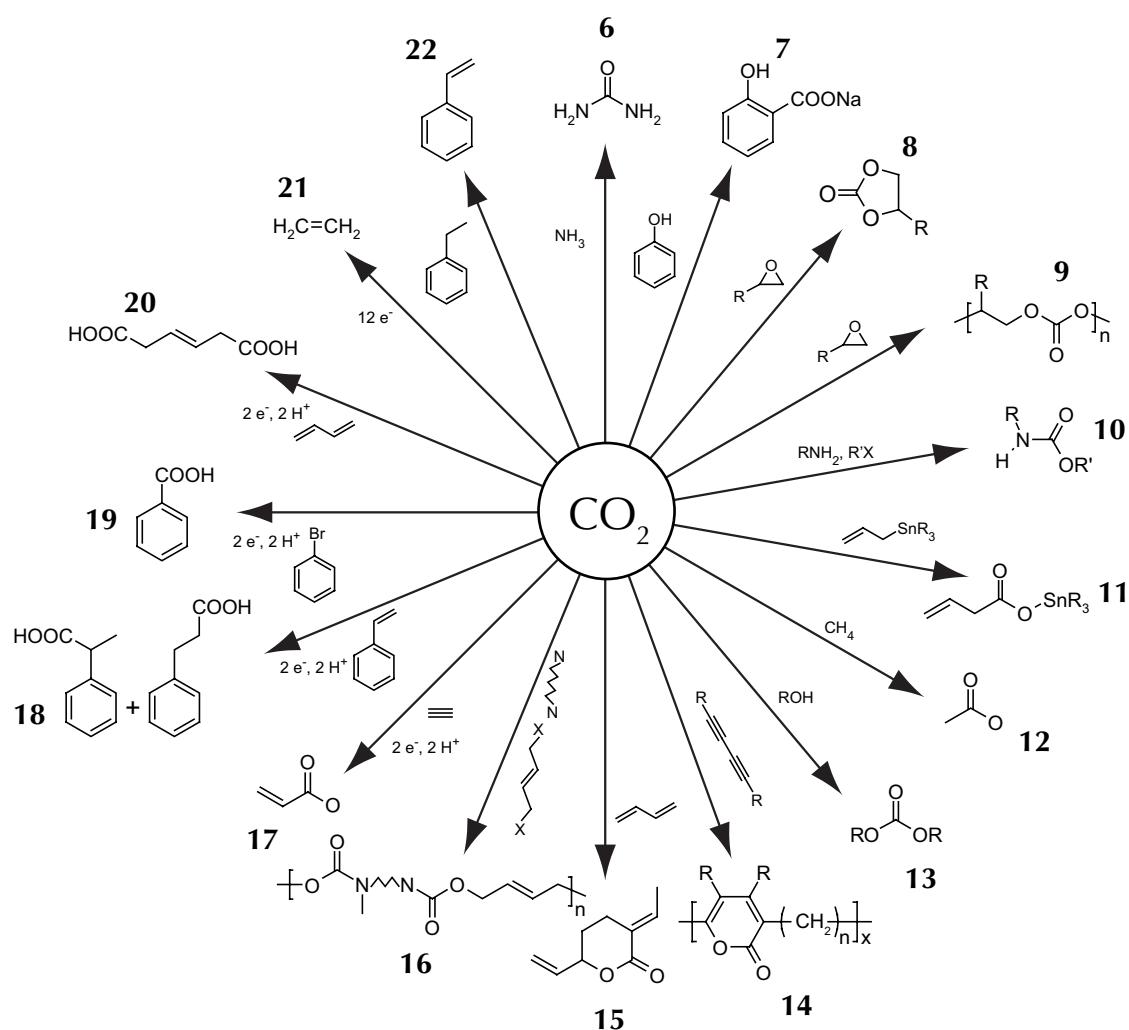


Figure 1-2: Qualitative schematic phase diagram of CO₂ with the supercritical fluid region (SCF), the triple point (tp) and the critical point (cp).

covered from ammonia and hydrogen plants, these plants could use a substantial amount of CO₂ for urea production.^{19,38} Salicylic acid is a crucial reactant for the synthesis of Aspirin. More than 100 years ago, the Kolbe–Schmitt reaction was developed in the chemical industry and it is still a topic of research.^{39–42} The synthesis of cyclic carbonates from CO₂ is focused in this thesis and discussed in detail in paragraph 1.3.3. Polycarbonate production is related to that of cyclic carbonates.^{43–46}

In addition to these commercial processes using CO₂, there are a lot of interesting approaches for the application of CO₂: These reactions differ in the way CO₂ is reduced during reaction. The simplest kind of reaction is the insertion of CO₂ e.g. to obtain carbamates **10**,^{47,48} carboxylated allyl derivatives **11**,⁴⁹ acetic acid **12**,^{50,51} dialkyl carbonates **13**,^{52–55} polypyrones **14**,⁵⁶ lactones **15**,^{57–59} and polyurethanes **16**.^{60,61} Reductive carboxylations are more complex than insertion reactions. Such reactions can result in propenic acid **17**,^{62,63} the coupling of CO₂ with styrene **18**,^{64–67} carboxylation of aromatic halides **19**,⁶⁸ and carboxylic acids from alkenes **20**.⁶⁹ Remarkable 12-



Scheme 1-2: Chemical transformations of CO_2 .¹⁰

electron reductions lead to C_2 -compounds like ethylene 21.^{70,71} Finally, CO_2 can be used for dehydrogenation of hydrocarbons 22.⁷² In this reaction, CO_2 is not incorporated into the product.

1.3 Organic Carbonates

Carbonic acid is not stable at ambient temperature and decomposes into CO_2 and water. The esterification of carbonic acid leads to stable organic species,

known as organic carbonates. Different carbonates can be distinguished according to the type of substituents of the hydroxy groups. Typical compounds are dialkyl-, diaryl- or diallyl carbonates, mixed forms and cyclic carbonates.

1.3.1 Physical Properties and Applications of Propylene Carbonate

PC is soluble in water to extent of 25 g of PC to 100 g of water at 25 °C; PC is a polar and aprotic solvent,⁷³ and it is liquid at typical application temperatures ($T_m = -55$ °C; $T_b = 242$ °C).²⁴ Compared to other organic solvents, PC has a relatively high flash point of $T_{fp} = 132$ °C, which makes it a quite safe solvent. Because of these properties, PC is used in the synthesis of polymers and it is also important for extractive separation of mixtures and as additive in hydraulic fluids. As PC features a good solubility in polyethylene oxide or other polymer electrolytes and has an advantageous effect on the ionic conductivity, PC is used in modern lithium-ion batteries.⁷⁴ Furthermore, it is an ingredient of more than 230 cosmetics and personal care products.⁷⁵

1.3.2 General Methods of Preparation of Organic Carbonates

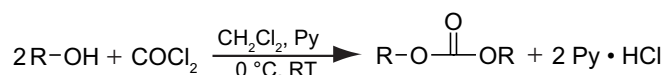
Organic carbonates can be synthesized in different ways.⁷³ The common methods are:

- phosgenation method
- oxidative carbonylation of alcohols and phenols
- reaction of urea with alcohols or phenols
- carbonate interchange reactions
- synthesis of cyclic carbonates by CO₂ fixation

The listed techniques are shortly described; the synthesis of carbonates by CO₂ fixation is focused on in more detail in paragraph 1.3.3.

Phosgenation Method

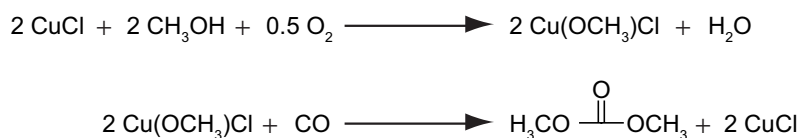
Alcohols or phenols are dissolved in an inert, anhydrous solvent with excess pyridine, and phosgenated at or below ambient temperature (Scheme 1-3). Pyridine acts as base and reacts with phosgene, and an ionic adduct is formed. This adduct formed is more reactive than the corresponding chlorocarbonic acid esters. Other nitrogen-based bases can also be used instead of pyridine. Nearly all organic carbonates can be prepared by this method; symmetric carbonates are obtained in one step, whereas unsymmetrical are obtained by a two-step reaction. The advantages of this method are the high yields and the possibility to synthesize functionalized and activated carbonates. The obvious disadvantages are the use of toxic and hazardous chemicals like phosgene and pyridine, the neutralization of excess pyridine and the removal of the by-products.⁷⁶



Scheme 1-3: Synthesis of cyclic carbonates with phosgene in presence of pyridine and solvent.

Oxidative Carbonylation of Alcohols or Phenols

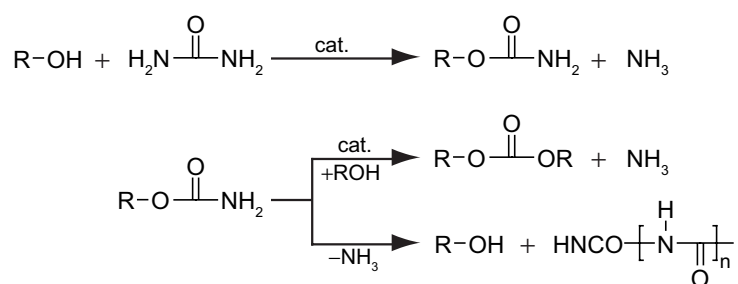
The formation of dialkyl carbonates from the reaction of alcohols and carbon monoxide is promoted by transition metal and post-transition metal compounds (Scheme 1-4).^{77,78} Often palladium, mercury or copper based catalysts were used. However, copper is the only species that can be directly re-oxidized. This is a suitable method for alkyl carbonates, but the synthesis of other carbonates gives only low yields.



Scheme 1-4: Oxidative carbonylation of alcohols catalyzed by copper.

Reaction of Urea with Alcohols or Phenols

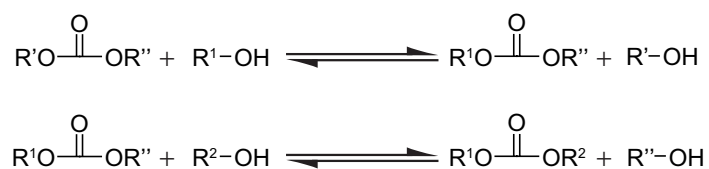
The reaction of urea with alcohols in combination with metal salts like zinc acetate or lead acetate leads to the synthesis of carbamates (Scheme 1-5).⁷⁹ These carbamates can react to carbonates with triphenyl phosphine as co-catalyst. Main by-products are isocyanuric acid and similar compounds. In principle, the produced ammonia can be recycled for the synthesis of urea. Adequate catalysts are dibutyl tin oxide and triphenyl tin chloride. Even heterogeneous catalysts such as antimony trioxide and aluminum trioxide can be used.



Scheme 1-5: Two-stage synthesis of carbonates from urea via carbamates.

Carbonate Interchange Reactions

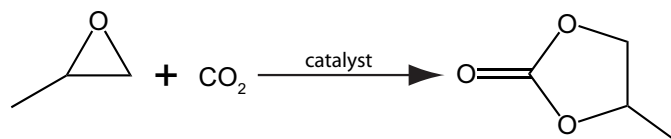
Carbonate interchange reactions can be defined as a catalytic process wherein one carbonate is converted with an adequate alcohol to another carbonate (Scheme 1-6).^{80,81} Normally, the more nucleophilic alcohol substitutes the less nucleophilic compound. If both compounds exhibit a similar nucleophilicity, the less volatile alcohol substitutes the more volatile alcohol. A broad range of different reactants and catalysts are used; the reaction conditions differ a lot, too.



Scheme 1-6: Carbonate Synthesis by interchange reactions.

1.3.3 Synthesis of Cyclic Carbonates by Carbon Dioxide Fixation

The synthesis of PC by the use of CO₂ as C₁-building block is a step toward production of PC (Scheme 1-7) according to the principles of green chemistry. Toxic and hazardous reactants such as phosgene and carbon monoxide can be substituted by CO₂ which simultaneously serves as a solvent.^{10–12,73}



Scheme 1-7: Reaction of CO₂ fixation by insertion into PO and formation of PC.

Present industrial processes for PC synthesis from PO and CO₂ use alkali metals or bromide as catalysts and ethylene glycol as solvent.⁸² The high substrate/catalyst ratio of 1/100 and the substitution of glycols or other solvents by CO₂ (acting as reactant and solvent) initiated the search for alternative catalyst systems. Alkali metal salts with crown ethers or ammonium compounds,^{83–85} halides with nitrogen or phosphorus bases as co-catalysts,^{86–89} transition metal or aluminum catalysts with nitrogen or phosphorus containing ligands,^{43,46,90–99} complex multi-metal catalysts,^{100,101} and catalyst systems involving ionic liquids^{102–105} have been reported.

However, for an environmentally benign process heterogeneous catalysts instead of homogeneous catalysts would be desirable due to easier product separation and because the process can be simplified.¹⁵ Hence in recent years a number of heterogeneous catalysts were tested like smectite,^{106,107} lanthanide oxychloride,¹⁰⁸ Mg-Al mixed oxides,^{109,110} Cs-P-Si mixed oxides,¹¹¹ niobium oxide,¹¹² zinc bromide,¹¹³ hydroxyapatites,¹¹⁴ polyoxometalates,^{115,116} and solid bases.^{80,117} Even more complex synthesized catalysts were investigated. Among these catalysts are zeolites with encapsulated alkali metals,¹¹⁸ halides,¹¹⁹ or aluminum phthalocyanine complexes.^{120,121} Furthermore, on oxides an-

chored organic bases,^{122,123} or transition metal complexes,^{124–126} as well as on resins tethered transition metals complexes,¹²⁷ complex organic halides,^{128,129} or gold¹³⁰ were investigated. However, the catalytic activity of these heterogeneous catalysts is rather low and a significant gap in performance between homogeneous and heterogeneous catalysts exists. Moreover, studies of stability and recycling ability are hardly reported for heterogeneous catalysts in the cycloaddition of CO₂ to PO.

1.4 Heterogeneized Catalysts

A simple exchange of a well-known homogeneous catalyst against a heterogeneous one would be interesting for many industrial processes, when the heterogeneous catalyst works under the same conditions, but eliminates extensive work-up procedures. This demand can be met by the so-called ‘heterogeneization’ of metal complexes, which are used as homogeneous catalysts. The objective is to obtain a well defined complex that can be highly dispersed throughout the reaction medium while remaining in a separate phase. Common grafting possibilities of homogeneous catalyst on a support material are shortly introduced.^{131,132}

1.4.1 Immobilization Strategies

Typically, active metal complexes are synthesized on supports like inorganic polymers, silica, oxides, zeolites, polystyrene, etc.^{133,134} Even directly polymerized metal complexes are possible. Common immobilization strategies are shortly discussed below and can be distinguished by the nature of the bond, which anchored them onto the support:

- relatively weak interactions like adsorption or coordination
- encapsulation

- covalent bond
- electrostatic bond

In general, a precursor of the catalytically active complex is first anchored onto the support and then the complex is synthesized step by step, or previously prepared complex can be grafted entirely onto the support.¹³³

Anchoring via Adsorption, Coordination or Chemical Vapor Deposition

A well-known example is the deposition of carbonyl complexes onto charcoal, alumina or zeolites. The adsorption of cinchona alkaloids onto metal surfaces has been extensively studied in the field of enantioselective catalysis.¹³⁵ For heterogeneous catalyst, the coordinative bond of metal complexes enabled the immobilization of various homogeneous catalysts. Coordination of the metal, which is often the catalytically active center, by a tethered ligand will change the atomic geometry of the transition state during reaction. This could be disadvantageous for the catalytic activity. Another possibility is the immobilization of the ligand, for e.g., by sulfonic acid groups onto the support. Due to the weak interaction between support and catalytically active complex, catalysts prepared by these methods exhibit only weak stability, particularly when these catalysts are used in an environment which features a high solubility power.¹³²

Encapsulation

Encapsulation is the only immobilization process which does not require any interaction between the catalyst and the support besides sterical restraints that hinder the catalyst from diffusion out of the pores. Hence it is the only method in which unmodified homogeneous catalysts can be used, because no changes of the ligand or in the coordination sphere of the catalyst are required.¹³² The ligand is finally synthesized inside a cage of a porous material to a bulky complex, so that the entire complex can not leave the catalyst's pore. This method is well-known as 'ship in the bottle' technique. An other preparation variant is the assembling of the support around the catalyst (zeolite synthesis method). For

the flexible ligand method a preformed complex reacts with a transition metal previously introduced into the zeolite¹³⁶ or the layers of clay.¹³³ The disadvantages are that such catalysts are only applicable for relatively small products (diffusion through zeolite pores) or small transition states, and the high experimental expenditure.¹³⁶

Covalent Tethering

As an organic ligand is covalently bound onto the support, the environment of the catalytically active metal center is equal to that of the homogeneous complex. However, the ligand has to be modified for the immobilization process. One possibility is to attach defined molecular species to polymeric supports, but in this work focus was placed on the anchoring of transition metal complexes onto oxidic supports. In general, the support has to be modified, as explained in paragraph 1.4.2. Due to the bond strength, covalent tethering will produce stable catalysts,¹³² and it is possible on various different supports.^{133,134,137}

Chemical Fixation via Electrostatic Bond

Cationic or anionic metal complexes can be immobilized by ion exchange or impregnation into cages of, e.g., zeolites. It is a conceptually simple and facile method of grafting ionic catalysts. The stability can be comparable to that of covalent tethered catalysts, but suitable ligands are required.¹³²

1.4.2 Support Modification

The Grafting Method

Stable covalent bonds between an organic molecule and an inorganic support material are achieved by post-synthetic modification of the support in which the functional organic group is grafted onto the solid.^{133,137} The most common support for this treatment is silica, and the method for silica modification was developed for applications in gas chromatography;¹³⁸ the silylation with alkoxy-silanes has been researched in greatest detail.¹³⁹

The Co-condensation Method

Organofunctional groups can be incorporated into the solid matrix during the silica preparation by co-condensation of an organoalkoxysilane with a silica precursor.¹³³ The limits of this method are the comparatively small range of ligands that can be incorporated, because bulkier and charged molecules will interfere with the formation process of the support. Moreover, the organic complex has to withstand the reaction conditions of the silylation.

1.5 Spectroscopic Techniques

In situ spectroscopy is an important tool to gain information about phase behavior and catalyst structure under reaction conditions.^{16,17} *In situ* spectroscopy of CO₂ fixation reactions has to be performed under high pressure due to the reaction conditions. Only a few spectroscopic techniques allow such measurements during heterogeneously catalyzed reactions, including IR,^{140–142} ATR-IR,¹⁴³ Raman,^{144,145} ultraviolet-visible (UV-Vis),^{146,147} NMR,^{140,148–150} electron paramagnetic resonance (EPR),^{151–153} and XAS^{154–157} spectroscopy.

Due to its ability to measure smallest amounts of liquids in a high pressure gas atmosphere, ATR-IR spectroscopy is a powerful tool for phase behavior studies. Only XAS can provide element sensitive information about coordination symmetry and bond length as well as oxidation state in heterogeneously catalyzed reactions. Both homogeneous catalysts in liquid and gaseous-like phase as well as heterogeneous catalysts in the solid phase can be observed under high pressure conditions. ATR-IR and XAS spectroscopy are shortly introduced in the next paragraphs.

1.5.1 Attenuated Total Reflectance Infrared Spectroscopy

In situ measurements of small liquid phases in a larger volume filled by a gas under high pressure are difficult to achieve by transmission IR spectroscopy. The contribution from the gaseous phase has to be minimized and the absorption of infrared light in dense or liquid-like phases is high, thus a very short path length is required. This problem can be solved using an internal reflection element (IRE).^{158,159} In ATR-IR spectroscopy the infrared beam propagates inside the IRE and is totally reflected at the interface (Figure 1-3), if the angle of incidence θ_i is larger than the critical angle θ_c , which can be calculated according to Equation 1-1. In this equation, n_1 is the high refractive index of the IRE, and n_2 the lower refractive index of the probed medium.

$$\theta_c = \frac{1}{\sin(n_2/n_1)} \quad (1-1)$$

An evanescent electromagnetic field is generated, which penetrates into the sample, as shown in the inset of Figure 1-3. This electromagnetic field attenuates exponentially to a value equal to $1/e$ of its initial magnitude $E_{0x,y,z}$ at a distance z from the IRE, defined as the penetration depth d_p .

$$E_{x,y,z} = E_{0x,y,z} e^{-\frac{z}{d_p}} \quad (1-2)$$

The magnitude of d_p depends on the wavelength of the probing beam, which results in higher absorption intensities at longer wavelength λ , the angle of incidence θ_i , and the refractive indices:

$$d_p = \frac{\lambda_1}{2\pi \sqrt{\sin^2 \theta_i - \left(\frac{n_2}{n_1}\right)^2}} \quad (1-3)$$

where $\lambda_1 = \lambda/n_1$ denotes the wavelength in medium 1. Typically d_p is in the order of 1/10 of the probing wavelength and varies between a micron and a few microns, depending on the refractive indices of the two media. Note that Equation 1-3 is derived for a two phase system, with the approximation that the sample is a weak absorber, in other cases the equation becomes more complex.¹⁵⁸ The combination of transmission IR with ATR-IR spectroscopy allows simultaneous investigation of the gaseous phase and the liquid phase.

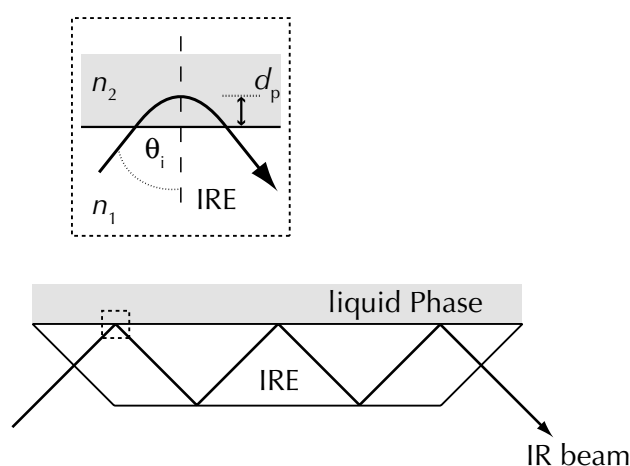


Figure 1-3: A coated trapezoidal internal reflection element (IRE) with 5 total reflections and angle of incidence θ_i of 45° for ATR spectroscopy. The inset shows the evanescent wave at the IR-probed medium interface and the penetration depth d_p to outline the principle of the ATR-IR technique.

1.5.2 General Aspects of X-ray Absorption Spectroscopy

XAS is based on the excitation of a core electron to an unoccupied orbital or continuum.¹⁶⁰ Each element has a particular binding energy for the core electron and therefore XAS is an element sensitive technique. If the core electron is excited, a higher X-ray absorption (absorption edge) is observed. To determine the absorption of the X-ray beam, a sample is typically placed between two ionization chambers, which measure the photon flux before and behind the sample. Often a reference sample situated between the second and a third ionization

chamber is used for energy calibration. The absorption of the X-rays which can be described with Lambert-Beer's law is then determined as a function of the energy. The overall spectral lineshape corresponds to the absorption threshold. When an electron of the K shell is excited, the observed absorption phenomenon is called absorption at the K-edge. The analogously denoted L-edge absorption occur at lower energies.

To determine the absorption as a function of energy, a tunable X-ray beam is necessary. This type of radiation is provided by synchrotrons or storage rings, which are normally used nowadays. The white X-ray beam is monochromized to a specific energy that is typically scanned stepwise during measurement. Besides noble gases or otherwise isolated atoms, a fine structure can be observed, which provides much more structural information than the mere absorption edge. This fine structure is a valuable tool for catalyst characterization.^{161–163} The part of the spectrum close to the absorption edge (Figure 1-4) is called the X-ray absorption near-edge structure (XANES), also known as near-edge X-ray absorption fine structure (NEXAFS). The oscillations occurring at higher energies than the edge (Figure 1-4) are the so-called extended X-ray absorption fine structure (EXAFS).

1.5.3 Basics of XANES and EXAFS

As electrons exhibit not only particle but also wave-like properties according to quantum physics, the excited electron can be regarded as outgoing electron wave, that is reflected by a neighboring atom. The backscattered wave results in a superposition, which causes minima and maxima in the fine structure, or more precisely, in the EXAFS (see Figure 1-4).^{164–166} The EXAFS modulation function can be extracted from the raw data (plotted as a function of the photon energy $h\nu$); for this purpose, the $h\nu$ regions above and below the energy used for EXAFS are cut off and the decreasing background as well as superimposed interferences of the XANES region are subtracted. Then the data from the energy

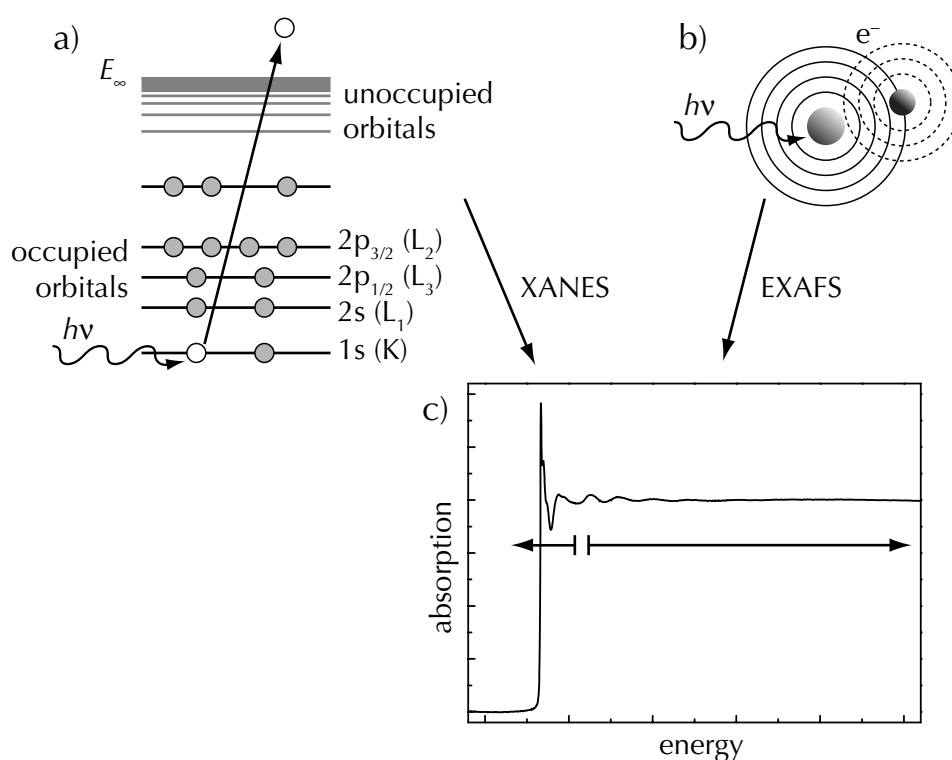


Figure 1-4: Principle of X-ray absorption: schematic presentation of a) the excitation of a core electron, b) the scattering of the electron wave by a neighboring atom, and c) the complete resulting spectrum with XANES and EXAFS region.

$h\nu$ -space is converted into the k -space, so that the minima of the superposition become equally spaced. The resulting $\chi(k)$ function is multiplied with k (or k^3) for further compensation of the progressive decrease in the EXAFS oscillations. Finally, the $k\chi(k)$ function is Fourier-transformed and typically the square is depicted (only the real part). The resulting function exhibits information about the distance of the neighboring atom. A complication is caused by a shift of the electron wave when it leaves the source and again, when it is backscattered. This shift is called the ‘phase shift’.

More information can be gained by fitting of a measured $\chi(k)$ function with a calculated function. Due to the energy of the emitted electron, multiple scattering of the electron can often be neglected. This approximation allows the calculation of the EXAFS $\chi(k)$ function (Equation 1-4). The short mean free path

length λ of only a few Ångström units makes EXAFS an ideal local sampling technique.

$$\chi(k) = \sum_j N_j S_0^2(k) F_j(k) e^{-2\sigma_j^2 k^2} e^{\frac{-2r_j}{\lambda_j(k)}} \frac{\sin(2kr_j + \phi_{ij}(k))}{kr_j^2} \quad (1-4)$$

The function is a sum, in which each term corresponds to a contribution from a different shell. The number of atoms in the same shell is represented by N_j , r_j is the distance between the absorber atom i and the neighboring atom j ; $\phi_{ij}(k)$ is the phase shift; the exponential term including the Debye–Waller factor σ_j is a damping factor due to thermal and static disorder; the exponential term including $2r_j/\lambda(k)$ regards the attenuation by the lifetime of the photo electron; $S_0(k)$ is the passive electron reduction factor originating from the positive charge after excitation; and $F_j(k)$ is the backscattering amplitude. One of the limitations of EXAFS analysis is that it is difficult to distinguish between atoms with similar mass like nitrogen and oxygen.

In general, the overall absorption strength is influenced by the number of electrons that occupy the initial core level. Only these electrons can participate to the absorption process. Furthermore, the absorption depends on the density of the unoccupied orbitals available for the X-ray-assisted excitation (see Figure 1-4 a), and, in addition, XANES is affected by the transition probability. Both phenomena are determined by the chemical bond formation process. Hence XANES allows to gain information about the oxidation state and the coordination geometry. In the XANES region, the X-ray photon energy is only slight above the edge energy. If the energy of the excited electron is low, the penetration depth will be rather long. Due to this fact, multiple scattering has to be taken into account. This makes the interpretation of the XANES region more difficult and often XANES is used like a ‘fingerprint’ by comparison to reference spectra.

1.6 Scope of the Thesis

The scope of this thesis was the development of catalysts for the synthesis of PC by fixation of CO₂ to PO. PC was used as representative for cyclic carbonates and exhibits a manifold application range.

The crucial step is the activation of the rather inactive CO₂ molecule by adequate catalysts. For this purpose, homogeneous catalysts—chosen by screening (Cr-based) or reported in literature (Zn-based)—were heterogenized onto oxidic supports. Different grafting strategies were tested and the deactivation behavior of the resulting catalysts investigated. Focus was placed on not only the type of bonding toward the support, but also the integrity of the catalytically active center.

The application of different analytic techniques was important, so that information about the success of the immobilization process could be gained. Besides NMR for the structural identification of the synthesized ligands and homogeneous complexes, ICP-OES, EA, TA, BET, XPS, and IR spectroscopy were used for characterization of the solid catalysts. Particular focus was laid on XAS, which should be used to obtain structural information of the catalyst, the structure/activity relationship, and the reaction mechanism.

Based on better comprehension of the reaction mechanism, in a final step less complex catalyst systems were developed that allow easier access to heterogeneous catalysts thus minimizing the effort in synthesis and cost. For that purpose, variations of the support, addition of a co-catalyst and a simplification of the catalyst synthesis were investigated.

Finally, phase behavior studies aimed at gaining more insight into the reaction itself. In such experiments, ATR-IR spectroscopy assisted by visual observation was used to study the phase behavior and enhanced the identification of the phase composition.

Chapter 2

Experimental

In this chapter the different experimental equipment, analysis methods and general techniques applied in this work are described. Specific experimental procedures are given in detail in the corresponding chapters.

2.1 Carbon Dioxide Insertion Reaction

2.1.1 High-Pressure Batch Reactor

The coupling of CO₂ and PO was performed in a 250 ml high pressure stainless-steel autoclave (Medimex, HPM-P) with teflon coated viton sealing (Figure 2-1). For safety reasons, the entire reactor system was placed in a high-pressure chamber. The reactor was equipped with a magnetically coupled stirrer (Emod EEDF 56L/2A), which speed could be adjusted manually. The autoclave was heated by an inner copper jacket equipped with electric heating elements and cooled by water through an outer aluminum jacket. A thermostat (Eurotherm 900 EPC) controlled the temperature. The reactor withstands a temperature up to 200 °C and a pressure up to 200 bar; the pressure was measured by a piezoelectric pressure gauge and in addition by a membrane based pressure gauge. Further, a pressure relief valve was connected to an expansion vessel, and the autoclave could be vented with an outlet valve, purging the gas to the exhaust gas system of the high-pressure chamber.

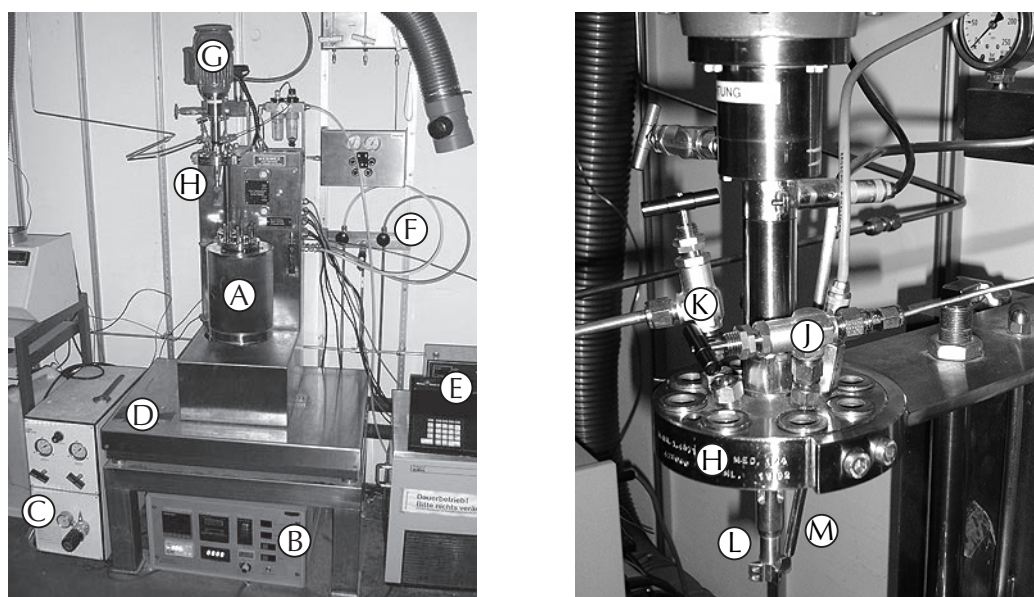


Figure 2-1: Batch reactor for PC synthesis. The reactor (A) is shown in the middle of the left picture, the controller unit (B) of the reactor (stirring, temperature, pressure) is standing on the floor. The CO₂ compressor (C) is on the left side of the balance table (D), the balance controller (E) and the cooling water connections (F) are on the right. The stirrer motor (G) is placed on top of the reactor. On the right picture, the reactor cover (H) equipped with in- (J) and outlet (K) valves and the stirrer (L) is shown. The tubing next to the stirrer below the cover is the thermocouple (M).

Liquid CO₂ from a cylinder with plunge pipe (Pangas 99.995%) was compressed by the help of a compressor (NWA PM-101). The whole reactor system was placed on a balance (Mettler Toledo IP5 Multirange) to measure the amount of used CO₂, which was filled into the reactor via the inlet valve.

Safety note: The experiments described in this work involve the use of high pressure and require equipment with an appropriate pressure rating. Due to the use of PO sufficient ventilation is required.

2.1.2 Procedure of the Insertion Reaction

Typically, PO, the corresponding catalyst and, if required, co-catalyst were weighted and poured into the reactor. Then the reactor was once flushed with CO₂. A certain quantity of CO₂ was pressed into the reactor, followed by heating and stirring of the reaction mixture. The stirring rate was always 1000 min⁻¹. After a certain reaction time the reactor was cooled down to ambient temperature, and CO₂ was released by opening the outlet valve. This decompression was done very slowly over a 30 min period.

2.1.3 Analysis

The compounds were analyzed by a gas chromatograph (Hewlett Packard, HP-6890) equipped with a capillary column (Valcobond VB-FFAP, 30 m × 0.32 mm × 0.25 μm) and a flame ionization detector (FID). First, 1 ml of *tert*-butylbenzene was added as internal standard to the reaction mixture and then 40 μl of this dilution was dissolved in 1.2 ml diethylether in a vial. Finally, 0.5 μl of the resulting solution was injected on-column at an inlet temperature of 32 °C. The initial oven temperature was 35 °C for 5 min, then the oven was heated to 220 °C at a ramp of 15 K min⁻¹ and held constant for 15 min.

Products were identified by gas chromatography (Hewlett Packard, HP-6890) coupled with mass selective detection (Hewlett Packard, HP-5973) and reference chemicals. As co-products only propylene glycol and dipropylene glycols were found. For quantitative analysis, a calibration curve was recorded to calculate the compound ratio from the measured peak areas.

2.1.4 Evaluation

The conversion X was calculated as the ratio of all products and the amount of PO charged (Equation 2-1), whereas the yield Y is the ratio of formed PC and

initial amount of PO (Equation 2-2). The ratio of Y and X is the selectivity S of PC (Equation 2-3). In each equation n represents the amount in terms of mol.

$$X = \frac{\sum n_k}{n_{PO}} \quad (2-1)$$

$$Y = \frac{n_{PC}}{n_{PO}} \quad (2-2)$$

$$S = \frac{Y_{PC}}{X_{PO}} \quad (2-3)$$

The turnover number TON was calculated to quantify the activity of a catalyst. It is defined as the amount of produced molecules per catalytically active center (Equation 2-4). Note that in this work each transition metal center was considered to be an active center (ac) unless otherwise noted. Therefore a 'real' TON would show higher numbers, but this definition is well-suited for the conclusions drawn in this thesis. The turnover frequency TOF in h^{-1} is the ratio of TON and the reaction time t in h (Equation 2-5).

$$TON = \frac{n_{PC}}{n_{ac}} \quad (2-4)$$

$$TOF = \frac{TON}{t} \quad (2-5)$$

2.2 X-ray Absorption Spectroscopy

2.2.1 XAS Under Demanding Conditions

As high pressure and temperature are usually required for reactions in and with CO₂, spectroscopic studies are more demanding than in conventional reactions. In heterogeneous catalysis often structural changes of the catalyst will influence its activity. Hence a deeper knowledge of these changes during the reaction is essential. For this purpose two spectroscopic batch reactor cells were designed and constructed to monitor the changes occurring in the bulk liquid and at the liquid/solid interface of heterogeneous catalyzed reactions at elevated pressure and temperature. *In situ* observations are also required to elucidate the reaction mechanism or a possible deactivation mechanism like leaching.

The penetration depth of X-rays through the solvent and through the window materials is critical at energies below 10 keV (see Table 2-1). At these low energies, beryllium or other light elements are required as window material. For this reason, *in situ* batch reactor cells with beryllium windows were constructed as described in the following paragraph.

Table 2-1: Thickness that leads to 25% absorption of X-rays.¹⁶

energy	beryllium 1.85 g cm ⁻³	quartz 2.65 g cm ⁻³	aluminum 2.70 g cm ⁻³	CO ₂ 0.7 g cm ⁻³
7.0 keV	1.10 mm	21 μm	15 μm	0.3 mm
10.0 keV	3.5 mm	61 μm	43 μm	0.9 mm
20.0 keV	>10 mm	500 μm	350 μm	8.4 mm

Note: The required path length through air to observe 25% absorption at 7.0 keV is more than 40 cm, even at 2.7 keV the path length is about 2 cm. 100 μm Kapton foil absorbs less than 5% at 7.0 keV.

2.2.2 *In Situ* XAS Batch Reactor Cell

The *in situ* batch reactor cell was designed in a way that it was possible to record XAS spectra of the liquid/solid interface at the cell's bottom (one pair of windows with 10 mm distance) and of the liquid phase with a path length of 15 mm (second pair of windows). These four windows of 5 mm × 1 mm size served to let the X-ray beam pass through the batch reactor cell at two positions (see X-ray path in Figure 2-2 and 2-3). The total volume of the spectroscopic cell is 10 ml and the cell withstands a pressure up to 250 bar and a temperature up to 200 °C. A teflon O-ring was used as sealing. The cell was heated by two 160 W cartridge heaters (SUVAG), which were built in at both sides of the *in situ* cell; the temperature was controlled using a commercial controller (PMA, KS 20-1 Omni Ray) and measured by a NiCr/Ni thermocouple in the cell's mantle. Further, the reactor is equipped with a magnetic stirrer and a cover containing an inlet and an outlet. For compact design, the motor with magnet was installed below the batch reactor cell.

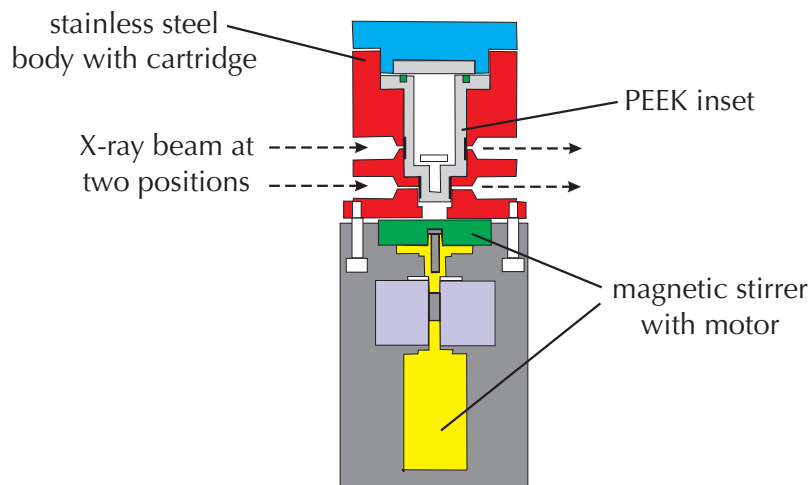


Figure 2-2: Batch reactor cell for *in situ* XAS experiments with PEEK inset, Be windows for two X-ray beam pathways and built-in stirrer/motor unit.

In the inner part a PEEK (polyetheretherketon, density 1.3 g cm^{-3}) container (Figure 2-2) was embedded, which has high chemical resistance and a high transparency for X-rays above 9 keV.¹⁵⁶ The bottom windows provided a path length of 4 mm and the upper windows were 10 mm above the bottom windows. In order to avoid any damages of the PEEK container at high pressure, 0.5 mm thick Be disks (Brushwellman, 7.8 mm diameter) were placed between the PEEK container and the windows of the *in situ* cell. Note that the PEEK polymer has a high tensile strength itself and therefore Be disks were even not necessary at temperatures below 150 °C. The cover was equipped with an additional thermocouple, which penetrated into the reaction volume, because the insulating PEEK container could influence the inside temperature. Furthermore, the reactor was connected to a valve, a burst plate (Swagelok, 190 bar), a pressure transducer (Wika), and the CO₂ supply system consisting of a compressor unit (NWA PM-101) and a flow controller (Rheonik, RHM015). With the latter, the amount of CO₂ filled into the batch reactor was measured, which requires a certain volume (>5 ml) so that dosing is accurate enough and stirring (mixing) is possible.

Additionally, a second batch cell was designed (Figure 2-3) without an embedded PEEK container, which allows a window distance at the bottom of 3 mm, so that spectra of higher quality than with the PEEK inlet can be obtained. For this purpose, a sequence of teflon, beryllium, and teflon disks was used to seal the reactor. This sequence of disks was pressed to the window by a hollow screw, that let the X-ray beam pass. To achieve the shortest possible path length, the bottom windows are slightly tilted with respect to the X-ray beam; in the side view both windows are mounted in 'V'-shape (see also Figure 2-3), which makes the construction of the batch cell rather complex. Due to the conical design of the lower part of the reactor volume, the path length could be minimized to 3 mm. The distance from the bottom to the upper windows is in this cell 13 mm. Because of the absence of a PEEK container, an additional thermocouple was not required.

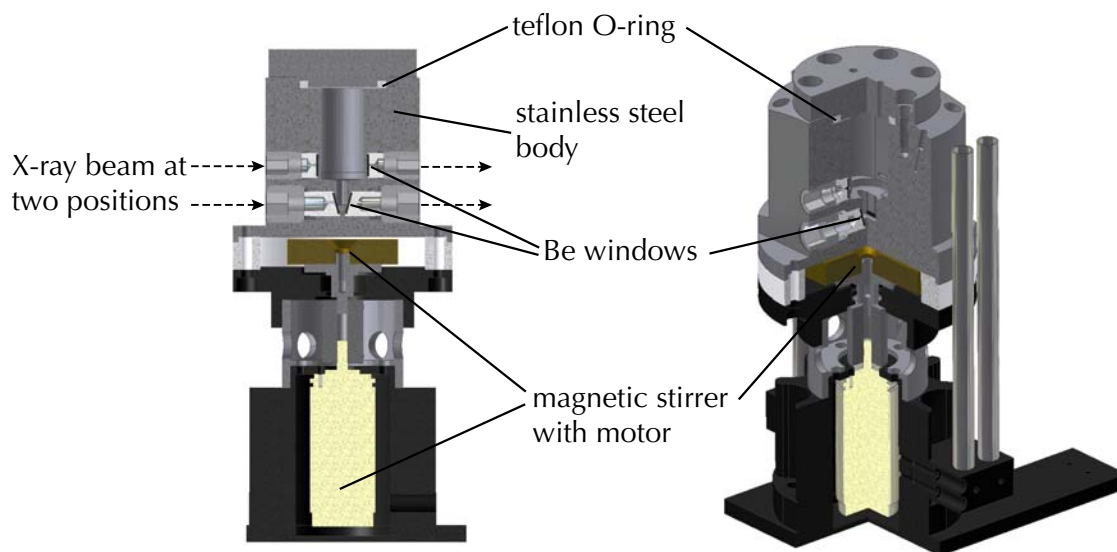


Figure 2-3: 3-dimensional views of the batch reactor cell with the built-in Be windows and two pathways to monitor the liquid/solid interface of heterogeneous catalysts and the liquid phase.

Another crucial point was the alignment of the cell in the X-ray beam. For this purpose, the entire cell was mounted on an x, z, θ -table shown in Figure 2-4. The apparatus can be moved between the two positions using the z -translation even during the XAS measurements by a remote controlled actuator.¹⁵⁷

2.2.3 Beamline Setup and Data Analysis

An overview of the XAS theory and principle technical requirements is given in paragraph 1.5. The experiments were performed at ESRF (Grenoble, France), HASYLAB (Hamburg, Germany) and at ANKA (Karlsruhe, Germany), for details of the synchrotron radiation see Table 2-2.

A typical beamline setup is shown in Figure 2-5. White X-ray radiation is provided by a positron or electron storage ring. The radiation occurs at bending magnets on insertion devices such as undulators, or wigglers, in which the positrons/electrons are accelerated perpendicular to the trajectory. The X-rays are focused by mirrors and cut to the desired size by different slits, which belong

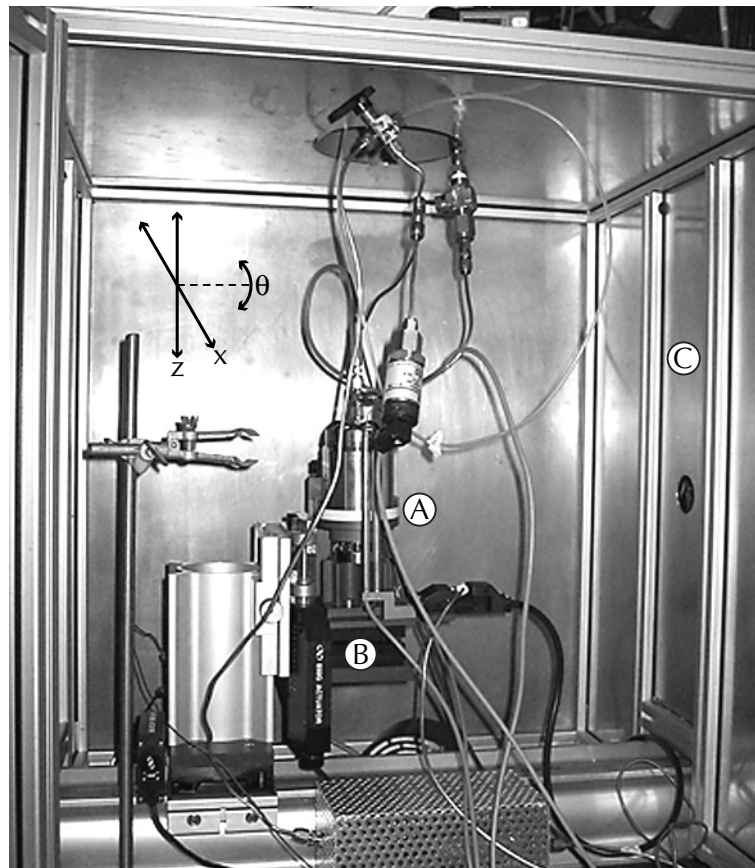


Figure 2-4: *In situ* XAS cell (A) placed on an x,z,θ -table (B). For safety reasons, a protection box (C) surrounded the experimental setup.

Table 2-2: Overview of the used synchrotron facilities.

facility	ring energy	beamline	source	monochromator
ANKA	2.5 GeV	XAS	bending magnet	double crystal
ESRF	6.0 GeV	BM1/SNBL	bending magnet	channel cut
HASYLAB	4.5 GeV	X1	bending magnet	double crystal

to the optical devices of the beamline. For monochromization of the X-rays monochromators such as double crystal or channel cut crystals are used. In both cases the incoming X-rays are scattered on a particular plane of a single crystal, like Si(111), Si(311), or Si(511), depending on the desired energy. Channel cut monochromators consists of two single crystals, which are attached together.

The X-ray beam is scattered from one crystal toward the other, and scattered again. Due to the Bragg condition, only X-rays of a particular energy can pass a second system of slits. Different energies can be chosen by different angles of the monochromator, which can be moved around a rotation axis. Channel cut monochromators are easier to install, but manufacturing errors will reduce the quality of the X-ray beam. Such errors can be corrected, when the two crystals can be moved independently of each other, but the implementation of the control equipment is much more sophisticated compared to a channel cut monochromator. Further optical devices including slits cut the X-ray beam to the desired size behind the monochromator. The intensity of the incoming beam is measured with a first ionization chamber, and after penetrating the sample with a second one. The difference of the X-ray beam intensity between the ionization chambers allows calculation of the absorption via Lambert-Beer's law. Simultaneously, a known reference can be measured with a third ionization chamber for energy calibration.

For *ex situ* experiments, the catalysts were pressed to pellets with polyethylene as additive or placed in thin quartz capillaries (Hilgenberg, 1.0 mm diameter, 20 μm thickness). The *in situ* experiments were accomplished in a batch reactor cell (see paragraph 2.2.2), in which a pellet of the catalysts without additives was placed at the bottom in an upright position. After taking the first spectrum, CO_2 was added and the next spectrum was recorded. CO_2 was removed and 3 ml of PO were filled in the cell. During continuous monitoring, CO_2 (7 g) was added again and the reactor was heated to 140 $^\circ\text{C}$. The raw data were energy calibrated (except for the *in situ* experiments with too low concentration), background-corrected and normalized using WINXAS 3.0 software.¹⁶⁷ After extraction of the $\chi(k)$ function from the EXAFS data (see also paragraph 1.5.3), Fourier-transformation was performed on the k^1 -weighted data in the interval $k = 3.5 - 14.0 \text{ \AA}^{-1}$. Data analysis in R -space was performed using Zn-Br and Zn-O/N shells calculated by FEFF 6.0.¹⁶⁸ Only the first coordination shells were used for the fittings. In contrast to the bond length ($\pm 0.02 \text{ \AA}$), determination of

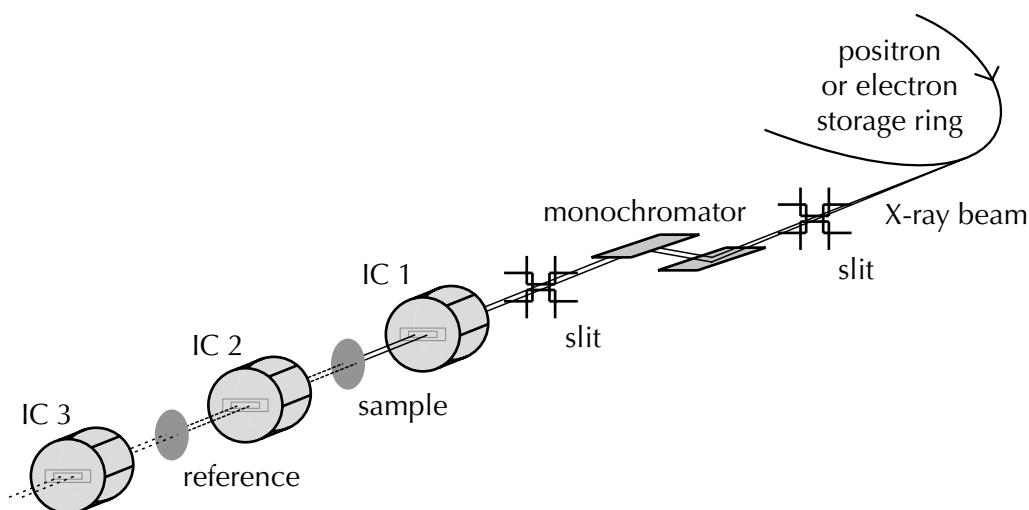


Figure 2-5: Typical beamline setup. White X-ray radiation is provided by a positron or electron storage ring. The X-ray beam is cut by different slits, which belong to the optical devices of the beamline. Only an X-ray beam of a defined energy can pass the monochromator (see text). Further optical devices (indicated by a slit) focus the X-ray beam again. The intensity of the incoming and transmitted beam is measured with ionization chamber IC 1, and after penetrating the sample with IC 2. Simultaneously, a known reference can be measured for energy calibration by comparison of the intensity of IC 2 and IC 3.

the coordination numbers is not as accurate, and deviations of ± 1 could appear (see also short introduction in EXAFS theory in paragraph 1.5.3).

2.3 Experimental Setup for Phase Behavior Studies

Spectroscopic measurements of the phase behavior were carried out in a stainless steel high-pressure view cell as depicted in Figure 2-6.^{169,170} This cell allows pressures up to 180 bar and temperatures up to 110 °C. The amount of CO₂ was measured with a flow controller (Rheonik, RHM015). The volume of the autoclave cell could be varied between 32 and 68 ml by a movable cylinder and was equipped with a magnetic stirrer. On the other site of this cylinder, a sapphire window allowed visual observation by a Nikon Coolpix digital camera. A

lamp connected with fiber optics through the movable cylinder was used to enlighten the autoclave. In addition, infrared spectroscopy could be used to probe the upper and lower part of the spectroscopic cell. At the upper part of the cell, transmission IR spectroscopy via ZnSe windows (diameter 8 mm, length 19.2 mm, path length 0.4 mm) was used. At the lowest point of the cell, the bottom was equipped with an IRE (ZnSe crystal, trapezoidal shape, angle of incidence 60° , length 27 mm, height 2 mm, depth 10 mm) for ATR-IR measurements (Figure 2-7). To record the IR spectra, the whole cell was installed in a spectrometer (Bruker IFS-66/S), typically accumulating 256 scans at a resolution of 4 cm^{-1} . The exact experimental conditions are described in Chapter 6.

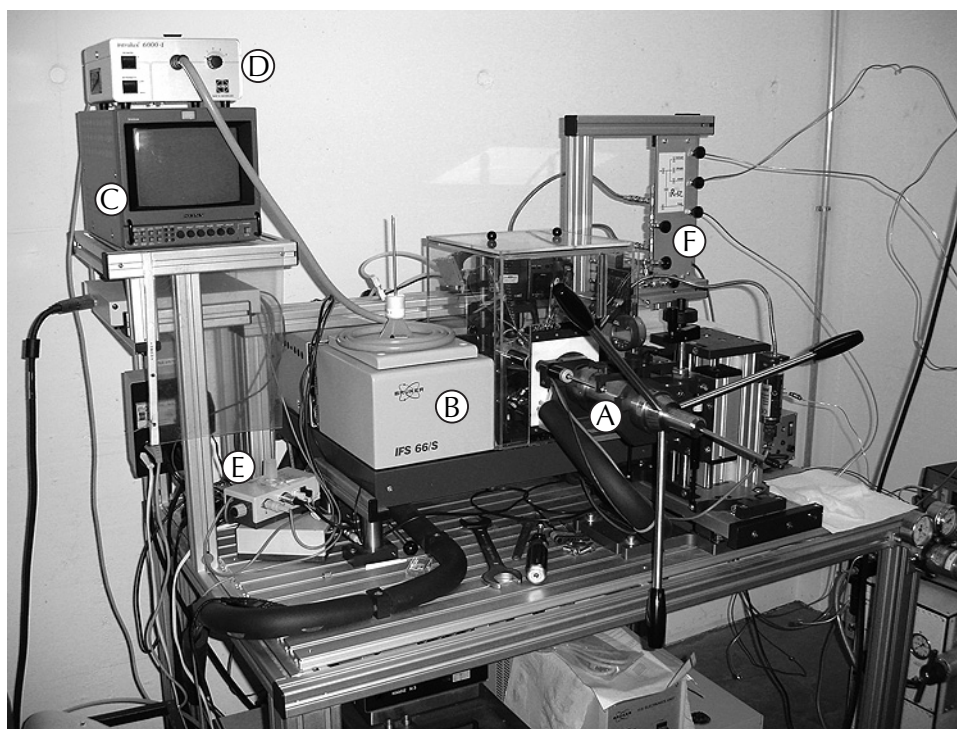


Figure 2-6: View cell (A) for phase behavior studies integrated in a Fourier transformed infrared spectrometer (B). The monitor (C) for visualization of the Nikon Coolpix images, the light source (D) for back side illumination, the stirring controller unit (E), and the gas in- and outlet system (F) are also shown.

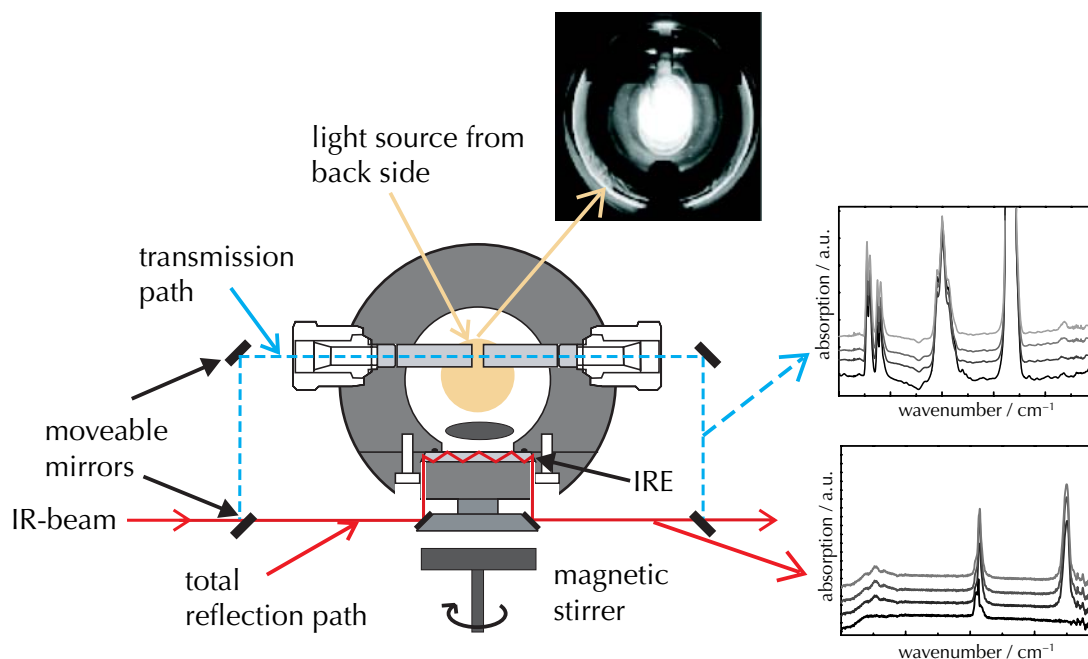


Figure 2-7: Front view of the spectroscopic cell for IR measurements. A set of mirrors allow to record IR spectra via the total reflection or the transmission path. In addition, a light source from back side in combination with a Nikon Coolpix digital camera enables visual observation.

2.4 Catalyst Characterization Methods

2.4.1 X-ray Photoelectron Spectroscopy

Surface analysis of the immobilized catalysts by XPS was performed on a Leybold Heraeus (LHS11 MCD) instrument using Mg K_{α} (1253.6 eV) radiation. The apparatus is described in detail in refs.^{171,172} The sample was pressed into a sample holder, evacuated in a load lock to 10^{-6} mbar and transferred to the analysis chamber (pressure $<10^{-9}$ mbar). The peaks were energy-shifted to the binding energy of the C(1s) peak to correct for the charging of the material. The surface composition of the catalysts was determined from the peak areas of C(1s), O(1s), N(1s), Si(2p), Cl(2p) and Cr(2p) which were computed after sub-

traction of the Shirley type background by empirically derived cross-section factors.¹⁷³ The relative error of the analysis was $\pm 5\%$.

2.4.2 Thermal Analysis

TA investigations were performed on a Netzsch STA 409. The samples were heated up to 800 °C in a gas stream of 20 vol% oxygen in helium. A quadrupole mass spectrometer (Balzers QMC 420) was used to detect the formation of CO₂ and water (traces $m/e = 44$ and 18, respectively). After heating, a known pulse of CO₂ was injected into the sample chamber to calibrate the area of the $m/e = 44$ signal. This calibration enabled calculation of the sample's carbon content. The mass losses of the samples were monitored during the measurements.

2.4.3 Further Analytical and Physicochemical Characterization

DRIFTS spectra were recorded at ambient temperature in a spectrometer (Bruker Equinox 55), accumulating 100 scans at a resolution of 4 cm⁻¹, the measured range was 4000 – 400 cm⁻¹. Solid samples were diluted in potassium bromide.

The chemical and structural properties of the catalysts were characterized by ¹H- and ¹³C-NMR, EA, and BET. The content of metal or halogen of the heterogeneous catalysts was measured by ICP-OES, performed by ALAB AG (Urdorf, Switzerland).

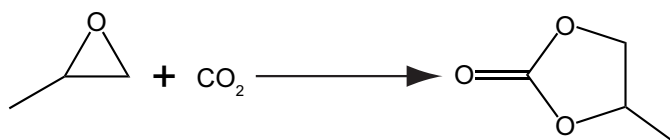
Chromium Salen Complexes: Bridging Homogeneous and Heterogeneous Catalysis

“The design of ... catalysts is feasible ... when the active site is situated at the extremity of the tether, and is free to flutter in the molecular breeze during the process of the catalytic conversion.” (Sir John Meurig Thomas)

Various homogeneous chromium salen complexes were synthesized and tested concerning their catalytic performance in the synthesis of PC from CO₂ and PO. The most active complexes were immobilized on a silica support and tested in the same reaction. Different immobilization methods were applied including anchoring of the complex through coordination with the metal, and covalent bonding via the ligand. Rates up to 300 mol_{PC} (mol_{Cr} h)⁻¹ at 98% selectivity were achieved with the heterogeneous catalysts without the use of any additional solvent or co-catalyst. The coordinatively bound complexes exhibited low stability and a very strong deactivation during reuse, whereas the correspondingly covalently bound complexes hardly showed any chromium leaching during catalyst recycling experiments. The catalysts were characterized by means of XPS, TA, ICP-OES and DRIFTS in as-prepared state and after use.

3.1 Introduction

Homogeneous chromium salen complexes were reported as active homogeneous catalysts for CO₂ fixation.^{43,94,174} Due to the use of chelate complexes with high complexation ability, the immobilization of these complexes represents an attractive strategy toward heterogeneous catalysts with improved stability. Different immobilization strategies have been reported in literature,¹³³ among them is coordination of the metal center to a modified support surface or covalently-bound inorganic complexes.



Scheme 3-1: Synthesis of PC from PO and CO₂.

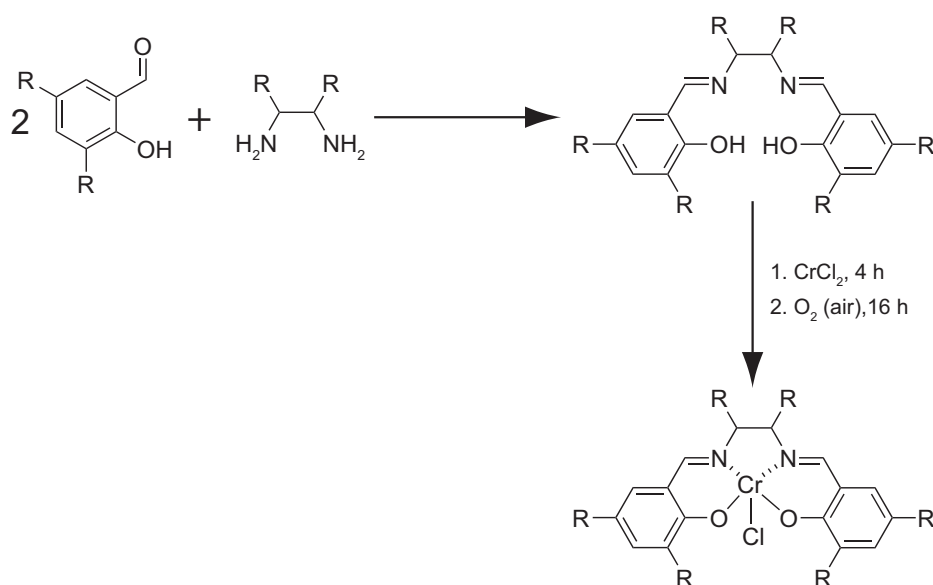
In this chapter, the focus was placed on heterogeneous catalytic synthesis of PC in a solventless process. In the first step, suitable homogeneous catalysts were searched that were also sufficiently active in the absence of co-solvents. By variation of the structure of salen ligands of the corresponding chromium salen complexes, the influence of these ligands on the catalytic behavior was investigated. In a further step, the most promising homogeneous complexes were grafted onto a silica support using different immobilization methods. Finally, the resulting heterogeneous catalysts were compared with respect to their catalytic performance and their re-usability.

3.2 Experimental Section

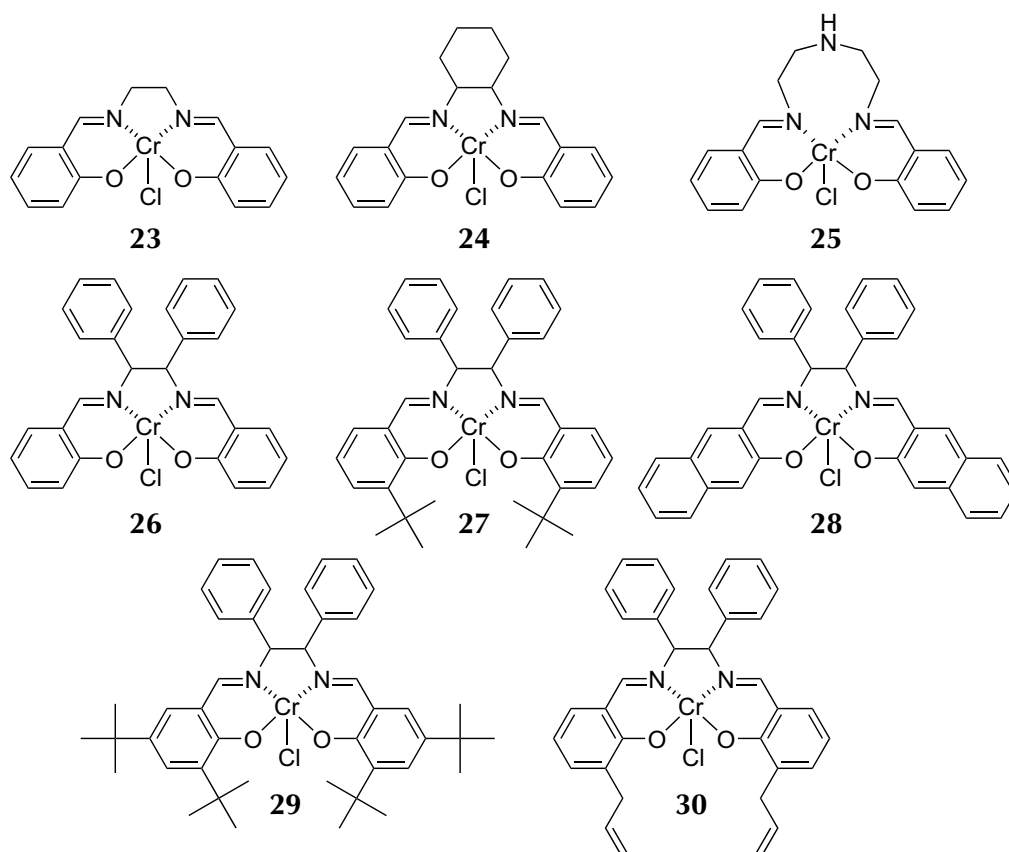
3.2.1 Syntheses of the Homogeneous Complexes

In general, the chemicals were used without any further purification, and the liquids were of spectroscopic grade. All products were analyzed by NMR and EA.

According to Scheme 3-2, the syntheses of the complexes **23** – **30** (Scheme 3-3) were performed similarly to literature.^{175,176} All reactants for the syntheses were commercially available except 3-allylsalicylaldehyde, an essential reactant of complex **30**. It was synthesized as described by Hwang et al.¹⁷⁷ The yield of the different supported complexes ranged from 42 to 86%. In the last step, chromium dichloride was added to the ligand and oxidized in the presence of air.



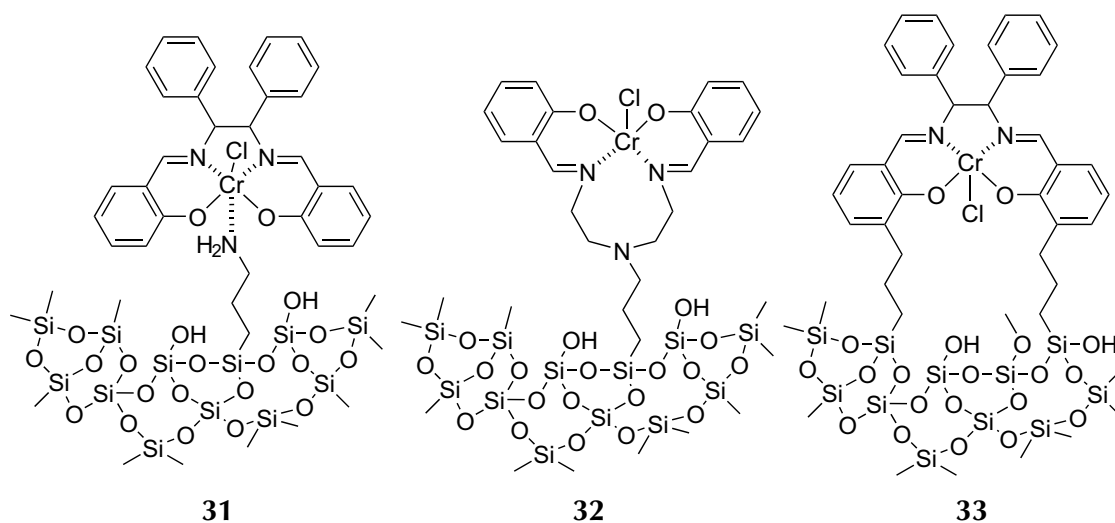
Scheme 3-2: General route applied for the synthesis of the different chromium salen complexes.



Scheme 3-3: Overview of the chromium salen complexes used in homogeneous catalysis.

Synthesis of 3-Allylsalicylaldehyde

Tributylamine (4.35 g, 80 mmol) and tin(IV) chloride (4.125 g, 20 mmol) were given to a solution of 2-allylphenol (25.05 g, 187 mmol) in toluene (500 ml). After stirring for 20 min at ambient temperature, paraformaldehyde (9.05 g, 0.4 mmol) was added. The mixture was heated to 100 °C for 8 h, then quenched in cold water (75 ml), and a pH 2 was adjusted with hydrochloric acid (2 N). The water phase was extracted three times with diethyl ether (20 ml), and finally the organic phases were united. After removal of the solvent, the remaining dark yellow oil was purified by chromatography (ethyl acetate : hexane = 1:9). Yield was 11.67 g (28% based on 2-allylphenol). For analytical data see paragraph C.1.1.



Scheme 3-4: Immobilized chromium salen complexes: **31** coordinated complex; **32** covalently-bound complex **25**; **33** covalently-bound complex **30**.

3.2.2 Syntheses of the Heterogeneous Catalysts

An overview of the immobilized catalysts is given in Scheme 3-4.

Synthesis of Catalyst **31**

a) Modification of the silica. Silica (16.0 g; Fluka Silica Gel 60; BET surface area, $460 \text{ m}^2 \text{ g}^{-1}$; mean pore size, 5.1 nm) was filled into a three-neck flask. Under argon, triethylamine (1 ml) in chloroform (100 ml) was given to the silica. After 30 min of stirring, 3-aminopropyltriethoxysilane (8.89 g, 40.2 mmol) in chloroform (100 ml) was slowly dropped to the suspension. Then the mixture was refluxed for 4 h at $60 \text{ }^\circ\text{C}$. The silica was cleansed in Soxhlet extractor with dichloromethane (200 ml) and dried under vacuum. Yield of the modified silica denoted in the following as ‘silica-NH₂’ was 17.36 g.

b) Anchoring of the Cr salen complex. Dichloromethane (50 ml) was added to silica-NH₂ (2.16 g) in a two-neck flask under argon. After addition of complex **26** (0.92 g, 1.8 mmol), the suspension was refluxed for 3 h at $40 \text{ }^\circ\text{C}$ and stirred overnight at ambient temperature. Yield was 2.48 g.

Synthesis of Catalyst 32

a) **Modification of the silica.** Under argon, triethylamine (1 ml) was added to silica (15.5 g) and toluene (150 ml) in a three-neck flask. Then 3-chloropropyltriethoxysilane (9.00 g, 37 mmol) in toluene (15 ml) was slowly dropped to the mixture. The slurry was heated for 4 h at 80 °C. Soxhlet extraction with a mixture of ether and dichloromethane (1:1, 200 ml) was carried out for 3 h. Yield was 20.64 g of white silica modified powder denoted 'silica-Cl'.

b) **Anchoring of the ligand via the aminopart.** In toluene dissolved *N,N'*-bis(2-hydroxybenzylidene)-3-aza-1,5-pentanediamine was dropped to a two-neck flask filled with silica-Cl (10.01 g) and toluene (180 ml). Thereafter, this mixture was refluxed for 8 h at 110 °C. The yellow silica material obtained was cleansed with Soxhlet extractor with dichloromethane (200 ml) for 3 h until the solvent was colorless. After drying under vacuum, ligand modified silica was obtained as a yellow powder (7.90 g).

c) **Complexation of the immobilized ligand.** Chromium(II) chloride (1.175 g, 9.61 mmol) was added to the immobilized ligand (7.00 g) in toluene (150 ml). The suspension was stirred for 4 h at ambient temperature under argon. Then the silica was transferred into Soxhlet extractor and washed for 2.5 h with dichloromethane (200 ml). The silica was filtrated and dried under vacuum. Yield was 7.21 g of a greenish brown powder.

Synthesis of Catalyst 33

Two different preparation routes were used to synthesize catalyst 33 depending on the sequence of the reaction steps.

a) **Variant 33a: Immobilization starting with the ligand.** *N,N'*-Bis(2-hydroxy-3-allylbenzylidene)-1,2-diphenylethylene-1,2-diamine (2.83 g, 5.65 mmol) was dissolved in a mixture of cyclohexane (10 ml) and toluene (10 ml). Then triethoxysilane (1.64 g, 10 mmol, 2 eq.) was added and the mixture was heated to 40 °C. Hexachloroplatinic acid was previously dried at 150 °C for 4 h, and

finally a spatula tip of hexachloroplatinic acid was dissolved in PC (20 ml). This catalytic solution was dropped to the reaction mixture at 40 °C. After 1 h of stirring, dried silica (10.9 g) was added, and the suspension was stirred overnight at ambient temperature. The silica was separated and washed with diethyl ether. 12.5 g of brownish silica was obtained. Secondly, chromium(II) chloride (0.75 g, 6.14 mmol) was added to a suspension of the modified silica (10.00 g) in tetrahydrofuran (100 ml). The suspension was stirred for 4 h at ambient temperature under argon. Finally, the silica was transferred into Soxhlet extractor and washed for 2 h with dichloromethane (200 ml). The silica was filtrated and dried under vacuum. Yield was 9.3 g of a green powder.

b) Variant 33b: Immobilization of the entire Cr complex. Firstly, complex 30 (3.0 g, 6.0 mmol) was dissolved in toluene (50 ml) and PC (2 ml). After heating to 40 °C, triethoxysilane (4 ml) was added, followed by a spatula tip of hexachloroplatinic acid. The solution became maroon colored. The mixture was stirred 4 h at 40 °C and after cooling down to ambient temperature, stirred overnight.

In parallel, dried silica (5.81 g) was suspended in purified toluene (75 ml) and activated with triethylamine (1 ml). After 1 h of stirring, the maroon-colored solution was dropped into the suspension with the help of a syringe. The mixture was stirred overnight. The yellow green catalyst was filtrated and washed with diethyl ether. Yield was 6.83 g.

3.3 Results and Discussion

3.3.1 Syntheses of the Free Complexes

The preparation of the salen ligands and the corresponding chromium complexes according to Scheme 3-2 was straightforward and thus, successful as described in the experimental section. Partly, the yields (42 – 86%) were

somewhat lower than expected but the main goal of this work was to obtain pure catalysts with reasonable effort. Hence intensive work-up of the complexes was omitted at this stage. NMR of the ligands and EA of the complexes confirmed the desired structure. Strong coordination of solvent molecules to the chromium center usually hampered the removal of these molecules by high vacuum, so the EA showed a slight difference in the calculated and measured values. This behavior is also reported in literature for similar compounds.⁹⁴

3.3.2 Catalytic Activity of the Homogeneous Catalysts

In a first step, the diamine part of the ligand was varied, and the most active component was aromatic diphenylethylene diamine (Scheme 3-3, catalyst **26**), but the catalytic activity toward PC in terms of the *TOF* of the other substituted diamines (catalysts **24** and **25**) was quite similar (150 h^{-1} vs. 170 h^{-1}). Note that for the calculation of the *TOF* it is assumed that all Cr-complexes were active. This is certainly a conservative estimate of the *TOF* since some of the complexes may not contribute to the reaction due to possible agglomeration or incomplete dissolution. The higher conversion using catalyst **26** could be due to the higher solubility of the aromatic rings in CO_2 .

Hence diphenylethylene diamine was used for further testing of the catalysts prepared from different hydroxybenzaldehydes. Alkyl chains in *ortho* position to the hydroxy group decreased the activity due to steric reasons (see Table 3-1), either by blocking the access to the active center or inhibiting the transition state. A condensed aromatic ring in *meta* position (catalyst **28**) halved the activity, alkyl chains in *ortho* position even decreased the activity to one-third of the non-substituted complex. Catalyst **29** showed no further drop in activity compared with that of catalyst **27**. So, additional substitution in *para* position had no negative effect on the activity of the complex. The most active catalyst prepared from hydroxybenzaldehyde was the catalyst derived from the unsubstituted hydroxybenzaldehyde itself.

Table 3-1: Catalytic activity of the different catalysts (Scheme 3-3 and 3-4) in the reaction of PO and CO₂.

catalyst	Y^a / %	TOF^b / h ⁻¹	PO / catalyst ratio
23	26.6	90	1000
24	47.3	150	1000
25	47.1	150	1000
26	62.0	170	900
27	17.9	60	1000
28	24.4	90	1100
29	18.4	60	1000
30	12.3	50	1100
31	41.0	330	2500
32	29.7	200	2000
33a	0.9	7	2400
33b	9.2	70	2400

^a) Reaction was carried out in 10 ml (140 mmol) of PO, catalyst, CO₂ (480 – 550 mmol, 3.4 – 3.9 eq.), reaction time was 3 h at 140 °C. Yield of PC was based on PO, the selectivity was always higher than 98%. ^b) Turnover frequency see paragraph 2.1.4.

The homogeneous chromium salen catalysts exhibited good catalytic performance reaching a TOF of 170 h⁻¹ at a conversion of 70% and a selectivity >98% in the cycloaddition of CO₂ to PO. It should be stressed that this performance has been achieved without any additional solvent or co-catalysts as applied in ref.^{43,94,174}, which has distinct advantages because the reactant can easily be separated from the product. The variation of the diamine compound (catalysts 23 – 26) had a strong influence in line with the results of Paddock and Nguyen,⁹⁴ although these authors used a Lewis-base and an additional solvent. The diphenyl compound exhibited also the highest activity in their experiments; however, the difference to the cyclohexane compound was much higher than the one of this work.

The choice of the benzaldehyde component was also important, though the substitution position seemed to have a stronger influence on the activity than the structure of the side chain itself. Substitution in *ortho* position of the hydroxy group (catalysts 27, 29, 30) hampered the reaction much more than a condensed aromatic ring in *meta* position (catalyst 28). The influence of a group in *ortho* position is much bigger than a corresponding substitution in *para* position, though the double-substituted catalyst 29 showed no additional decrease in activity compared with catalyst 27. Similar results were achieved by Lu et al. for cobalt salen complexes for the synthesis of ethylene carbonate in the presence of additional solvents.¹²⁵ The additional group in *para* position also lowered the activity in this study by 25%. A group in *ortho* position decreased the yield by 65% (catalyst 26 and 27). In conclusion, the impact of substitution seems to be more related to steric factors than to the solubility or the electronic properties of the different ligands. In contrast, Darensbourg et al. found an opposite effect for the influence of groups on the phenolic ligand.¹⁷⁸ They used a different substrate and an additional co-catalyst, so the solubility of the salen complexes was probably more important than steric factors.

3.3.3 Syntheses and Characterization of the Immobilized Catalysts

Considering the results from the homogeneous catalysts, corresponding salen complexes were immobilized using different grafting methods (Scheme 3-4). Catalyst 31 was prepared by anchoring the metal to a modified silica surface by coordination of the Cr³⁺-center to an amine group. As there is no special requirement for the complex structure, the most active complex 26 was chosen. The modification of the silica surface by reaction with different ethoxysilanes is well-known in literature, and preliminary tests with ²⁹Si-NMR-measurements demonstrated the good feasibility of this synthesis. The NMR spectra showed mainly silicon bound by two oxygen atoms to the bulk silica (−58 ppm) and the rest by three oxygen atoms (−66 ppm). Single bound silicon was not found.

3.3.3 Syntheses and Characterization of the Immobilized Catalysts

Immobilization via the amino part of the salen ligand could be easiest achieved with complex **25** by modification of the amino group and using hydroxybenzaldehyde as an aldehyde component (see paragraph 3.2). This led to one covalent bond (catalyst **32**). In contrast, modification of the aldehyde part resulted in the immobilization via two covalent bonds on the silica surface (catalyst **33**). In this case, complex **30** was chosen, because the synthesis with a vinyl group in *ortho* position is less complex than the one in *para* position, and the interest in the heterogeneous catalysts was triggered by their stability.

For characterizing the immobilized catalysts, DRIFTS spectra were recorded (Figure 3-1). The bands of the C=N imine vibration appeared at 1636 and 1613 cm^{-1} for the immobilized ligand of catalyst **32** without chromium in accordance with literature.¹⁷⁵ After addition of the chromium, the signals were shifted to 1619 and 1598 cm^{-1} .¹²⁴ The intensive bands of catalyst **31** appeared at higher wavenumbers (1628 and 1602 cm^{-1}); the bands of catalysts **33a** and **33b** appeared at significantly lower wavenumbers. Catalyst **33b** showed bands at about 1620 and 1592 cm^{-1} , whereas catalyst **33a** only showed a very weak, but broad signal at 1630 cm^{-1} . This indicates a small total amount of C=N bonds and in addition, that both chromium salen complexes and uncomplexed ligands are present. Obviously, the structure of the salen complex was destroyed during the synthesis of the catalyst. Hence chromium was not coordinated to the grafted ligand. The spectra of catalysts **31**, **32** and **33b** showed all the typical shifted bands of the C=N group. Consequently, in this cases the chromium was well immobilized in an intact anchored complex. Additionally, with both catalysts **33a** and **33b** weak bands appeared between 1700 and 1670 cm^{-1} together with bands over 3000 cm^{-1} due to small amounts of residual vinyl side chains.

TA measurements were conducted to gain information on the ligand loading for the immobilized catalysts by determination of the carbonaceous compounds (Figure 3-2). Note that only the chromium-free immobilized ligands were examined to avoid contamination of the TA equipment. The sterically-demand-

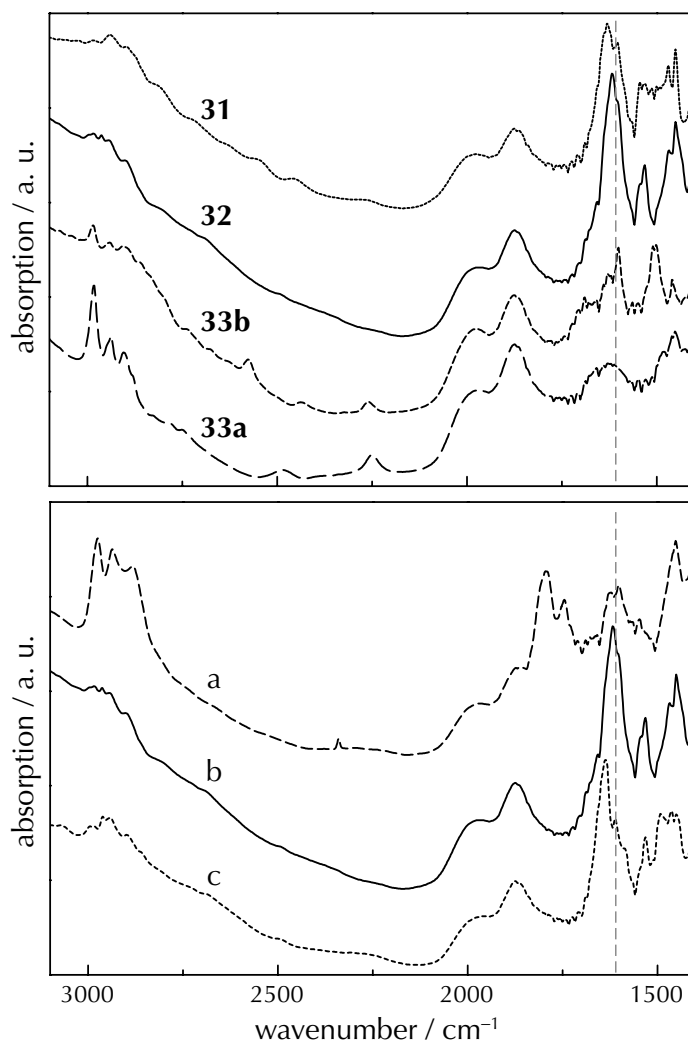


Figure 3-1: DRIFTS spectra of the immobilized catalysts (top). The labels of the catalysts correspond to those indicated in Scheme 3-4. Different states of catalyst **32** (bottom): a) after one reaction cycle; b) catalyst **32** as prepared; and c) immobilized salen ligand without chromium. The dotted line serves as a guide for the eyes for better comparability.

ing ligand of catalyst **33a** exhibited a carbon loading of 1.0 mg(C) g^{-1} . The combustion of carbon occurred in a narrow temperature range with a maximum at $478 \text{ }^\circ\text{C}$. This is typical for species that were placed on the same part of the surface. The small aminopropyl anchor of catalyst **31** decomposed in a broad temperature range with two different narrow maxima at 308 and $390 \text{ }^\circ\text{C}$. The loading (2.2 mg(C) g^{-1}) was higher than for the sterically-demanding

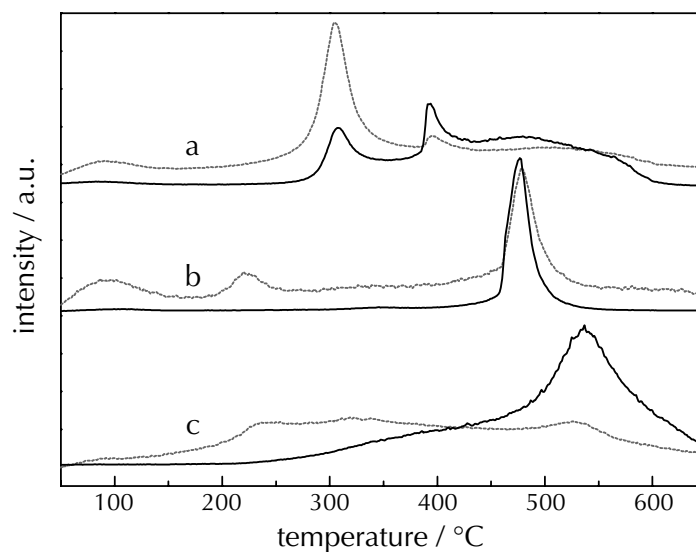


Figure 3-2: TA measurements of a) aminopropyl grafted on silica-precursor of catalyst **31**; b) immobilized ligand of catalyst **32** without chromium; c) grafted ligand of catalyst **33a** without chromium. The samples were heated in 20 vol% oxygen in helium. The solid black lines are the signal of $m/e = 44$, corresponding to CO_2 , the grey dotted lines are the signal of $m/e = 18$, due to water formation.

complex **33a** probably because the molecule is smaller and immobilization is sterically less hindered. Finally, the highest carbon loading of the silica surface exhibited complex **32** (3.1 mg(C) g^{-1}), due to the sum of immobilized complex **25** and 3-chloropropyltriethoxysilane. The curve of the mass loss of carbon as function of temperature looked like the superimposed curves of the former two experiments. This could be traced to the method of catalyst preparation. First, the silica surface was modified by grafting of 3-chloropropyltriethoxysilane. Then complex **25** reacted partly with the already immobilized precursor. Thus the results of the TA indicated that not all grafted precursors reacted with the salen complex.

The highest bulk chromium content (1.5%) quantified by ICP-OES was found for catalyst **32**. Catalyst **31** and the two variants of catalyst **33** exhibited similar metal content (about 0.6%). In contrast, the chromium surface concentration of catalyst **33a** determined by XPS (Table 3-2) was higher than the sur-

face concentration of catalyst **33b**. This supports the observation from IR measurements that in catalyst **33a** chromium was not found as Cr salen complex on the surface, because XPS is surface sensitive and thus more sensitive for uncomplexed chromium (in case of catalyst **33b** the bulky salen ligands can shield the chromium). XPS further showed that in catalyst **33a** both Cr and Cl are adsorbed on the surface. As expected, catalyst **31**—grafted on a silica surface with aminopropyl anchors—had the highest nitrogen content on the surface. Also catalyst **33a** exhibited a high nitrogen content, whereas the nitrogen content of catalyst **33b** was very low. This implied a higher ligand loading of catalyst **33a** compared with **33b**, but the ligands of catalyst **33a** did not coordinate to any chromium center.

Table 3-2: Surface analysis of the heterogeneous catalysts by XPS.

element / %	31	32	33a	33b
C (1s)	13.0	10.7	17.8	8.7
O (1s)	68.0	69.6	63.8	73.8
N (1s)	2.3	1.1	2.1	0.3
Si (2p)	14.8	15.7	13.3	16.3
Cl (2p)	0.5	1.2	1.4	0.2
Cr (2p)	1.4	1.7	1.7	0.8

3.3.4 Catalytic Activity of the Heterogeneous Catalysts

The activity in terms of *TOF* of the immobilized catalysts (**31**, **32**) for PC formation (Scheme 3-1) was higher than that of the free complexes. One reason for this behavior may be the site isolation of the immobilized complexes, whereas the complexes used as homogeneous catalysts may partly agglomerate during reaction. Note that also the concentration of the Cr-complexes in the reaction mixture was higher in case of the homogeneous catalysts (cf. Table 3-1). Homo-

geneous catalysts with comparable catalytic activity were reported in literature to be more active only in presence of additional solvents.⁹⁴

The simplest approach for anchoring the active complex to a support was applied for the preparation of catalyst **31**. The fresh catalyst showed a very high *TOF* of 330 h⁻¹. Also the activity of catalyst **32** is high in comparison to the homogeneous catalysts. Catalyst **33a** was nearly inactive, whereas the activity of catalyst **33b** prepared by a different procedure was higher by one order of magnitude. This is perfectly in line with the structural analysis of the complexes which showed that only in the procedure where the complete complex was grafted, the salen complex was intact in the resulting heterogeneous catalyst (catalyst **33b**). The catalytic activity of catalyst **33b** was lower than that of catalyst **32** due to its side chains in *ortho* position, as also observed for the homogeneous counterparts **30** and **25**.

In conclusion, both catalysts **32** and **33b** exhibited the same dependence on structural influences as the homogeneous ones and even the catalytic activity was comparable for the free and the grafted complexes. Hence the presented strategy to immobilize the most active salen complexes was a reasonable approach.

3.3.5 Reuse of the Heterogeneous Catalysts

An important criterion for heterogeneous catalysis is the reusability. Catalyst **31** showed a strong loss of activity (Figure 3-3). After one use, the yield dropped from 41 to 1.4%. Since one-third of the chromium content remained on the catalyst, not only leaching of the salen complex, but also deactivation of the remaining chromium species occurred. A similar deactivation of coordinatively-bound catalysts was observed for a styrene oxide system with additional solvent by Garcia et al.^{124,126}, but no leaching was reported in refs.^{179,180} In conclusion, anchoring via the Cr metal atom was not strong enough for the title reaction and led to leaching and ligand exchange. This may be traced back to the

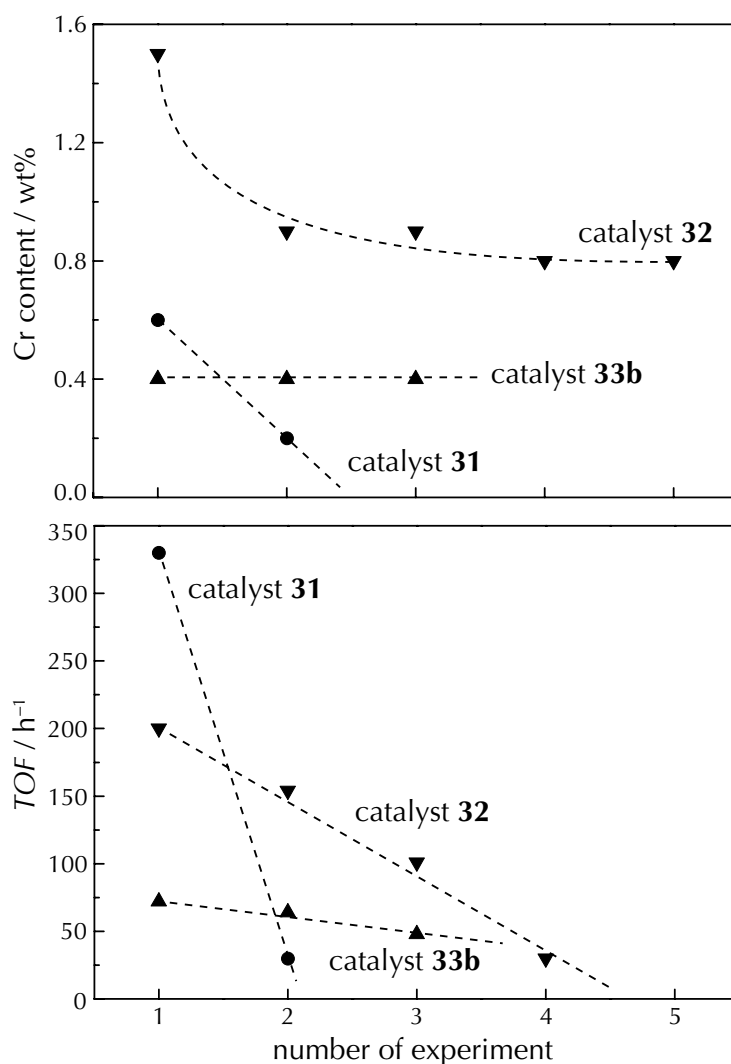


Figure 3-3: Chromium content (top) and catalytic activity (bottom) of the different immobilized catalysts (Scheme 3-4) after reuse in the synthesis of PC. (Activity is expressed as *TOF*.)

rather drastic conditions during the reaction or the strong propensity for complexation of PO and its derivatives. In summary, this simple approach is not suitable and the observed activity probably originates from homogeneous catalysis.

Significantly more stable were the covalently-bound catalysts **32** and **33b** (Figure 3-3). However, this required a compromise in the catalytic activity, since either the amine or benzaldehyde component had to be modified. A cer-

tain loss of the chromium content was observed for catalyst **32** after the first use. The high stability in subsequent runs indicates that this may have resulted from adsorbed chromium that was not removed at the work-up of the synthesis by washing under atmospheric conditions. Catalyst **32** was prepared step by step on the silica surface and finally the chromium chloride was added. This final step could have caused the high adsorption of chromium. In contrast no strong 'washing' effect was observed with catalyst **33b**. In the latter case the complete complex was grafted, the chromium content was stable over the whole time. The observed loss in activity of catalyst **33b** was less pronounced than that of catalyst **32**.

DRIFTS measurements of a used catalyst **32** showed decreased signals at 1622 and 1600 cm^{-1} (Figure 3-1). In accordance with the loss of chromium content the signals of the C=N vibration became weaker. This indicated that the entire complex and not only the chromium was washed out during reaction. Further, strong bands appeared in the DRIFTS of the used catalyst **32** at 2977, 2935 and 2883 cm^{-1} , and at 1794 and 1745 cm^{-1} , corresponding to the adsorbed PC species. Strong adsorption of PO and similar compounds was also reported by Uphade et al.¹⁸¹ Hence polymerization probably occurs as a side reaction during the cycloaddition of CO_2 to PO leading to some deactivation of the catalyst during reuse. This may also explain why the activity of both catalysts **32** and **33b** still decreased while hardly any leaching was observed. Thus, the decreasing *TOF* at stable chromium content was caused by blockage or disintegration of an active chromium center. Note that no deactivation was reported in literature for a related substrate, ethylene oxide,^{120,127} probably due to less pronounced adsorption on the silica support.

Therefore the use of modified silica or other supports which are less polar together with the immobilization strategies shown in this study, may lead to catalysts with improved stability for PC synthesis from PO and CO_2 .

3.4 Conclusions

A series of chromium salen complexes with different ligands has been synthesized and tested for CO₂ fixation in PO without additional solvents and co-catalysts. The structure of the salen ligand had a strong effect on the catalytic activity, whereas selectivity to PC was always high (>98%). The most active complexes were immobilized on silica by coordinative or covalent bonding.

The study demonstrates that only covalently-bound complexes exhibit reasonable stability under reaction conditions. Coordinated complexes are too weakly anchored during PO reaction with CO₂ under high pressure. No advantage of double tethered complexes compared with complexes anchored by single covalent bond was found. Instead, the structure of the ligand had a pronounced influence on the catalytic activity, similarly as observed with the corresponding homogeneous catalysts.

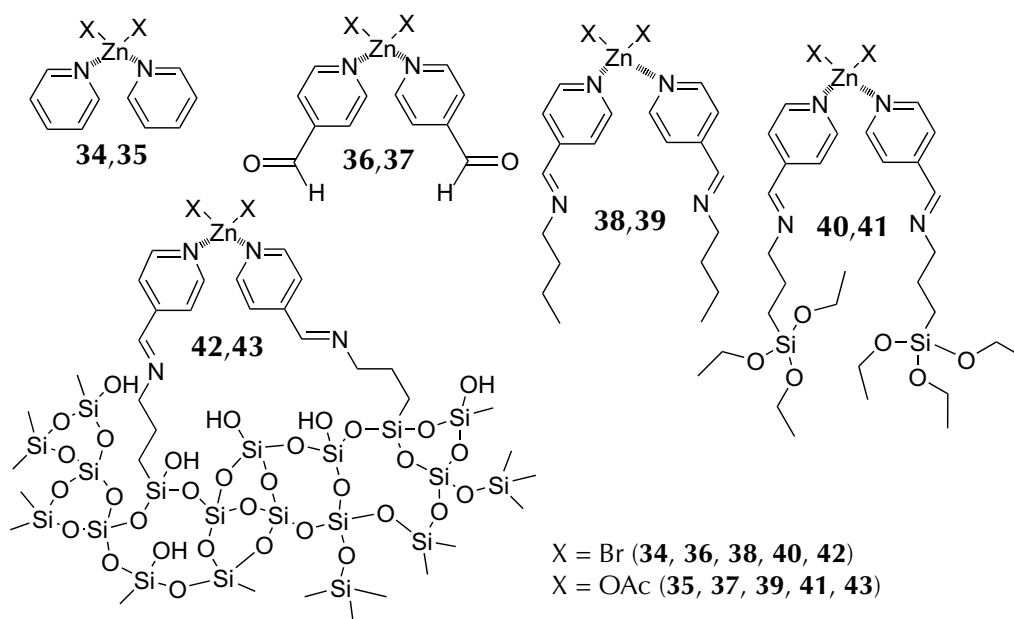
Behavior of Homogeneous and Immobilized Zinc-based Catalysts

Homogeneous and heterogeneous zinc-based catalysts were tested in the reaction of PO and CO₂ to PC without the use of additional solvents. For the preparation of the heterogeneous catalysts, the homogeneous zinc pyridine bromide and acetate complexes were modified for chemical anchoring on a silica surface. All intermediate stages of the series starting with the zinc pyridine based complex and ending with the anchored complex were catalytically tested and characterized. The immobilization process was monitored by DRIFTS which confirmed the successful fixation of the zinc pyridine bromide complex on the silica matrix. *TOF* >1100 h⁻¹ were obtained with the homogeneous zinc pyridine bromide-based catalysts and 330 h⁻¹ with the corresponding heterogeneous catalyst. Using acetate instead of bromide as a ligand significantly decreased the performance. The differences in activity could be traced to structural differences unraveled by X-ray absorption spectroscopy. For the heterogeneous catalysts, special attention was paid to the deactivation behavior and the reusability.

4.1 Introduction

The aim of the work described in this chapter was to investigate the performance of a catalyst step by step from a homogeneous catalyst to its immobilized coun-

terpart. For this purpose we started from simple and well-performing zinc pyridine bromide complexes,^{93,127} and immobilized them according to Scheme 4-1. The materials were tested for the fixation of CO₂ and characterized by EXAFS, TA, and ICP-OES. Special emphasis was laid on the immobilized catalyst with respect to structure, deactivation and reaction mechanism.



Scheme 4-1: Series of used zinc complexes. (Complexes designated by an odd number X = Br, complexes designated by an even number X = acetate.)

4.2 Experimental Section

4.2.1 Materials

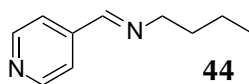
The synthesis of the complexes summarized in Scheme 4-1 involved the following materials: 3-aminopropyltriethoxysilane (99%), 4-pyridinecarboxaldehyde (98%), both purchased from Acros Organics, and silica as silica gel 60 from Fluka, all used as received. *n*-Butylamine (Acros), ethanol, pyridine, dichlo-

romethane, chloroform, and diethyl ether were of spectroscopic grade. Zinc bromide and acetate were purchased from ABCR and Acros, respectively.

4.2.2 Syntheses of Homogeneous Catalysts

Catalysts **34**, **35**, **36**, and **37** were prepared similarly as reported by Darenbourg et al.⁹⁰: To a suspension of zinc bromide (1.126 g, 5.0 mmol) in dichloromethane (40 ml) 2 eq. of pyridine (0.788 g, 10.0 mmol) or 4-pyridinecarboxaldehyde (1.070 g, 10.0 mmol) were added resulting in complex **34** and **36**, respectively. For the corresponding zinc acetate catalysts **35** and **37**, zinc acetate (917.4 mg, 0.005 mmol) was used instead of zinc bromide. The suspension was stirred overnight at ambient temperature, then the solution was concentrated and the white precipitate filtrated. The remained traces of pyridine were removed by heating the white crystals under vacuum.

Catalyst **38**, **39**, **40**, and **41** were prepared in the following manner: 4-Pyridinecarboxaldehyde (0.788 g, 10.0 mmol) was added to a solution of *n*-butylamine (0.731 g, 10.0 mmol) or 3-aminopropyltriethoxysilane (2.214 g; 10.0 mmol) in dichloromethane (20 ml). The spontaneously formed yellow imine **44** was stirred for 2 h at ambient temperature. Then zinc bromide (1.126 g, 5.0 mmol) was added and the reaction mixture was stirred overnight. Zinc acetate instead of zinc bromide was added for synthesis of catalysts **39** and **41**. Subsequent steps were as described earlier. See Appendix C for analytical data.



Scheme 4-2: This yellow imine **44** was used for the synthesis of catalysts **38** and **39** as well as reference compound for IR spectroscopy.

4.2.3 Syntheses of the Immobilized Catalysts

The immobilized catalysts **42** and **43** were synthesized by two different procedures, in one approach, the complete complex was synthesized before immobilization (catalysts **42a** and **43**).¹⁸² For this, silica (3 g) was added to a solution of complex **40** or **41** (2.5 mmol) in ethanol (40 ml). The suspension was stirred overnight, filtrated, and washed three times with ethanol, then three times with diethyl ether and finally dried under vacuum. A second approach (catalyst **42b**) began with the immobilization of the ligands, followed by the addition of zinc, as described previously.¹³³ The ligand was built up on the silica surface by immobilization of 3-aminopropyltriethoxysilane (4.43 g, 20.0 mmol) on silica (8 g), denoted by 'SiO₂-NH₂'. For this purpose, the ligand and the support were dissolved/suspended in chloroform (100 ml) and stirred for 20 h, and then the modified silica was filtered off and washed with ethanol. To a suspension of the modified silica (2 g) in ethanol (30 ml), catalyst **36** (1.4 mmol) was added and treated as described earlier. Only the first approach was used for the synthesis of catalyst **43** (starting from catalyst **41**) and the adsorption of catalyst **38** on silica. For analytical data, see also Appendix C.

4.2.4 Leaching Tests

For the leaching tests the heterogeneous catalyst **42** was separated from the reaction mixture by filtration and washed with diethyl ether, afterwards dried under vacuum. The used catalyst was applied as mentioned in paragraph 2.1.2. To detect the catalyst, which was dissolved in the liquid reaction phase, PO was added to the used and filtrated reaction mixture, which was analyzed before the reaction by gas chromatography and filled in the reactor without further addition of catalyst. Then the reaction was performed as the other catalytic reactions.

4.3 Results

4.3.1 General Catalyst Characterization

The preparation of complex **34** – **43** was checked in different steps of the synthesis. The chemical composition of complexes **34** and **36** was identified by accordance between the theoretical value and the results of the EA. The successful synthesis of the pyridine-based ligands for catalysts **38** – **41** was corroborated by $^1\text{H-NMR}$ and the measured values of the EA (see Appendix C). The reaction of aminopropyltriethoxysilane and, accordingly, of catalyst **41** with the -OH groups of the silica support to gain $\text{SiO}_2\text{-NH}_2$ or catalyst **43** was evidenced by the characteristic signals of the $(\text{SiO})_3\text{Si-CH}_2$ group (-67.25 ppm) and the $(\text{SiO})_2(\text{O-H/CH}_2)\text{Si-CH}_2$ group (-60.32 ppm) in the $^{29}\text{Si-NMR}$ -spectra (not given).

Both TA and ICP-OES were used to characterize the immobilized complexes (Table 4-1). For this purpose, catalysts **42** and **43** were compared with the 3-aminopropyltriethoxysilane-modified silica $\text{SiO}_2\text{-NH}_2$ and catalyst **38**. In TA all samples demonstrated a loss of water with a peak maximum at 90 °C. No CO_2 was detected at this temperature. Hence this water stemmed from adsorbed water, not from the combustion of immobilized organic compounds. Only traces of hydrocarbons were found, due to incomplete removal of solvents and chemicals after synthesis or to adsorption of hydrocarbons on the silica in the laboratory atmosphere. The water content is also given in Table 4-1. The carbon content of the immobilized 3-aminopropyltriethoxysilane alone on silica (intermediate step during synthesis of catalyst **42b**), was 2.6%. CO_2 was formed in two sharp temperature ranges with maxima at 305 and 393 °C (50 K width), and one broad signal from 360 to 600 °C. The first signal at 305 °C disappeared after the grafting of the pyridine zinc complex leading to sample **42**, and a new strong signal arose at 520 °C. The two sharp signals of the modified silica could originate from different positions of the immobilized aminopropyl group. One

of these anchors reacted with the zinc complex; the other may have been sterically hindered by its position on the silica. Catalyst **42a** demonstrated hydrocarbon combustion over a broader temperature range with maxima at 432 and 574 °C. No signal due to free aminopropyl groups was discernible at 390 °C. Both catalysts seem thermally rather stable. The higher combustion temperature of catalyst **42b** was caused by changes in the immobilized complex compared with catalyst **42a**. The same results as for catalyst **42a** were obtained for catalyst **43**, except that the second peak was shifted to lower temperatures because of the lower thermal stability of the acetate groups.

Table 4-1: Analytic results of the immobilized complexes measured by thermal analysis and ICP-OES.

catalyst	H ₂ O ^{a),b)} / %	C ^{a)} / %	Zn ^{e)} / %
SiO ₂ -NH ₂	0.9	2.6	–
38 ^{d)}	1.2	0.7	1.3
42a	1.8	1.4	1.5
42a ^{e)}	–	–	1.3
42b	0.7	3.9	1.8
42b ^{e)}	–	–	1.4
42b ^{f)}	–	–	1.3
43	1.2	4.7	3.2

^{a)} Measured by thermal analysis. ^{b)} Content of absorbed water. ^{c)} Results of ICP-OES. ^{d)} Adsorbed complex **38** on silica. ^{e)} After one use. ^{f)} After second use.

In contrast, catalyst **38** on silica exhibited combustion over a very broad temperature range, with a maximum at 465 °C, and the lowest carbon content of all samples. But the zinc content was too high compared with the measured carbon content. The covalently anchored complexes in catalysts **42** and **43** had a higher carbon content than the adsorbed complex in catalyst **38**. A favored coordina-

tion of zinc by hydroxyl groups of the silica could explain the higher zinc content. The hydroxyl groups on the silica surface were not blocked by a silylation reaction as occurred for the chemically bound complexes. The higher carbon content of catalysts **42b** compared with those synthesized by the first approach (catalysts **42a** and **43**) was likely due to the free aminopropyl groups on the silica surface.

4.3.2 Ex Situ X-ray Absorption Measurements

The XANES region of an X-ray absorption spectrum provides information on the first coordination shell of the excited atom, such as coordination geometry and the oxidation state. Additional structural information can be obtained by EXAFS spectroscopy.^{161,162} The post-edge region in the XAS can provide information on the bond length, coordination number, and nature of scattering atoms around the absorbing center.

The Br K-edge XANES spectra of the bromide-containing catalyst series (complex **34**, **40**, and **42**) (Figure 4-1) demonstrated no change in the near-edge region. Hence the local structure of the bromide remained similar during the immobilization series. This finding is supported by the fact that in the spectrum of dissolved KBr, the edge energy and the shape of the Br K-edge XANES changed. Small changes indicating a different local structure were seen at the Zn K-edge (Figure 4-2). In particular, the catalysts **36**, **40**, **42**, and **43** exhibited greater absorption at 9.668 keV than did catalysts **34** and **38**. The greatest absorption was seen for catalyst **43**, in which zinc is surrounded by 6 N/O atoms; this seems to lead to the whiteness and the additional feature at 9.668 keV. Ethoxy groups of the molecule or silanol groups of the silica surface could provide additional coordination via oxygen atoms for the catalysts **40** and **42**. Only a small feature at 9.668 keV and strong whiteness were seen for catalyst **36**, in which steric reasons hindered an inner molecular oxygen coordination of the zinc. In contrast to the bromide catalysts, a striking whiteness is missing for the

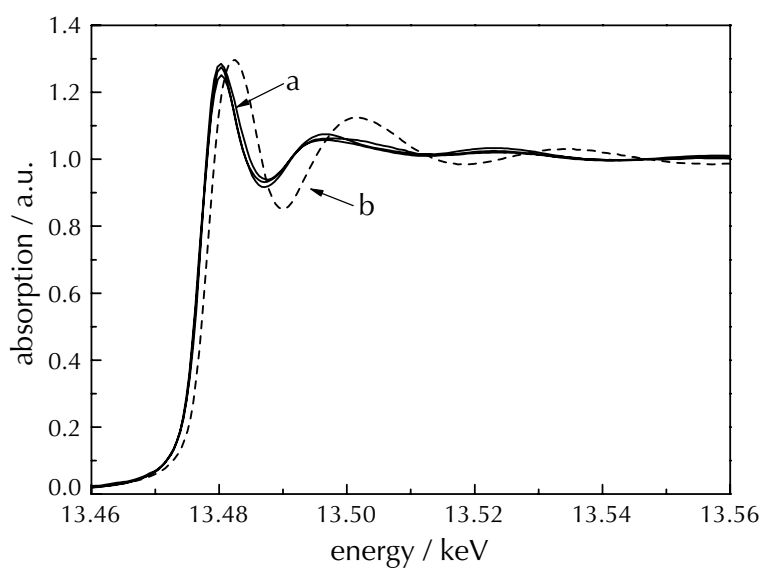


Figure 4-1: *Ex situ* XANES spectra at the Br K-edge. a) catalysts 34, 40, and 42. b) KBr as reference.

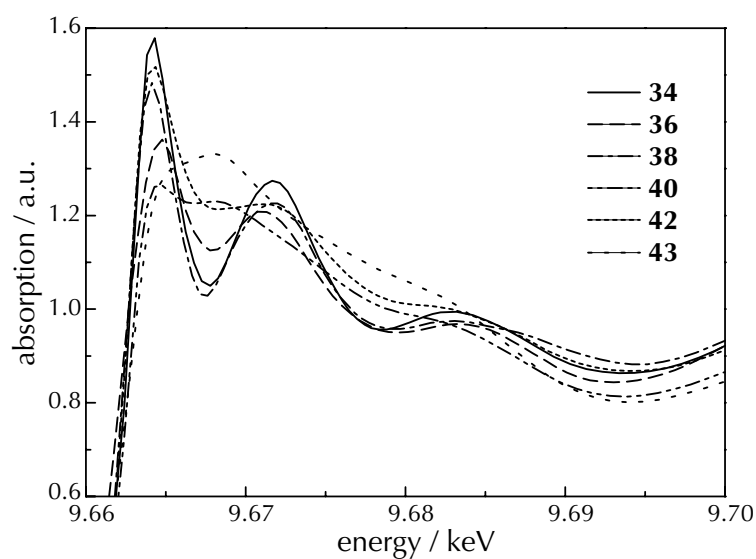


Figure 4-2: *Ex situ* XANES spectra of Zn-complexes 34, 36, 38, 40, 42, and 43 at the Zn K-edge. The labels of the catalysts correspond to those indicated in Scheme 4-1.

immobilized acetate complex **43**, possibly due to differing symmetries (tetrahedral vs. octahedral).¹⁸³

Figure 4-3 and 4-4 show the extracted Zn K-edge EXAFS functions and the corresponding Fourier-transformed k^1 -weighted EXAFS spectra at the Zn K-edge. The spectra of the zinc pyridine bromide catalysts **34**, **36**, **38**, **40** and **42** demonstrated contributions from both N and Br. Because of the similar back-scattering amplitude of N and O, one cannot differentiate between these two neighbors in the measurements. Zn–Br distances were identical with data for similar zinc pyridine bromide complexes obtained by X-ray crystallography,^{90,93} and the bond length was coincident in Fourier-transformed spectra of Zn and Br K-edge. The structural parameters are given in Table 4-2. Although it is significant that the ratio of the coordination number of the Br and N/O neighbors is >1.6 for the catalysts **34**, **36** and **38**, it is about one or even <1 for catalysts **40** and **42**. This finding can be explained by coordination of the zinc atom with oxygen atoms from the ethoxy groups of the molecule or the silanol groups of the surface. Striking differences were also found in the Fourier-transformed spectrum for complex **40** compared with **34** and **38**, indicating a greater number of oxygen and/or nitrogen neighbors. Complex **42a** demonstrated higher coordination by oxygen neighbors than **42b**. Note that by catalyst **42b**, the complex was immobilized by reaction with former installed molecules on the silica surface, and catalyst **42a** was an immobilized complex **40** exhibiting coordination of the zinc by ethoxy groups. It is possible that only one anchor was used for the immobilization and the free anchor was additionally coordinating the active center.

4.3.3 IR Studies for Structural Analysis

The additionally performed infrared spectroscopic studies proved also the successful immobilization (Figure 4-5). For comparison the catalyst **42** itself and three precursors (**38**, **40**, **44**) were measured (Scheme 4-1 and 4-2). The spectra

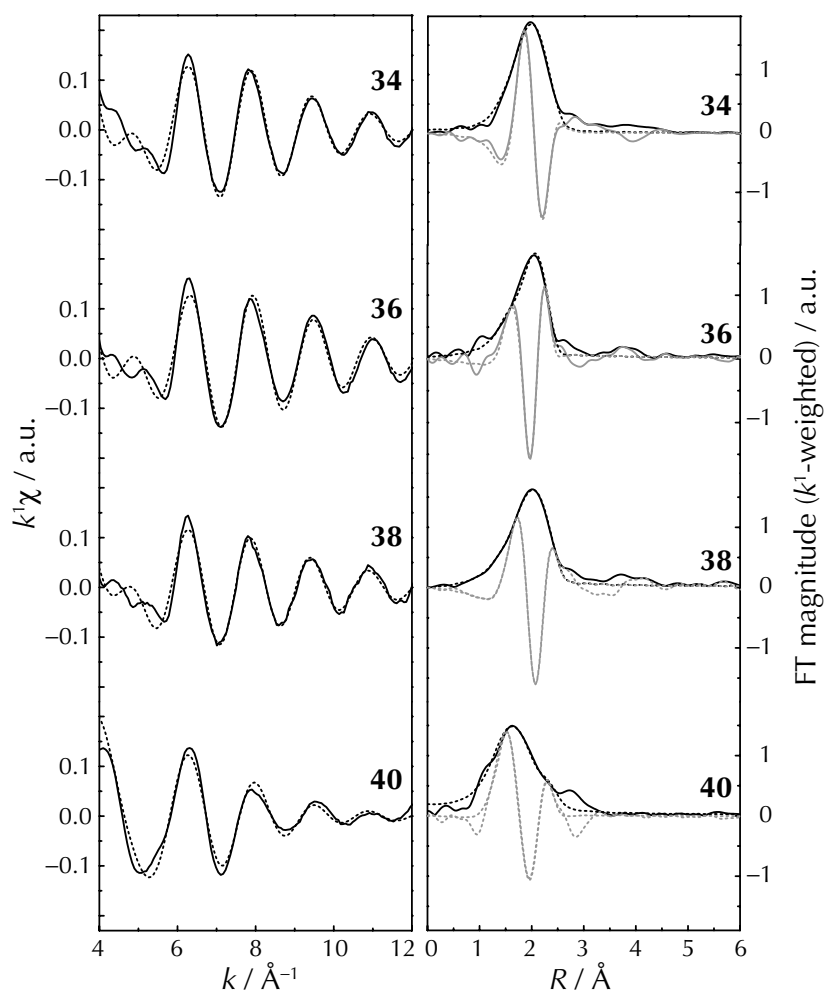


Figure 4-3: Experimental and fitted k^1 -weighted $\chi(k)$ functions and their Fourier-transforms of the different homogeneous complexes **34**, **36**, **38**, **40** at the Zn K-edge. Experimental data are shown by solid lines, the fitted data by dotted lines. Grey lines in the right part reflect the imaginary part of the Fourier-transform. The labels of the catalysts correspond to those indicated in Scheme 4-1.

of the free ligand **44** and of the zinc bromide complex **38** differ markedly in the range of $1750 - 1500 \text{ cm}^{-1}$ due to the additional zinc bromide coordinated to the ligand.¹⁸⁴ The signals at 1410 , 1379 , 1321 , and 816 cm^{-1} were shifted to 1424 , 1375 , 1318 , and 827 cm^{-1} . Further, a change at the end of the side chain from methyl (**38**) to a triethoxysilyl rest (**40**) of the zinc complex did not shift the bands at 1646 , 1617 , 1028 , 827 , and 648 cm^{-1} . In addition, very strong signals were found stemming from the ethoxysilane groups at 1165 , 1101 , 1074 ,

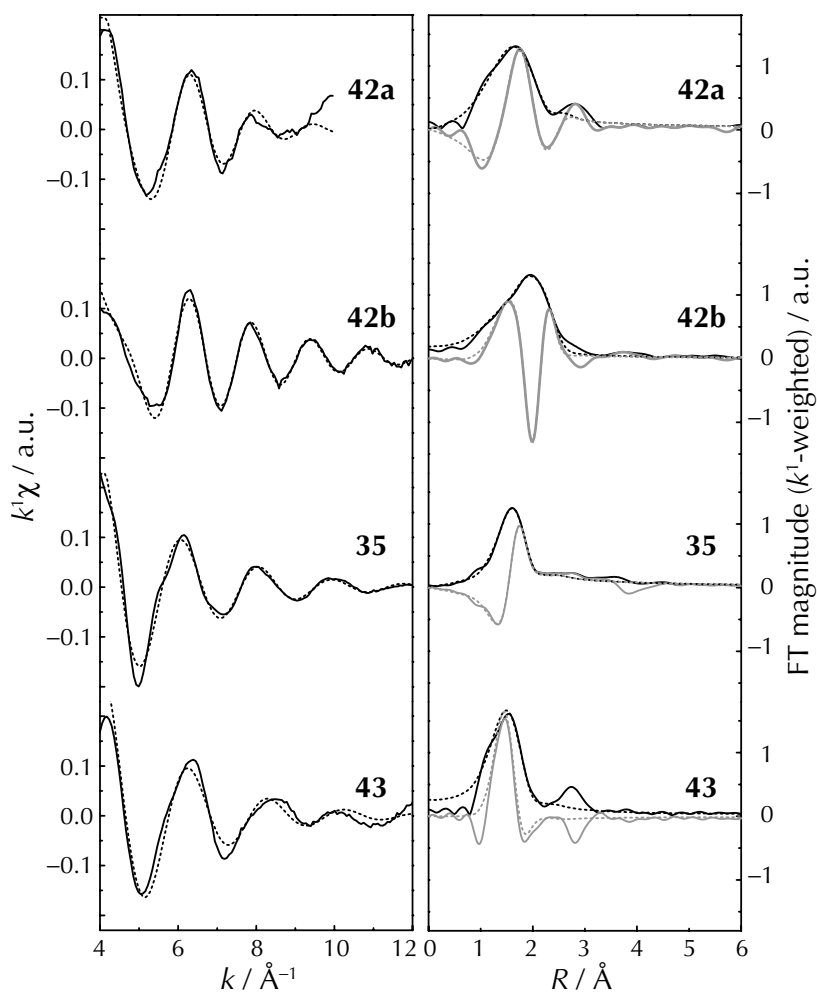


Figure 4-4: Comparison of experimental and fitted k^1 -weighted $\chi(k)$ functions and their Fourier-transforms of heterogeneous bromide and the acetate complexes (Zn K-edge). Experimental data are designated by solid lines, calculated by dotted lines. Grey lines in the right part are the imaginary part of the Fourier-transform. The numbers are corresponding to the catalysts shown in Scheme 4-1, **42a** is designated for catalyst **42** synthesized by the first variant (see paragraph 4.2.3), **42b** is catalyst **42** synthesized by the second variant.

955, 788, and 771 cm^{-1} . On the basis of these measurements, the XAS analysis and the spectrum of the immobilized catalyst **42**, it can be inferred that the complex kept its structural integrity upon immobilization.

Table 4-2: Structural parameters determined from the EXAFS spectra at the Zn K-edge and the Br K-edge.

cat.	$A^a-B^b)$	$r^c) / \text{\AA}$	$N^d)$	$\sigma^{2e}) / \text{\AA}$	$\Delta E_0^f) / \text{eV}$	residual $g)$	$k\text{-range} / \text{\AA}^{-1}$
34	Zn-Br	2.375	2.7	0.006	2.2	5.4	3.5 – 14.0
	Zn-N	1.985	1.6	0.001	-5.4		
35	Zn-N/O	1.998	3.6	0.006	3.8	1.8	3.5 – 14.0
36	Zn-Br	2.356	2.9	0.005	0.4	6.0	3.5 – 14.5
	Zn-N	1.970	1.8	0.003	-9.2		
	Br-Zn	2.347	1.2	0.005	-0.2		
38	Zn-Br	2.376	2.8	0.006	1.8	4.3	3.5 – 14.0
	Zn-N	1.997	1.7	0.004	-2.9		
40	Zn-Br	2.365	3.0	0.008	0.8	6.5	3.5 – 14.0
	Zn-N/O	1.971	3.4	0.007	5.2		
42a	Zn-Br	2.370	2.1	0.015	1.8	3.7	4.0 – 10.0
	Zn-N/O	1.950	3.2	0.019	-0.6		
42b	Zn-Br	2.377	2.7	0.005	-1.1	3.6	3.5 – 12.0
	Zn-N/O	1.985	2.5	0.003	-2.3		
	Br-Zn	2.375	1.7	0.006	0.9		
43	Zn-N/O	1.946	4.7	0.008	4.4	10.8	3.5 – 14.0

a) Absorber. b) Backscatterer. c) Distance. d) Coordination number. e) Dybye-Waller factor. f) Shift of the energy threshold. g) Quality of fit according to ref.¹⁶⁷

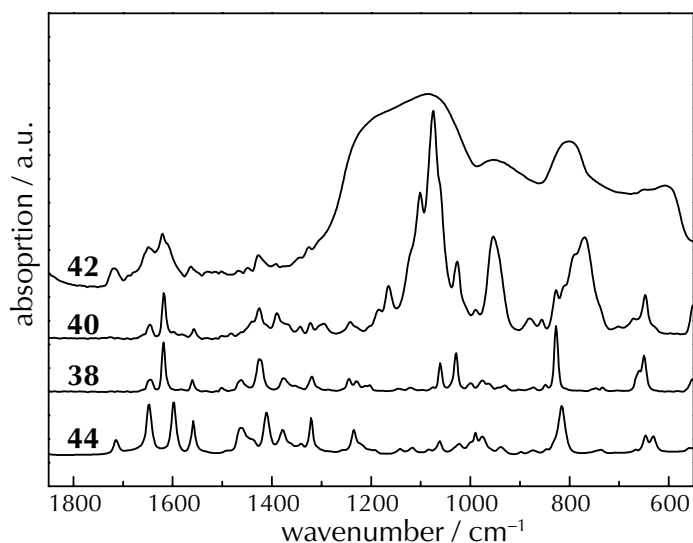


Figure 4-5: IR spectra of ligand 44, zinc bromide complex 38, zinc bromide complex with triethyl silyl groups 40, and immobilized catalyst 42 (see for the structures also Scheme 4-1 and Scheme 4-2).

4.3.4 Catalytic Performance in Carbon Dioxide Fixation

The catalytic results from the cycloaddition of CO₂ and PO to the homogeneous and heterogeneous catalysts are given in Table 4-3. The difference in activity between the pyridine complex 34 and the modified complex 38 is insignificant. Interestingly, the activity of catalysts 36 and 40 was significantly lower. Note that the coordination geometry determined by EXAFS for catalyst 40 was different; the coordination number for N/O neighbors was higher. Comparative reactions with the acetate complexes (high N/O coordination number and no bromide) also demonstrate the importance of bromide in this reaction. Lower rates were observed with the heterogeneous catalyst system 42. This may be due to mass transfer limitations, as discussed later.

The only by-products were propylene glycol and dipropylene glycols. These always appeared in similar (small) amounts. This results from the residual water in the batch reactor, because the addition of 73 mmol water decreased the selectivity from 99 to 71.8%. However, this also explains the very low selectivity with

Table 4-3: Catalytic results of zinc-based catalysts in the synthesis of PC.

catalyst	$Y^a) / \%$	$S^b) / \%$	TON	TOF / h^{-1}
34 ^{c)}	90.7	99.3	910	228
34	66.7	99.4	3376	1125
35	3.1	86.3	111	37
36	38.2	100.0	1972	657
37	1.3	56.1	46	15
38	62.5	99.5	3165	1055
39	5.6	88.2	200	67
40	42.3	98.5	1979	660
41	2.7	76.2	95	32
38 ^{d),e)}	1.4	57.7	39	13
42b ^{d)}	51.8	98.5	994	331
42a ^{d)}	18.9	98.2	597	199
43 ^{f)}	18.1	95.1	209	9
42b ^{d),g)}	31.9	99.7	862	287
42b ^{d),h)}	42.1	71.8	865	288

^{a)} Yield of PC based on PO; the reaction was carried out in 10 ml (140 mmol) of PO, catalyst (0.03 mmol, 0.0002 eq.), CO₂ (480–550 mmol, 3.4–3.9 eq.), reaction time was 3 h at 140 °C.

^{b)} Selectivity of PC. ^{c)} Catalyst (1.4 mmol, 0.001 eq.), reaction time 4 h. ^{d)} 250 mg of solid catalyst was used (0.08–0.15 mmol, 0.0006–0.001 eq.). ^{e)} Adsorbed on silica, the TOF is based on the mol of Zn.

^{f)} Reaction time 24 h. ^{g)} After one use. ^{h)} Unused catalyst with addition of 73 mmol water.

the adsorbed catalyst **38** on silica. The same experiment also illustrated that it is not sufficient to adsorb a homogeneous catalyst on a surface. Simple washing of the catalyst removed the active component. The low activity of the adsorbed catalyst could be explained by small amounts of complex **38** that remained adsorbed after preparation. After the first reaction, the reused catalyst exhibited no activity. The low rates in terms of TOF of catalyst **38** on silica was due to the

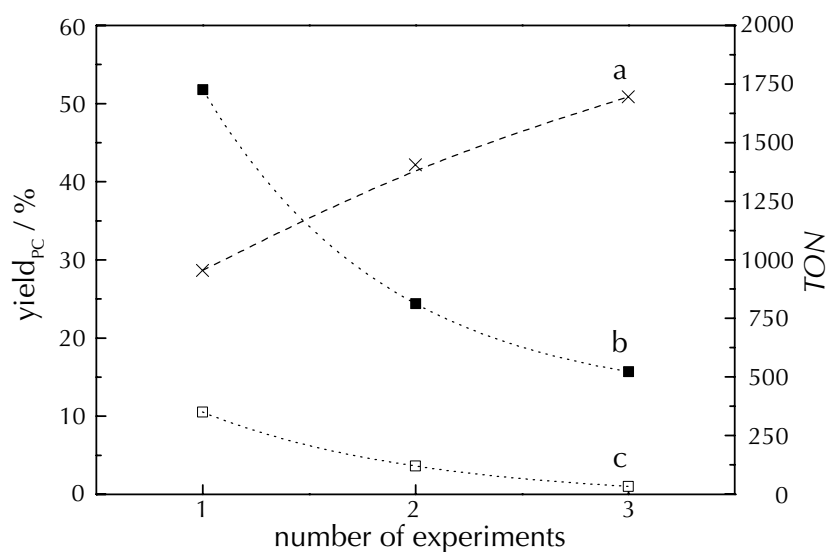


Figure 4-6: Deactivation experiments of catalyst **42b**. a) *TON* summarized over all recycle steps. b) Exponential decrease of the yield of PC by reuse of the solid catalyst. c) Yield of the leaching test. The test itself could not explain this behavior.^{185–187} After the first reuse, there is no active catalyst left in the liquid phase.

relatively high zinc content compared with the carbon and bromide content. The *TOF* was calculated with zinc considered an active component, and as discussed earlier (paragraph 4.3.1), the zinc on this catalyst was coordinated by hydroxyl groups of the silica support. Thus, this zinc was not catalytically active.

An important feature of heterogeneous catalysts is their long-time behavior during catalytic runs and, accordingly, their behavior toward deactivation during reuse. Therefore, emphasis was placed on studying leaching of the metal and/or ligand from the support. A simple way to gain insight into this issue is to reuse both solid and liquid phases.^{185,186}

Figure 4-6 shows that reuse of catalyst **42b** led to an exponential decrease in activity. Actually, after two repeats, the activity was comparable to that of the fresh catalyst **43** (Figure 4-6). Despite this deactivation, however, only low catalytic activity was detected in the liquid phase. This activity corresponds to a loss of about 4.5 μmol of active component in the first use; the second use saw a loss of about 1.5 μmol , calculated with the data of catalyst **40**. But this represents

<8% of the total amount of the active component and thus cannot explain the deactivation phenomenon. When the catalyst was reused a second time, the liquid phase exhibited no catalytic activity and thus no leaching of an active catalyst. The leaching of active catalyst from the support to the liquid in the first two uses could be explained by the removal of adsorbed species from the silica surface, because the reaction mixture itself is more 'aggressive' than the liquid used for washing the synthesized catalyst after preparation. Nevertheless, leaching of the active component could not explain the detected deactivation.

4.4 Discussion

4.4.1 Immobilization and Structure of the Catalysts

The different analytical methods confirmed successful immobilization of the zinc pyridine complex. The covalent fixation via the silylether groups was indicated by the ^{29}Si -NMR spectra. EA confirmed the composition of the homogeneous catalysts, and both ICP-OES and TA identified the constitution of the immobilized catalyst 42. There were no significant changes in the EXAFS spectra of the series toward the immobilized species. Fourier-transformed EXAFS spectra at the Br K- and the Zn K-edge, as well as fit results, indicated two different neighbors in the coordination sphere of the zinc atom with distances of 1.98 and 2.37 Å, respectively. The catalysts containing silylether or acetate groups 40, 42 and 43 exhibited a tendency toward higher coordination numbers. This may be due to an additional coordination of the oxygen, because XANES indicated a change in geometry and EXAFS revealed variation in the coordination number. Usually, a tetrahedral coordination of zinc would be expected; however, small ligands like water can lead to a change from a tetrahedral to an octahedral environment. In addition, the ratio of the peak areas of Br and N/O neighbors changed. For catalysts 34, 36 and 38, the bromide contribution

was dominant (Figure 4-3), but the ethoxy group containing catalyst **40** exhibited more pronounced N/O backscattering compared with the bromide. This finding was also seen for catalyst **42a**, which could be regarded as immobilized catalyst **40**. An equal signal contribution demonstrated catalyst **42b**. Here it was not possible to coordinate the zinc by the flexible ethoxy groups, because these groups were previously bound to the silica support. Only the remaining ethoxy groups, short free silanol groups of the surface or even free immobilized pyridine precursors, could coordinate to the zinc center. In the EXAFS spectra, no typical Zn–Zn contributions were found; however, Darensbourg⁹⁰ reported not only monomeric zinc pyridine bromide complexes, but also di- and trimeric species coupled by zinc bridges. Also DRIFTS measurements confirmed the successful immobilization of a zinc pyridine bromide complex on silica by comparison with its precursors. In summary, the complete series of catalysts from the homogeneous complexes **34**, **35** to the heterogeneous counterparts **42**, **43** could be prepared and the structure of the active center preserved.

4.4.2 Comparison of Homogeneous and Heterogeneous Catalysts

As discussed earlier, the strategy of modifying the pyridine step by step toward an immobilized complex proved successful. The catalytic data demonstrate that each intermediate was catalytically active. This indicates no significant change of the catalytically active center. It is the first time that the metamorphosis from a homogeneous toward a heterogeneous catalyst for PC formation was presented in all steps, which allows to compare the catalytic results and to study the effects of the immobilization process.

The selectivity of these catalysts to PC is high, reaching nearly 100%. The formation of trace amounts of polymeric materials, such as polypropylene oxide or polypropylene carbonate, cannot be ruled out. By-products detected in low quantities were propylene glycol and dipropylene glycol, which can be explained

by traces of water in the reactor, and in the ligand sphere of the catalyst or its surface.

The activity of the bromide-containing homogeneous catalyst series is high compared with that of other catalyst in this system.^{92,94,120,127,188} Figure 4-7 compares the catalytic data of selected catalysts of this work with those reported in previous studies. $TOF > 1000 \text{ h}^{-1}$ were obtained for catalysts **34** and **38**. The catalytic performance of catalysts **36** and **40** with TOF above 600 h^{-1} is high as well. Compared with the highest achieved TOF of 1125 h^{-1} for catalyst **34**, only very recently reported homogeneous salen complexes with co-catalysts are more active (Figure 4-7). Note, however, that the very active salen-based catalysts require co-solvents to reach their high performance; for example, Cr salen catalysts with dichloromethane as additional solvent yielded a TOF of 916 h^{-1} .⁹⁴ The same group also reported an improved system (TOF up to 1200 h^{-1}) through the use of Co complexes and DMAP as Lewis base in dichloromethane. This work aimed to develop a solventless process using CO_2 as both solvent and reactant. The catalytic activity of the homogeneous Zn-based catalysts of this work is also higher than that of comparable catalyst systems reported by Kim et al.^{92,93,127} One reason may be the higher reaction temperature in this study ($140 \text{ }^\circ\text{C}$ compared with $100 \text{ }^\circ\text{C}$). Kim enhanced the performance of these complexes by substituting at the *ortho* position of the pyridine ring and using iodide instead of bromide. Accordingly, the potential exists to design more powerful catalysts by varying the catalysts of this work. Note also that recently, a complex mixture of different metals and co-catalysts resulted in even higher rates.¹⁰⁰

Focusing on the immobilized catalysts, a three-fold decrease in activity is observed compared with the homogeneous counterparts. Nonetheless, catalyst **42b** is the most active heterogeneous catalyst for the fixation of CO_2 to PC (Figure 4-7), allowing a TON of >5000 . Moreover, the gap between homogeneous and heterogeneous catalysts is smaller than has been reported in literature up to now. He et al.¹²⁰ achieved related TOF with similar selectivity only

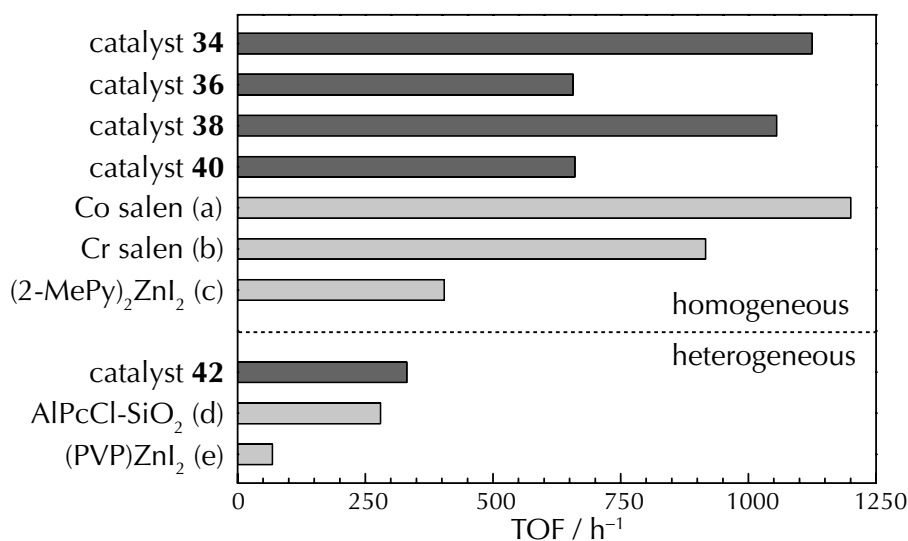


Figure 4-7: Comparison of catalysts in this work and other mono-metallic catalysts for the synthesis of PC by CO₂ fixation. Dark bars are designated to the catalysts of this work, the bright ones to examples of the literature. a) Co salen catalyst with DMAP as Lewis base co-catalyst and CH₂Cl₂ as additional solvent,¹⁸⁸ b) Cr salen catalysts in presence of CH₂Cl₂,⁹⁴ c) homogeneous zinc catalyst,⁹² d) aluminum phthalocyanine complex covalently bonded to MCM-41 silica with *n*-butylammonium bromide as co-catalyst,¹²⁰ e) PVP-supported zinc catalyst.¹²⁷

with an aluminum phthalocyanine complex covalently bonded to MCM-41 silica and *n*-butylammonium bromide as a co-catalyst. Until now, the best system without a co-catalyst was the resin-immobilized zinc iodide complex,¹²⁷ but an inorganic support would be more desirable for higher thermal and mechanical stability.

As outlined above, EXAFS found no difference in the coordination sphere for catalysts 34, 36 and 38, but catalyst 36 exhibited only half of the activity of the other two catalysts. The basicity of the ligands of these catalysts depends on possible electron-donating and withdrawing groups, and the strength of the Zn–N bond will decrease for the less-basic pyridine ligand.⁹³ The polarity of the complex is also important; this is significantly different for catalyst 36. The poorer performance of catalysts 40 and 42 compared with catalysts 34 and 38 can be explained by the greater coordination of the Zn with ethoxy or silanol groups.

The better catalytic performance of the homogeneous catalysts compared with their immobilized counterparts may be due to sterical constraints and decreased accessibility of the latter. Kim et al.⁹³ investigated the influence of additional pyridine and found decreased activity. They explained this effect as resulting from competition of the added pyridine and PO for coordination to the zinc center. Thus increased coordination of the active center decreased the catalytic activity of catalysts **40** and **42**.

Catalyst **42a** exhibited poorer performance than the immobilized catalyst **42b** which was synthesized by the second variant. The structural studies demonstrated a different structure, probably because complex **42a** was completely synthesized before immobilization (immobilized catalyst **40**). One of the anchor side chains caused an additional coordination by oxygen groups, which apparently decreased the activity of the complex.

Hence the structure of the active center needs to be as similar as possible to that of catalyst **34**. Consequently, the activity of the acetate containing catalysts **35**, **37**, **39**, **41** and **43** was poor compared with that of the bromide-containing catalysts. This finding underlines the important role of Br in the reaction and indicates that a higher coordination of zinc by oxygen atoms hampers the coordination of the PO to form an active species.

4.5 Conclusions

High rates during the addition of CO₂ to PO were obtained using homogeneous zinc pyridine bromide catalysts, even without additional solvents. By immobilizing of the active complex, this high activity was transferred to a heterogeneous catalyst, which also has high thermal stability because of the silica support. This work showed that structure and activity of all intermediate stages of the immobilization can be followed step by step by both spectroscopic measurements and catalytic results. Variations in the structure were unraveled by

XAS, and the change in catalytic activity could be related to a change in the coordination shell of the zinc and to the type of ligand in the catalyst.

Chapter 5

In Situ XAS Under High Pressure Conditions

“Not using in situ methods to examine catalytic processes is like studying a life with access only to the prenatal and postmortem states” (Gabor A. Somorjai)

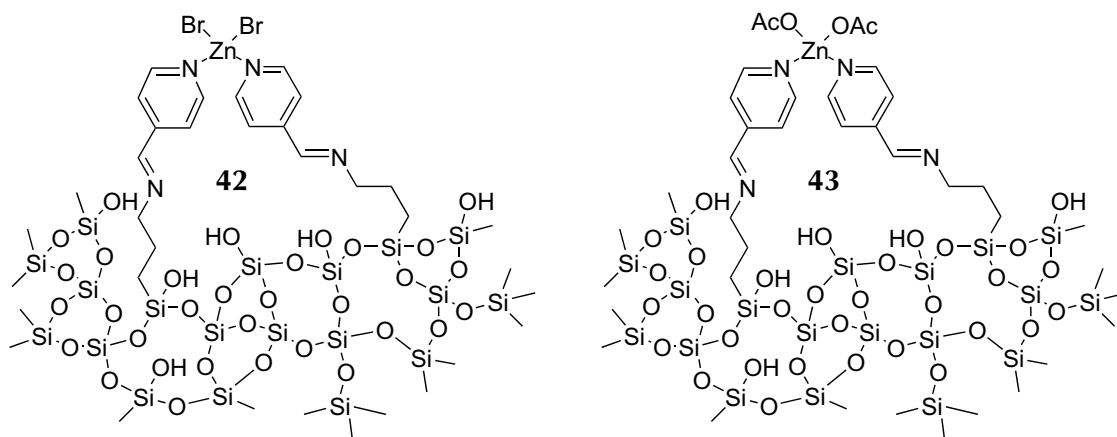
The structure of the catalysts was followed *in situ* by X-ray absorption spectroscopy using a specially designed batch reactor cell. This allowed to gain important information on the fate of zinc and bromide under reaction conditions and provided new insight in the reaction mechanism. Bromide is important for high reaction rates and due to the fact that it goes into solution under reaction conditions, catalyst deactivation is observed during reuse of the solid catalyst. ICP-OES measurements confirmed the results of the *in situ* XAS studies. As a consequence, it was possible to maintain the catalytic activity by addition of bromide as co-catalyst and its role is probably the nucleophilic attack of the epoxide.

In a further going case study, the batch reactor cell for *in situ* XAS measurements was also tested at lower X-ray energies with different nickel-based catalysts. Also in this study, a structure/activity relationship was observed and the halogen left the nickel-complex during reaction.

5.1 Introduction

As reported in Chapter 4, immobilized zinc pyridine complexes exhibited a high catalytic activity in the synthesis of PC from PO and CO₂. However, deactivation occurred, which could not be explained by leaching of the zinc or the entire complex. In structural studies of the transition state it was claimed, that PO was inserted between zinc and pyridine.^{92,93,104,113,127} The bromide played in these *ex situ* studies no role.

Hence element sensitive *in situ* studies were required to uncover the deactivation mechanism. For this purpose, XAS spectroscopy was chosen, because it can be performed at high pressure and information can be gained on the neighboring atoms, the coordination sphere and the oxidation state (see also paragraph 1.5.3).



Scheme 5-1: The two different immobilized zinc-based catalysts.

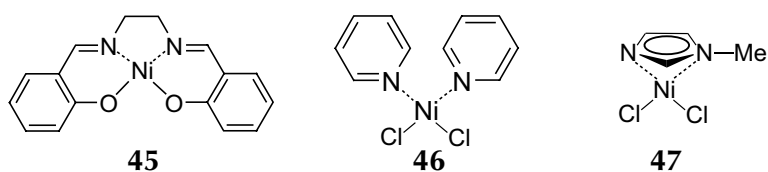
5.2 Experimental Section

The catalysts 42 and 43 (shown in Scheme 5-1) were synthesized according to paragraph 4.2.3. The *in situ* XAS setup has been reported in paragraph 2.2.2. Experiments at the Zn K-edge and the Br K-edge were performed both in the

batch reactor cell with PEEK inlet (Figure 2-2) and in the cell without (Figure 2-3); the spectra of the nickel catalysts were recorded using the batch reactor cell without PEEK inlet, because of the lower energy of the Ni K-edge, see also paragraph 2.2.1.

5.2.1 Syntheses of the Nickel Complexes

An overview of the different Ni catalysts is given in Scheme 5-2.



Scheme 5-2: Overview of the different Ni catalysts.

Synthesis of Complex 45

a) **SalenH₂ complex.** Salicylaldehyde (6.05 g, 49.5 mmol) was dissolved in toluene (100 ml), then ethylene diamine (1.2 g, 20 mmol) in toluene was added. The mixture was refluxed at 120 °C for 4 h, and cooled down to ambient temperature overnight without stirring. The yellow crystals were filtrated, washed with dichloromethane, and dried under vacuum. Yield was 4.3 g (81%).

b) **Nickel salen complex.** Nickel dichloride hexahydrate (0.71 g, 3.0 mmol) was added to a solution of salenH₂ (0.80 g, 3.0 mmol) in ethanol. The orange precipitate was filtrated and recrystallized in ethanol. After drying under vacuum, the nickel salen complex 45 was obtained as an orange powder (0.83 g, 83%).

Synthesis of Complex 46

Pyridine (0.7 g, 8.9 mmol, in 2.5 ml ethanol) was slowly added to a solution of nickel dichloride hexahydrate (1.8 g, 7.4 mmol) in ethanol (10 ml). The crystals

were filtrated, washed in a mixture of pyridine and ethanol (1:9), and dried under vacuum. Yield was 1.2 g (58%).

Synthesis of Complex 47

Nickel dichloride hexahydrate (0.71 g, 3.0 mmol) was dissolved in ethanol (20 ml), then 1-methylimidazole (0.33 g, 4.0 mmol) was added. The mixture was stirred for 30 min, then the solvent was evaporated. Afterwards, the yellow residue was washed with acetone and ethanol, and dried under vacuum. Yield was 0.45 g (70%).

5.3 Results

5.3.1 *In Situ* X-ray Absorption Measurements

To understand the catalyst structure in more detail under reaction conditions, the catalyst was monitored *in situ* with XANES and EXAFS spectroscopy. For this purpose a batch reactor with two Be windows (as described in paragraph 2.2.2) was applied. The lower window was directly over the bottom of the reactor, and the solid catalyst was analyzed. The spectrum of the liquid phase was measured through the upper window. To avoid a possible suspension of the solid catalyst in the liquid phase, stirring was stopped during measurements.

The XANES spectra at the Zn K-edge changed dramatically in a nonreversible manner after PO was added (Figure 5-1). Interestingly, the structural changes with PO were similar regardless of whether or not CO₂ was present. Merely the addition of PO changed the XANES spectra in a way to be more similar to the spectra of the bromide free acetate complex (compare Figure 5-1 with Figure 4-2). No change in the spectrum itself could be seen at the Br K-edge, but the edge jump decreased and the signal became increasingly noisy during the reaction (Figure 5-2). Also during the reaction, X-ray absorption spectra

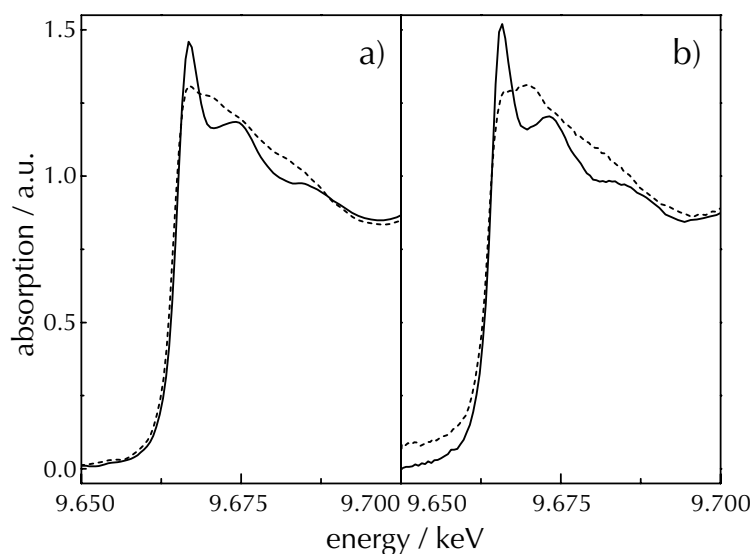


Figure 5-1: *In situ* XANES spectra of catalyst 42 at the Zn K-edge. A striking change appeared after the addition of PO (dashed lines), a) without CO₂, b) with CO₂.

were recorded for both the liquid phase and the solid catalyst. No absorption was found at the Zn K-edge in solution, but an intensive signal was detected at the Br K-edge. The XANES spectra at the Br K-edge were different from those of the bromide in the solid phase (Figure 5-2). This finding is reasonable, because although bromide will not dissolve in CO₂, small amounts added to the epoxide could be present in solution. Comparable XANES spectra have been reported for Br–C bonds.¹⁸⁹ Along with the XANES data, the *in situ* EXAFS experiments at the Zn K-edge (solid catalyst) indicate a significant change in the coordination shell of the zinc center (Figure 5-3). After a short contact time between the catalyst and PO, the strong signal at 2 Å in the Fourier-transformed EXAFS spectra at the Zn K-edge disappeared. The signal at about 2 Å is typical for the Br-backscatterer, demonstrating that Br dissolves. Correspondingly, in the spectra of the solid catalyst at the Br K-edge during reaction just a small and hardly interpretable signal remained, also demonstrating the loss of bromide. After the reaction, only the backscattering of N or O neighbors could be detect-

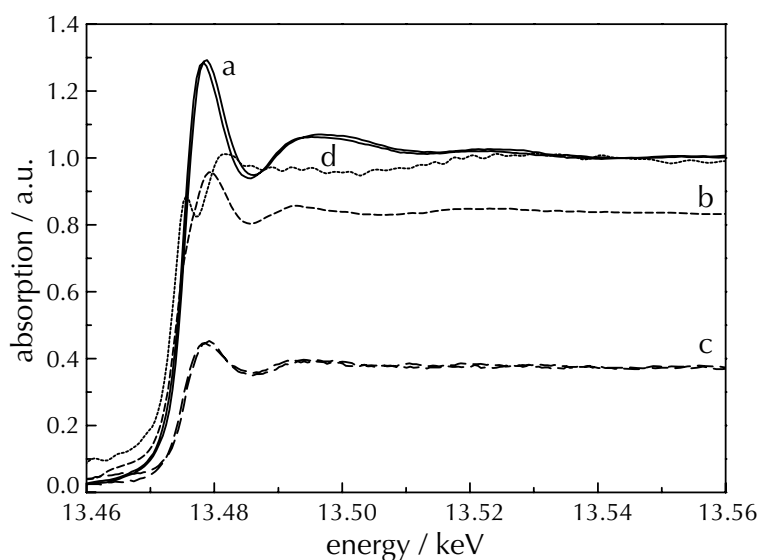


Figure 5-2: *In situ* XANES spectra of catalyst 42 at the Br K-edge. The spectra are related to the first spectrum to point out the loss of bromide with the exception of the spectra of the liquid phase. a) Spectra with catalyst as synthesized. b) After 30 min of addition of PC. c) After 3 h of reaction at 140 °C and after cooling down to ambient temperature. d) Spectrum through the liquid phase during reaction. On the anchored complex no change of the neighbors could be seen, but the bromide detected in the liquid phase had a completely different ligand sphere (normalized).

ed (Figure 5-3), and no Br surrounded the central zinc atom. There was little difference in the EXAFS spectrum at the Zn K-edge from catalyst 43.

In addition, the bromide concentration in the *in situ* batch reactor was estimated as follows: In the liquid phase (upper part of the reactor), the bromide was calibrated by solutions of known bromide concentration and resulted in a concentration of about 5 mmol l⁻¹. The bromide loss of the catalyst determined by the decrease of the edge jump (the lower part of the reactor) produced a concentration of 15 mmol l⁻¹. This greater amount may be related to a larger-than-expected volume of the liquid phase or to some abrasion of the pellet resulting from mechanical impact caused by the stirring. The difference in the edge jumps before and after the reaction lead to a bromide loss of 55% during reaction; this is less than the drop in bromide content measured by ICP-OES after a standard

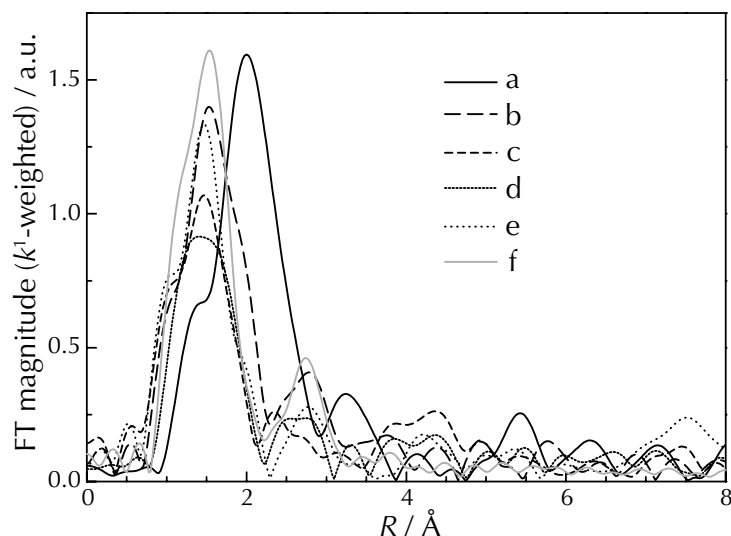


Figure 5-3: Fourier transformed *in situ* EXAFS spectra. Fourier transformed $k^1 \chi(k)$ function of catalyst 42 (a). A fast change in the spectra appeared after the addition of PO (b). The signal corresponding to the bromide is disappearing whereas the signal of N/O atoms becomes more dominant. Addition of CO₂ (c) and increase of the temperature to 140 °C during reaction (d) decreased the signal. After the reaction (e) there is no significant difference to the spectrum of the bromide free catalyst 43 (f).

reaction. But note that a pellet was used for the *in situ* experiments, and consequently intra particle mass transfer was less effective compared with the powder.

5.3.2 ICP-OES Measurements Including the Bromine Content

More information of the deactivation mechanism was gained by ICP-OES and XAS measurements of the reused catalyst samples. ICP-OES revealed that the zinc content decreased only slightly during the first experiment, whereas bromide was washed out with every further reuse. Thus the decreased bromide content occurred in parallel to the loss of catalyst activity (Figure 5-4).

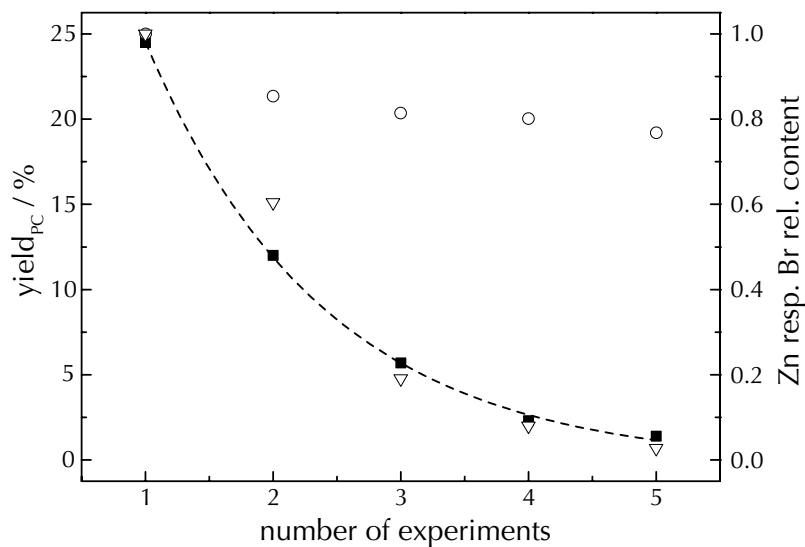


Figure 5-4: Deactivation experiments of catalyst 42a. Solid squares are designated to the yield of PC. The dashed line is an exponential fit of the decrease. Circles indicate the zinc content and triangles the bromide content, both measured by ICP-OES.

5.3.3 Reactivation of the Catalyst by Bromide Addition

Because bromide loss seems to be the main cause of the deactivation of the immobilized catalyst 42, it should be possible to regenerate the catalyst by adding bromide. Indeed, the addition of both potassium and ammonium bromide lead to a reactivation of the catalyst (Table 5-1). An increase in the Br content was obtained in ICP-OES measurements; however, EXAFS measurements showed that the coordination geometry around the zinc central atom was not regenerated. No signal of a backscattering Br neighbor with the typical Zn–Br distance was found. The additional Br on the catalysts was adsorbed on the surface of the silica and not assembled in the zinc complex; thus regeneration led not to structure 42 of the immobilized catalyst, but rather to bromide as a co-catalyst. This has significant effects on the mechanism.

Table 5-1: Catalytic results of the used and by addition of bromide reactivated catalyst.

catalyst	$Y^a) / \%$	$S^b) / \%$	TON	TOF / h^{-1}
42b	51.8	98.5	994	331
42b ^{c)}	31.9	99.7	862	287
42b ^{d)}	56.3	99.6	1520	507

^{a)} Yield of PC based on PO; the reaction was carried out in 10 ml (140 mmol) of PO, 250 mg catalyst, CO₂ (480–550 mmol, 3.4–3.9 eq.), reaction time was 3 h at 140 °C. ^{b)} Selectivity of PC. ^{c)} After one use. ^{d)} Used catalyst in presence of 0.14 mmol ammonium bromide.

5.4 Discussion

5.4.1 Behavior of the Catalyst Under Reaction Conditions

Important features of heterogeneous catalysts are their deactivation behavior and reusability. *In situ* EXAFS studies demonstrated that the Zn complex was well immobilized on the support even under reaction conditions. However, a loss of bromide into PO or a PO/CO₂ mixture was found that led to a deactivation of the catalyst. Interestingly, Kim et al.¹²⁷ found no such deactivation; however, their deactivation studies were performed in ethylene oxide instead of PO. The dissolution of bromide explains the deactivation of the catalyst during reuse, as well as the negative leaching tests. Such tests are usually performed to identify whether the active complex goes into solution.^{185–187} Because the entire active complex did not leach, no activity was found in the liquid phase. Consequently, the former activity could be recovered by adding bromide to the solid catalyst. Hence in this case, bromide was used as co-catalyst. Regeneration of the complex (i.e. the coordination of Br to Zn) was not seen on EXAFS.

5.4.2 Role of Bromide

The observation that bromide is dissolved in the liquid phase also has important implications for the mechanism. Kim et al.⁹³ and Lu et al.^{97,120} proposed mechanisms that first consider either activation of CO₂ or coordination of epoxide by the metal center. These authors found no changes in the bromide after the reaction. In the reaction mechanism, bromide is assumed to be coordinated with the zinc complex; however, this *in situ* study indicates that dissociation of the zinc bromide complex occurred. The role of bromide could thus be either to act as nucleophiles for epoxide opening or to serve as an easy-leaving group, making free coordination sites at the zinc more accessible. This possibility is supported by the observation that iodide is even better than bromide.^{93,127} Moreover, Br-species were observed that uncover the nucleophilic attack of the epoxide and the formation of a Br–C bond. Accordingly, the mechanisms in the homogeneous and immobilized complexes are similar; however, more *in situ* studies are needed to unravel the complete mechanism.

5.5 Case Study: *In Situ* Monitoring of Nickel Catalysts

5.5.1 Introduction

After the successful application of the batch reactor for *in situ* XAS measurements at the Zn K-edge, the ability of this setup toward lighter elements was tested, particularly with regard to the immobilized chromium salen catalysts (see Chapter 3).

In a screening of various transition metal complexes, nickel-based catalysts were found to be catalytically active in the solventless synthesis of PC in and with dense CO₂. Hence three different complexes were synthesized (Scheme 5-2), catalytically tested, and analyzed by XAS measurements. An *in situ* study provided insight into the relation of structure and catalytic activity.

5.5.2 Results and Discussion

The catalytic results are shown in Table 5-2. Catalyst **45** was strikingly less active than catalysts **46** and **47**. In the XANES spectra (Figure 5-5) at the Ni K-edge of these Ni catalysts the spectrum of catalyst **45** differs from the others. A pre-edge and the decreased whiteline indicate a square planar structure if compared to previous results in literature.¹⁹⁰ In the EXAFS region oscillations were missing at higher k -value due to the lack of heavier backscatterers such as the chloride neighbors of catalysts **46** and **47**. The expansion of the coordination sphere of the Ni center atom resulted in a higher catalytic activity.

Table 5-2: Summary of catalytic results of the nickel catalysts.

catalyst	Y^a / %	TOF / h^{-1}	PO / catalyst ratio
45	10.0	15	455
46	59.3	80	400
47	57.2	60	300

^a) Yield of PC based on PO; the reaction was carried out in 10 ml (140 mmol) of PO, 100 mg catalyst, CO_2 (480–550 mmol, 3.4–3.9 eq.), reaction time was 3 h at 140 °C.

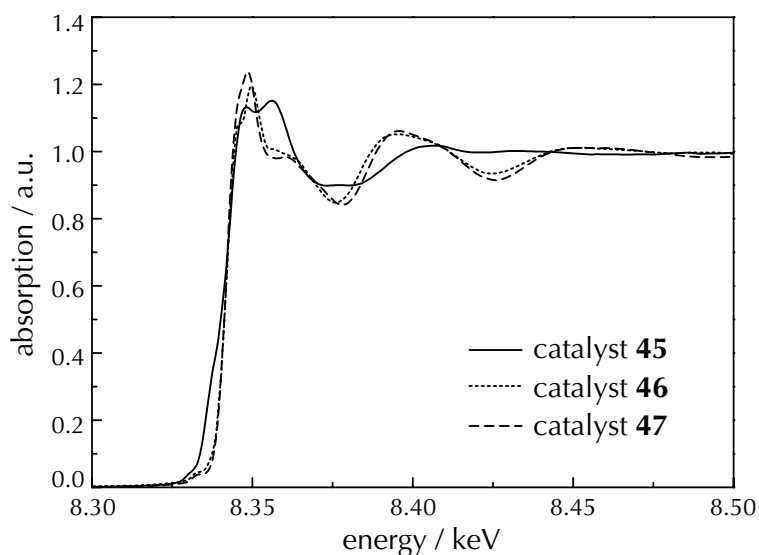


Figure 5-5: XANES spectra of the Ni catalysts.

The *in situ* XAS measurements with the Ni catalyst 47 showed no changes in the spectra during the addition of PO and CO₂. At a reaction temperature of 120 °C a pre-edge at the XANES spectrum appeared together with a decrease in the oscillation in the far *k*-space (Figure 5-6). This indicates a loss of chloride in the coordination sphere of the Ni. In the Fourier transformed $k^1 \chi(k)$ function of the *in situ* EXAFS (Figure 5-7), the signal of the first sphere shifted from 2.0 Å to 1.6 Å in accordance to the loss of the chloride (Table 5-3). Also the extracted $k^1 \chi(k)$ functions of the catalyst before and after reaction corroborate the loss of chloride and indicate the change from octahedral to tetrahedral coordination of the Ni.

Table 5-3: Structural parameters determined from the Ni K-edge EXAFS spectra of catalyst 47.

	<i>A-B</i> ^{a)}	<i>r</i> ^{b)} / Å	<i>N</i> ^{c)}	$\sigma^{2d)}$ / Å	$\Delta E_0^e)$ / eV	residual ^{f)}	<i>k</i> -range / Å ⁻¹
before reaction	Ni–N	2.135	2.4	0.008	–5.5	14.4	3.0 – 12.0
	Ni–Cl	2.492	4.0	0.010	9.2		
after react.	Ni–N	2.054	4.9	0.008	–3.0	7.2	3.0 – 12.0

^{a)} Absorber–Backscatterer pair. ^{b)} Distance. ^{c)} Coordination number. ^{d)} Debye–Waller factor. ^{e)} Shift of the energy threshold. ^{f)} Residual indicates the quality of fit.¹⁶⁷

Hence this evidences the relatively low stability of the Ni–Cl bond and explains, why the octahedral coordination of Ni did not hinder the substrates to interact with the active center. Due to the weaker binding of the chloride, the center atom of catalyst 47 was easier accessible than the center of the chelat salen complex 45 despite the lower coordination number of the Ni atom in the latter catalyst.

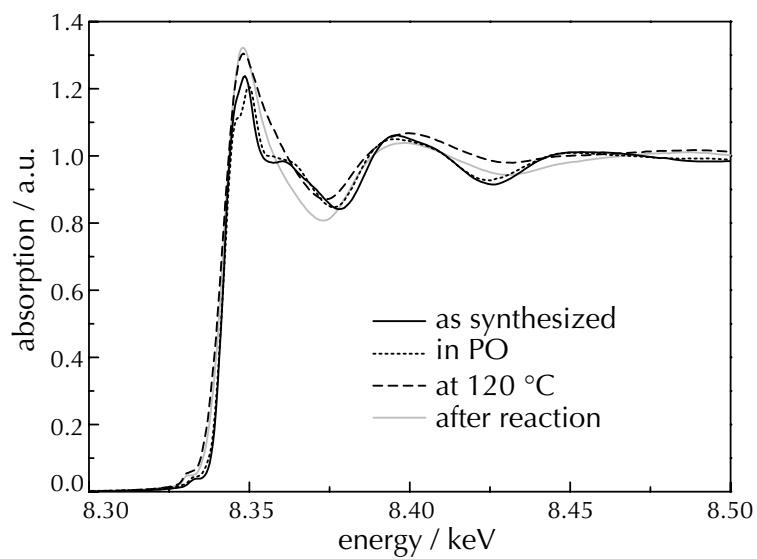


Figure 5-6: XANES spectra of the *in situ* measurements of catalyst 47 at the Ni K-edge.

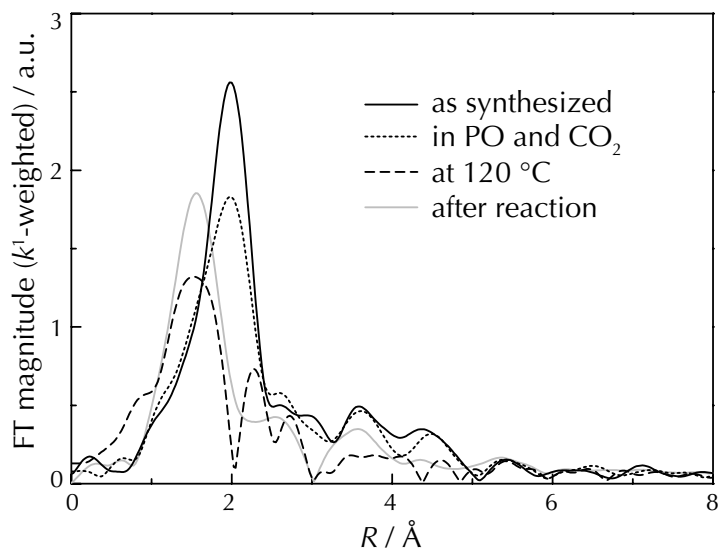


Figure 5-7: *In situ* EXAFS spectra. Fourier transformed $k^1 \chi(k)$ function of catalyst 47.

5.6 Conclusions

In situ X-ray absorption spectroscopy proved to be a well-suited technique for monitoring the structure of the catalyst under real reaction conditions, even at high pressure. Changes in the coordination sphere of the zinc and detachment of the bromide under reaction conditions were seen. Crucial for this was the possibility to monitor both the solid phase at the bottom and the liquid phase in the XAS-autoclave. The zinc itself is well immobilized. The observed presence of the bromide in the liquid-like reaction mixture not only provides insight into the mechanism, but also explains why bromide or similar ligands have been important in the design of active catalysts for the addition of CO₂ to epoxides. Obviously, the mechanisms have to be modified in a way that bromide is not attached to the complex but is responsible for the nucleophilic attack of the epoxide. These findings indicate that when designing heterogeneous catalysts for this reaction, bromide can be used as a co-catalyst, or the heterogeneized catalyst can be modified by additional immobilization of the bromide as an onium salt.

The second part of the study showed that the *in situ* XAS batch cell is even applicable at lower energies such as the Ni K-edge energy of 8.333 keV. At synchrotron facilities with high intensity and a critical energy of about 6 keV, this setup should also allow *in situ* measurements even at the Cr K-edge (5.989 keV). This may give further insight into the structure of chromium salen complexes reported in Chapter 3.

Phase Behavior Studies: Expanded Liquid Versus Supercritical Fluid

The synthesis of PO was optimized using phase behavior studies based on video monitoring, transmission and ATR-IR measurements. Phase behavior studies of the reaction mixture showed three different regions that influenced strongly the reaction rate: (i) At low overall density a biphasic region with small liquid phase (high molar ratio of PC) was observed. The catalytic activity of this system was poor. (ii) A decreasing CO₂ content at the same density resulted in an expanded liquid phase, which was up to a certain PO/PC ratio beneficial for the catalytic activity. However, at too low content of CO₂ (ratio CO₂/(PO+PC) < 4) the rate decreased again, because CO₂ is not only solvent but also reactant in the synthesis of PC. (iii) Finally, experiments at higher pressure led to a single-phase system ('supercritical conditions'). Despite of optimal mass transfer properties the lowest conversion was achieved under these reaction conditions. These observations provided important insight into the reaction system. *In situ* ATR-IR studies of the catalyst surface during reaction revealed drastic changes in the phase behavior in the first minutes and gave important insight into the solid/fluid interface under reaction conditions.

6.1 Introduction

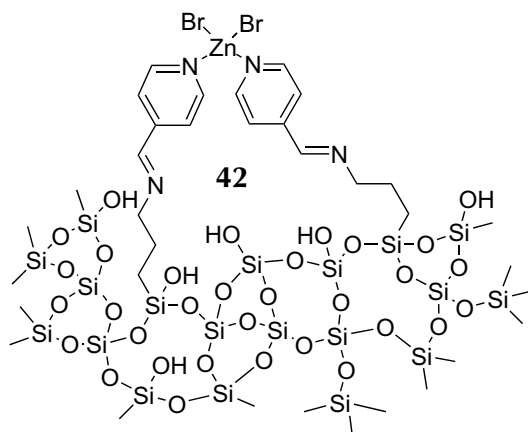
Due to the moderate critical parameters of CO₂ ($T_c = 31$ °C, $p_c = 73.8$ bar), single-phase conditions can be reached at rather low pressure and temperature. Note that the term ‘supercritical’ was used in this chapter for single-phase conditions in general although it is well-defined only for pure substances.^{17,28} Due to the altered properties of dense CO₂ in comparison to conventional solvents, not only supercritical conditions, but also expanded liquids can be beneficial solvents in reactions due to altered mass transfer and solvation properties.^{191,192} In a number of heterogeneously catalyzed reactions, phase behavior studies have been found crucial for optimization since a phase transition can strongly influence the external mass transport.^{193–195} Supercritical solvents may also directly affect the diffusion coefficients, and the reaction mixture composition may be significantly different at the solid/fluid interface and in the bulk fluid phase.¹⁶

So far none of the studies have investigated the influence of the phase behavior. The three fluids involved in this reaction differ in their physical properties. CO₂ is gaseous and apolar, PO has a boiling point of 33.9 °C ($T_c = 215$ °C, $p_c = 54.4$ bar),¹⁹⁶ while that of PC is 241.7 °C. The latter two fluids are polar. Interestingly, several authors report a lower reaction rate at higher CO₂ pressure.^{94,109,111,117} Therefore, focus was placed on this aspect, using one of the best catalyst systems reported so far for a solvent-less process.

The catalytic insertion of CO₂ in PO was performed using an immobilized zinc bromide pyridine complex on silica. The phase behavior of the reaction mixture was studied with a high-pressure view cell by visual observation. In addition, IR spectroscopic measurements at the top (transmission IR) and at the bottom (ATR-IR) of the cell were performed to gain information on the phase composition.^{16,169} With this approach it was also possible to observe minor liquid phases that were not observed by visual inspection. Finally, the phase behavior was determined in the presence of the solid catalyst which also provided insight into the solid/fluid interface.

6.2 Experimental Section

The synthesis of the catalyst shown in Scheme 6-1 is described in detail in the experimental section of Chapter 4.



Scheme 6-1: Structure of the immobilized Zn-complex **42** used for the *in situ* spectroscopy.

6.2.1 ATR-IR Spectroscopy

The signals of the different substances were integrated for further interpretation. Used bands were 3049, 2998 and 2940 cm^{-1} (CH stretching) for PO subtracted by the weaker bands of PC in this region, and about 1801 cm^{-1} (transmission) and 1849 cm^{-1} (ATR) for PC (C=O stretching), and 3727, 3703, 3624 and 3597 cm^{-1} (transmission, overtones) and 2341 cm^{-1} (ATR) for CO_2 .

The penetration depth of the IR radiation in ATR-IR measurements was calculated to be about 0.56 μm for PC at a wavelength of 1849 cm^{-1} and for CO_2 about 0.37 μm at a wavelength of 2340 cm^{-1} .¹⁹⁷ The calculation was based on refractive indices of ZnSe of 2.40,¹⁹⁷ liquid PC of 1.39,²⁴ and CO_2 of 1.06.¹⁹⁸

6.3 Results

6.3.1 Phase Behavior

Phase behavior experiments were performed with different ratios of PO and PC ($x_{\text{PO}} = 0, 0.5, 0.9, 1$). In these cases the ratio of PO and PC to CO_2 was always $n_{\text{PO+PC}} : n_{\text{CO}_2} = 1:4$. The different physical properties of the reaction components such as boiling point and polarity of PO and PC lead to a complex phase behavior during reaction. In order to quantify the described qualitative observations by video monitoring, the concentration of PO and PC was estimated at the bottom of the reactor by ATR-IR spectroscopy and in the middle by transmission IR spectroscopy. Typically for PC the carbonyl stretching band located around 1800 cm^{-1} and for PO the CH stretching bands around 3650 cm^{-1} were used (see paragraph 6.2.1). Note that significant shifts were observed. The carbonyl band of PC in CO_2 without PO located at 1791 cm^{-1} in ATR-IR measurements was shifted to higher wavenumbers with increasing PO ratio (1798 cm^{-1} at $x_{\text{PO}} = 0.5$; 1811 cm^{-1} at $x_{\text{PO}} = 0.9$). The same band was located at 1835 cm^{-1} in transmission mode. Interestingly, at low amounts of PC in the gas phase, a first signal appeared at the same position as in the ATR mode, but with increasing amount of PC only the signal at 1835 cm^{-1} was rising, whereas the signal that was also observed in ATR-IR remained constant. This is attributed to condensation of PC on the transmission window. When the concentration of PC in the gas phase was high enough, the signal of PC at 1835 cm^{-1} appeared.

In general, most of the PC was found in the liquid-like phase and PO mainly in gas phase. Due to the low vapor pressure of PC, the total pressure at the same overall density decreased with increasing amount of PC. Simultaneously, the CO_2/PC ratio decreased in the liquid phase and rose in the gas phase. Addition of gaseous PO caused the dissolution of PC in the gas phase, but a higher content of PO resulted in an increased CO_2/PO ratio in liquid phase and a de-

creased ratio in gas phase. Higher temperatures lowered the proportion of CO₂ in the liquid phase, as also observed by Ai et al.¹⁹⁹ and Trejo et al.²⁰⁰ at lower pressure and temperature.

In addition, studies were performed with a fixed ratio of PO and PC ($x_{\text{PO}} = 0.9$) and a varying ratio of these organic compounds to CO₂ ($n_{\text{PO+PC}} : n_{\text{CO}_2} = 1:2, 1:4, 1:8, 1:16$). This corresponds to a yield of 10% PC during the fixation of CO₂ in PO. This seemed to be a reasonable approach to the real conditions during reaction, because the CO₂ insertion is a slow reaction and a lower fraction of PC is not useful for investigations in the view cell. Varying the CO₂ ratio resulted in two remarkable phase behaviors. They are separately discussed in the following subsections.

Single Phase Region

Figure 6-1 depicts the typical transition to the single-phase region observed by visual inspection. The corresponding changes in ATR-IR spectra are shown in Figure 6-2. With varying CO₂ content, the critical pressure was nearly constant at a certain temperature. Therefore, in this work the overall density is referred and not the total pressure. Specifically, a higher CO₂ content resulted in a decreasing density of the single phase with higher CO₂ ratio, because more CO₂ causes higher pressures at the same overall density. When the critical point was reached, the intensity of the PC signal was strongly growing in the transmission spectra (Figure 6-3) as the liquid phase suddenly vanished and the evaporated PC led to a higher PC concentration in the gas phase. At the same time, the signal at 1807 cm⁻¹ measured by ATR-IR disappeared, due to the loss of the liquid PC in the near surface region of the ATR crystal (Figure 6-4). Simultaneously, the ν_2 band of CO₂ was shifted to higher wavenumber (658 cm⁻¹ at 130 bar to 662 cm⁻¹ at 139 bar). This is in accordance with measurements of the band shift in relation to the density.²⁰¹ Therein a ν_2 band of 662 cm⁻¹ is correlated to a density of about 550 kg m⁻³, which is the overall density at the transition to the single-phase system.

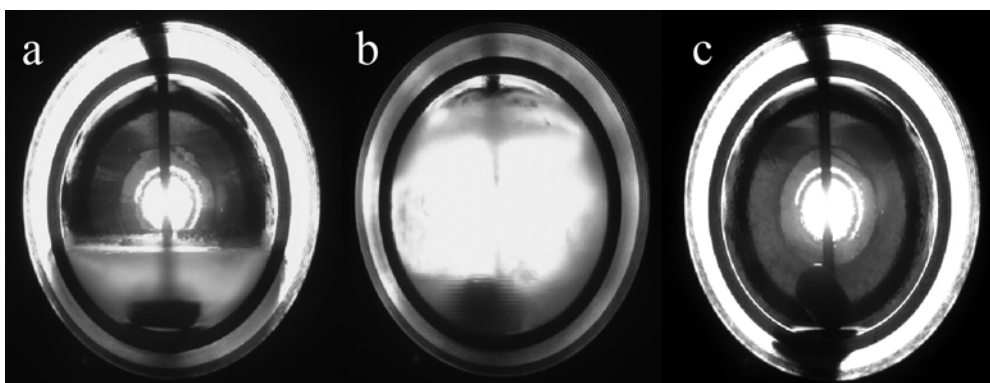


Figure 6-1: Transition to single phase. 81.8 mmol PO, 9.1 mmol PC and 364 mmol CO₂ at 100 °C. a) 2-phase system at 140.2 bar, b) critical point at 140.7 bar, c) single phase at 147.8 bar. The bright round spot at the opposite end of the cell is due to the sapphire window used for illumination; the outer white circle is caused by reflection of light at the outer flange of the front sapphire window; the vertical thermocouple and the magnetic stirrer at the bottom of the cell are also visible.

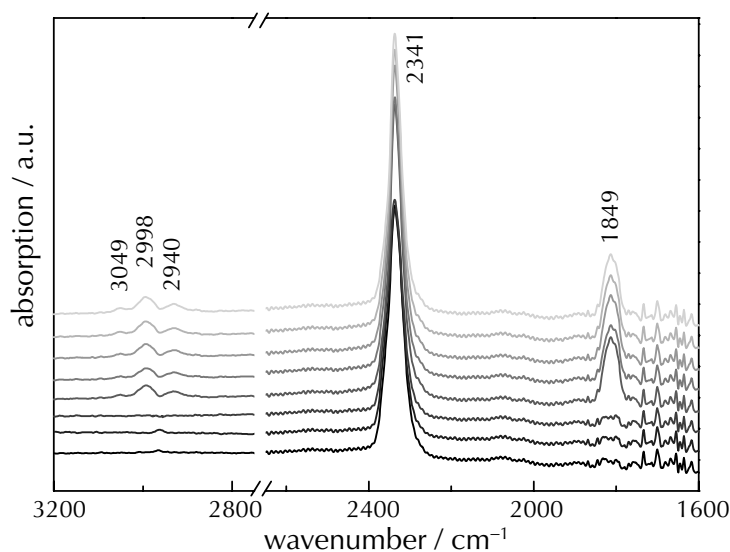


Figure 6-2: ATR-IR spectra of the transition between single and two phase system. The spectra were recorded from an overall density of 630 kg m⁻³ (darkest line) to 400 kg m⁻³ (brightest line). Temperature was 100 °C and the mole fraction $n_{0.9\text{PO}+0.1\text{PC}} : n_{\text{CO}_2} = 1:4$.

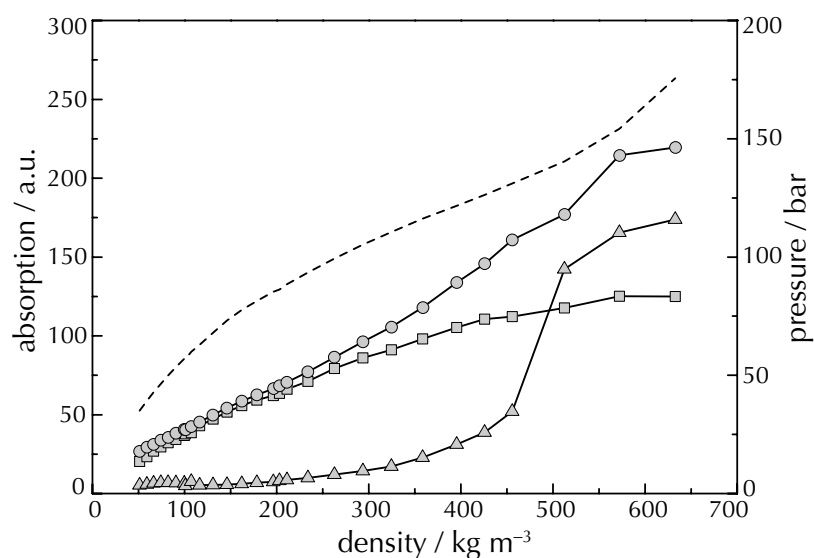


Figure 6-3: Variations in the absorption of transmission IR bands (gas-like phase) of PC (triangles), PO (circles) and CO₂ (squares) as function of the overall density. Conditions: 100 °C, $n_{0.9\text{PO}+0.1\text{PC}} : n_{\text{CO}_2} = 1:4$. Pressure is indicated by the dotted line.

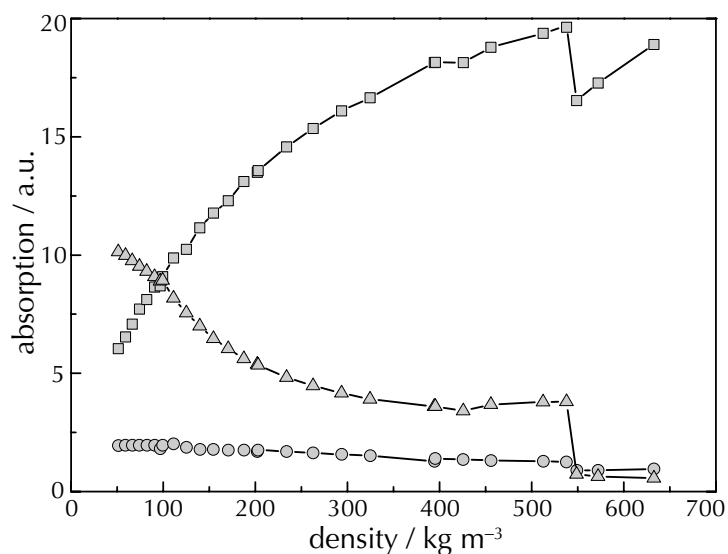


Figure 6-4: Variations in the absorption of ATR-IR bands (dense phase, at the bottom) of PC (triangles), PO (circles) and CO₂ (squares) as function of the overall density. Conditions: 100 °C, $n_{0.9\text{PO}+0.1\text{PC}} : n_{\text{CO}_2} = 1:4$.

Higher temperatures and higher CO₂ content shifted this single-phase transition to lower overall densities but higher pressures. However, it was difficult to inspect visually if it was really a single phase or if there were still small amounts of a liquid phase left. In this respect, ATR-IR and transmission IR measurements were particularly helpful not only to determine the composition of the phase but also to check whether a liquid phase was present. Since the IRE was mounted at the lowest position of the cell, liquid-like phases should preferentially condense on the IRE first.

Expanded Liquid Region

The two phase region showed a significant variation in the volume of the liquid phase with respect to the amount of CO₂ and the temperature. As expected, lower temperature (Figure 6-5) increased the amount of liquid phase. Moreover, less CO₂ at the same overall density also increased the liquid/gas volume ratio. The reason for this interesting observation is that nearly the same PO concentration existed in the gaseous phase at a certain overall density independently of the CO₂ content, and the excessive PO was added to the liquid phase. The factor of the expansion of the liquid phase was 1.5 at 100 °C, 2.5 at 80 °C, and 2.8 at 60 °C for this system at a CO₂ ratio of 4 ($n_{\text{PO+PC}} : n_{\text{CO}_2} = 1:4$). These factors were based on the total volume of PO and PC. At a fixed overall density below supercritical conditions, the mol fraction of PC in the liquid phase was increasing (Figure 6-6) with increasing content of CO₂. In addition, the influence of the temperature was decreasing with higher content of CO₂.

6.3.2 Catalysis

The impact of the phase behavior described above on the catalyst performance of catalyst 42 was examined (Table 6-1) under conditions corresponding to the different cases identified in the phase behavior studies (Figure 6-7, a – d). First, a series of four reactions at an overall density of 250 kg m⁻³ with different ratios

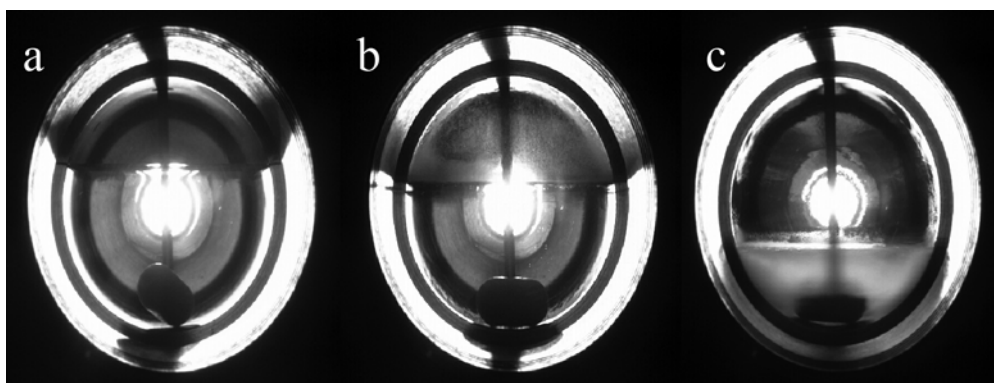


Figure 6-5: Decrease of the liquid phase with increasing temperature. 81.8 mmol PO, 9.1 mmol PC and 364 mmol CO₂ in a 30 mL cell at a) 60, b) 80, and c) 100 °C. For explanation of the general features of the snapshots cf. Figure 6-1.

of CO₂ was performed (following the trend in Figure 6-6). The reactions were carried out at 110 °C. Lower temperatures would have increased the liquid phase, but the low catalytic activity limited the study of the influence of the phase behavior.

With decreasing CO₂ ratio ($n_{\text{PO+PC}} : n_{\text{CO}_2} = 1:16, 1:8, 1:4$) the yield was increasing (Table 6-1) from 3.0 to 8.7%. The lowering of the CO₂ content had a strong influence on the phase behavior. The expanded liquid phase (Figure 6-7 a) increased, a higher concentration of PO around the catalyst was achieved and a high concentration of PC around the catalyst could be avoided (Figure 6-6). Note that high concentration of PC on the catalyst surface favors deactivation by polymerization. However, an lower CO₂ ratio ($n_{\text{PO+PC}} : n_{\text{CO}_2} = 1:2$) was not beneficial. In this case, the reaction rate decreased resulting in a yield of 5.6%.

In addition, the single-phase region with an overall density of 570 kg m⁻³ and a molar ratio $n_{\text{PO+PC}} : n_{\text{CO}_2} = 1:4$ was investigated (Figure 6-7 c). The conversion was lower compared with the two phase system (Figure 6-7 a and b). In a two-phase system the density of the liquid phase is higher than the density in a single-phase system near supercritical conditions (about 700 kg m⁻³ corre-

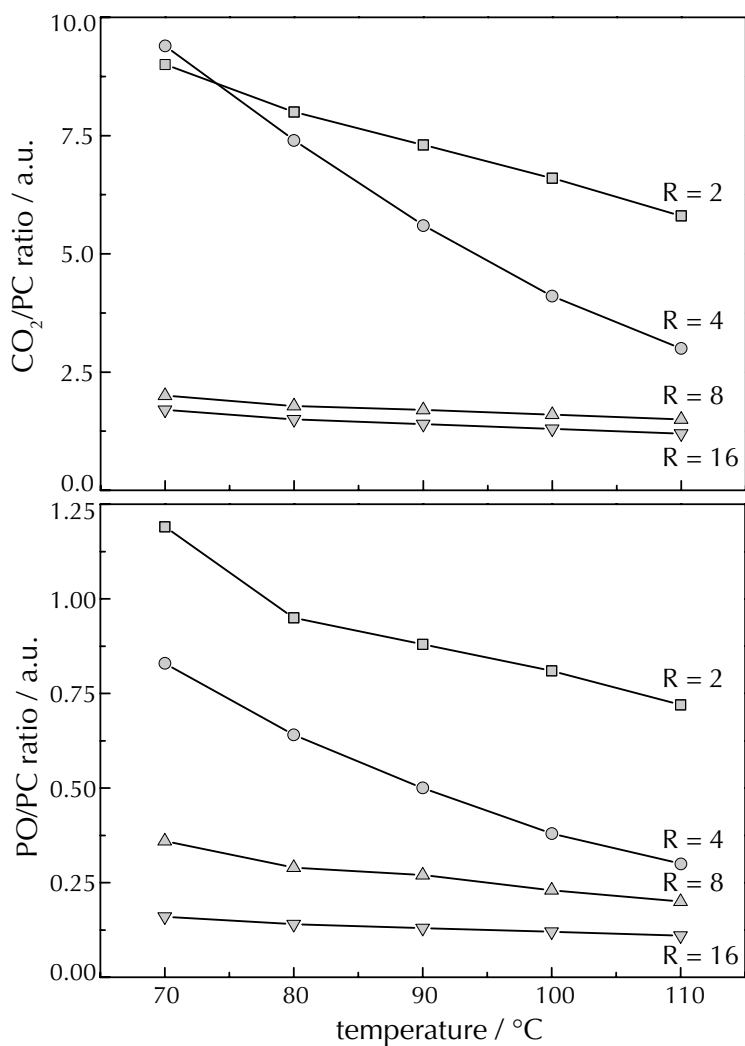


Figure 6-6: Ratio of the integrated signals of the ATR-IR bands for different mixtures of PC, PO and CO₂ at an overall density of 300 kg m⁻³. The mole fractions were 0.1 PC, 0.9 PO and the ratio $R = n_{\text{CO}_2} (n_{\text{PO}} + n_{\text{PC}})^{-1}$ of 2 (squares), 4 (circles), 8 (up-triangle) or 16 (down-triangle).

sponding to a ν_2 band of 658 cm⁻¹).²⁰¹ Hence the dissolution power of the less dense phase may not be sufficient for extraction of the PC out of the pores.

Table 6-1: Catalytic results of the PC synthesis with catalyst 42.

CO ₂ / PO ^{a)}	overall density / kg m ⁻³	pressure / bar	phase behavior (see Figure 6-7)	S / %	Y / %
2	250	64	a	94.4	5.6
4	250	76	a	95.0	8.7
8	250	92	b	92.9	3.9
16	250	96	b	91.8	3.0
4	570	149	c	86.7	3.4
4 ^{b)}	250	78	a	–	1.1

^{a)} molar ratio of CO₂ to PO at reaction time = 0; reaction conditions: n_{Zn-catalyst} : n_{PO} = 1:5000, temperature 110 °C, time 4 h. ^{b)} reaction time 20 min, no side products found, their concentration is supposed to be below the detection limit.

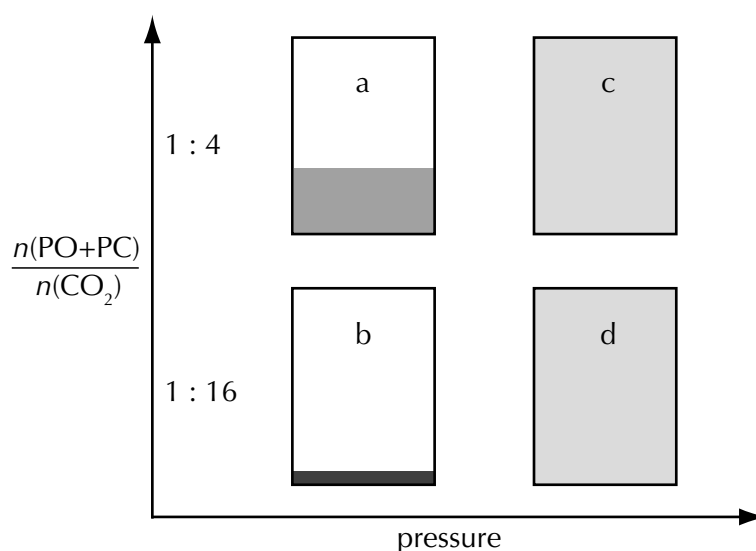


Figure 6-7: Phase behavior in the system PO, PC and CO₂ as a function of pressure and composition. Two different two-phase systems at lower pressure a) an expanded liquid at a low CO₂ content and b) a minor liquid phase at a high amount of CO₂; c) and d) single phase region at higher pressure.

6.3.3 *In Situ* Spectroscopy During Reaction

To shed more light into the relation between catalytic results and phase behavior, an *in situ* IR measurement was performed. Thus, a thin layer of catalyst 42 was deposited on the IRE and the view cell was charged with PO and CO₂ (ratio $n_{\text{PO}} : n_{\text{CO}_2} = 1:4$) at a fixed reaction volume and heated to 100 °C. The calculated penetration depth of the IR beam was about 0.56 μm and thus much smaller than the catalytic layer of $\gg 1$ μm.

During heating there was no signal of PC below 91 °C. The time of the last spectrum at this temperature was taken as the starting time of the reaction in Figure 6-8 to Figure 6-10. In this starting period, the reaction mixture consisting of PO and CO₂ was gaseous-like. Only a weak absorption at 2340 cm⁻¹ of CO₂ was observed (Figure 6-8); the ν_2 band at 658 cm⁻¹ was not observable.

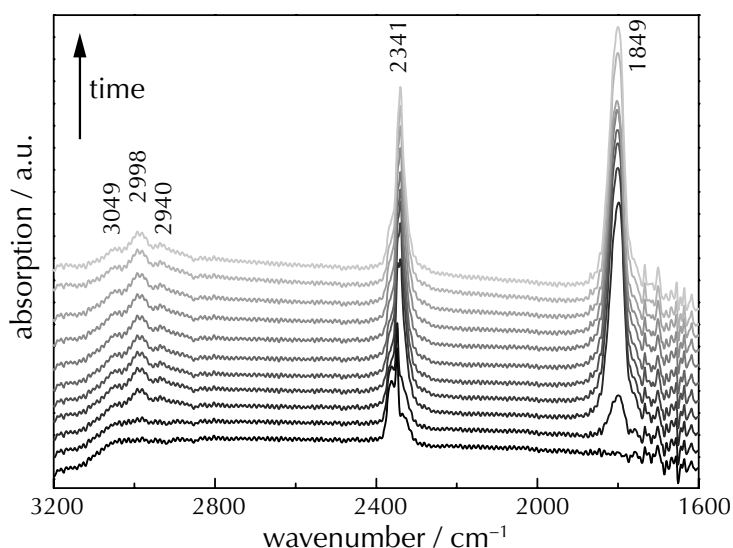


Figure 6-8: ATR-IR spectra during reaction of CO₂ and PO at 100 °C. The spectra were recorded at following times, starting with the solid black line and as indicated by the arrow: 2, 3, 5, 6, 7, 8, 12, 20, 35, 45, 55 min.

Five minutes later at a temperature of 99 °C the first signal from PC at 1800 cm⁻¹ was detected and simultaneously the ν_2 band of CO₂ trapped in the catalyst pores appeared at 658 cm⁻¹. The location of this ν_2 band indicates that

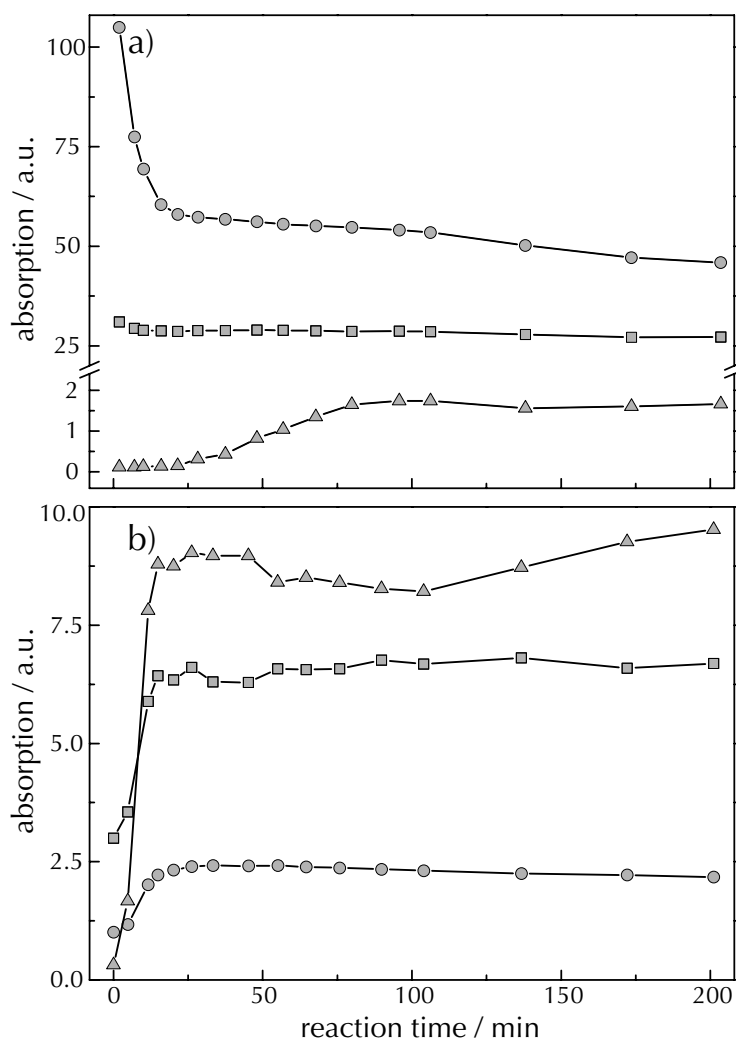


Figure 6-9: Integrated IR signals of CO₂ (squares), PO (circles), and PC (triangles) (a) in gas phase by transmission IR and (b) at the catalyst/fluid interface by ATR-IR spectroscopy during the CO₂ fixation in PO. Reaction conditions: 20 mmol PO, 54 mmol CO₂, 50 mg of catalyst 42, 100 °C, and 35.7 ml reaction volume.

CO₂ in the pores was liquid-like. Thus, the reaction mixture in the pores had a high content of PC (see paragraph 6.3.1). In the first minutes of the reaction nearly one-third of the PO was dissolved in the freshly formed PC, and also more CO₂ condensed (Figure 6-9). But the content of PC in the gas phase increased rather slowly (Figure 6-10), a hint for a hindered diffusion of PC out of the pores. An additional reaction of 20 min duration was performed to rule out

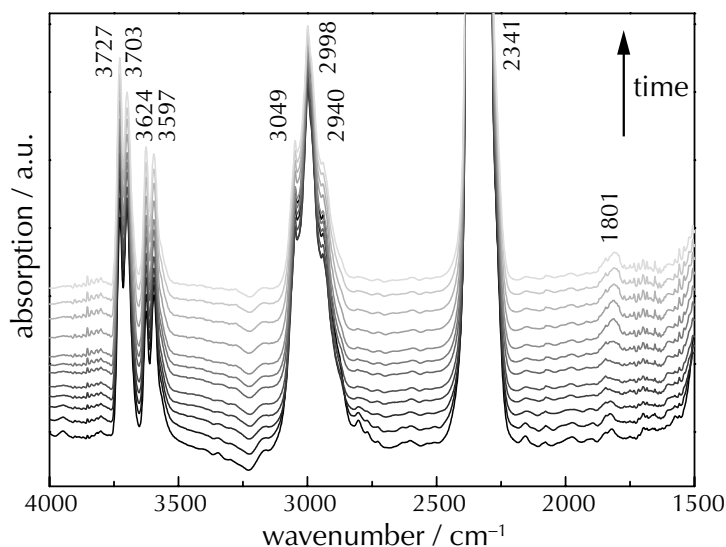


Figure 6-10: Transmission IR spectra during reaction of CO₂ and PO at 100 °C. The spectra were recorded at following times, starting with the solid black line as indicated by the arrow: 3, 5, 6, 8, 10, 20, 23, 26, 33, 36, 46, 60 min.

a fast reaction in the beginning. As Table 6-1 shows, the yield was 1.1% compared with 8.7% after 4 h indicating not a much higher reaction rate in the beginning of the reaction.

In the next minutes the composition of the reaction mixture was stable, only after a long reaction time the content of PC increased (Figure 6-9). As no further increase of the PC concentration could be measured in the gas phase, the synthesized PC seemed to be accumulated in the liquid phase thereby increasing its volume. A slight decrease in the PO ratio was observed during further reaction. After 200 min the reaction mixture was cooled to ambient temperature. The molar ratios in the gas phase corresponded to a conversion below 10% according to IR spectroscopy, though a relatively high amount of catalyst was used. This may have been due to the lack of sufficient stirring at the bottom of the view cell, compared with the batch reactor.

6.4 Discussion

The immobilized zinc-pyridine catalyst **42** was active in the solvent-less synthesis of PC by fixation of CO₂ into PO and reached a yield of 8.7% with a *TOF* of 110 h⁻¹ per zinc atom even at a reaction temperature of 110 °C. For process optimization the phase behavior was examined. Three different regions could be distinguished. There were two different biphasic systems, one with the expected amount of liquid phase derived from PO and PC and another one with an expanded liquid phase. In addition, a single-phase system was found at high overall pressure (Figure 6-7).

As the present study demonstrated, these regions had a strong influence on the reaction rate. The region where a non-expanded PC rich phase was present (high amount of CO₂) led to a significantly lower reaction rate than an expanded liquid. The main reason for this behavior seems to be that the non-expanded liquid phase had a too high concentration of PC with smaller amount of CO₂ and PO surrounding the catalysts. Hence the low concentration of the reactants and the low concentration gradient of PC (slow diffusion of PC out of the pores) seem to be at the origin of the slow reaction rate observed under these conditions.

The best catalytic results were achieved in expanded liquid phases. These expanded liquids were obtained at a relatively low $n_{\text{CO}_2}/n_{\text{PO}}$ ratio. However, there was a limitation of the expansion factor, and too low concentrations of CO₂ were counterproductive. In another recent study, Kerler et al. investigated the oxidation of cyclohexene in CO₂-expanded acetonitril.¹⁹¹ They found that a too high expansion factor was unfavorable for the catalytic activity, because the solvent polarity decreased with higher CO₂ ratio. This may also play a role in the present reaction, because the polarity of PC is significantly different to PO and CO₂. Besides this, CO₂ was a reactant in the herein discussed reaction.

Surprisingly, the single-phase region exhibited the lowest performance. In fact, in other studies the pressure dependence was also investigated. Usually, an

increase of the reaction rate was found with increasing pressure.^{89,108} However, several groups found at higher pressure a strong decrease in the reaction rate.^{94,109,117} Yasuda et al.¹¹¹, who used similar solventless conditions, observed a significant loss in activity over a Cs-P-Si oxide catalyst above 140 bar. This is in line with the observation that at higher pressure a single phase is formed that leads to much lower reaction rate. This is surprising since with many reactions the opposite effect was observed and supercritical conditions were advocated to be beneficial.^{16,17,30,194,202,203}

This is probably due to the too low solvent polarity as described before or due to a too low mean density of the reaction mixture. Ginosar and Subramaniam²⁰⁴ demonstrated the importance of the density of the reaction mixture for the deactivation behavior of a catalyst that was connected to extraction of organic compounds from the catalyst surface. In their case, near critical conditions were more favorable than gas or liquid-like conditions. Interestingly, Schneider et al.²⁰¹ investigated near-critical CO₂ in mesoporous silica and discovered that the fluid density of CO₂ inside the pores was higher than outside. This could be a hint for slow extraction of PC out of the pores under supercritical conditions.

In situ IR spectroscopy under real reaction conditions uncovered that after a short induction time the CO₂ in the pores of the catalyst became liquid-like during reaction. In the starting period PO and CO₂ were present as one single phase, also in the porous catalyst. The first appearance of PC led to a separation of a liquid phase containing PC, PO and CO₂, and resulted in a significant change of the PO concentration in gas phase. An additional batch reactor experiment performed for a short time period clarified that this loss in PO concentration in the gas phase was not due to a fast reaction within the first minutes. The relatively high concentration of PC at the catalyst/fluid interface shortly after the reaction start is an evidence for an initially fast reaction but a slow extraction of the product out of the catalyst pores. This supports the observation from phase behavior and catalytic studies that the high solvent power of the expanded

liquid phase combined with high PO and CO₂ concentration is important for achieving a high reaction rate.

6.5 Conclusion

In contrast to several other reactions reported in literature, a single-phase system was not beneficial for the solventless synthesis of PC from PO and CO₂. The higher density and solvent power of the dense liquid-like PO/PC-rich phase improved the reaction rate. The present study indicates that the earlier made observation that the reaction rate of PC synthesis shows a maximum when pressure is increased has to be traced to the unfavorable phase behavior at high pressure. Attention has to be given to the special behavior of the reacting fluid when entrapped in the pores due to changes in density and solvent power as the example of the CO₂ insertion reaction, presented in this study, demonstrates.

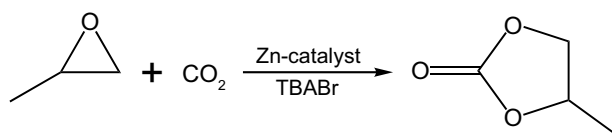
Simple Preparation Routes Toward Novel Zn-based Catalysts

Differently prepared supported and unsupported zinc-based catalysts were tested in the solventless synthesis of PC from PO and CO₂. ZnO-SiO₂ xerogels prepared by the sol-gel method and flame-made ZnO-SiO₂ materials synthesized by flame spray pyrolysis resulted in catalysts with high surface area (640 m² g⁻¹ and 460 m² g⁻¹, respectively) and exhibited in the presence of tetrabutyl ammonium bromide (TBABr) a good catalytic activity toward PC. Also undoped and doped zinc oxides prepared via flame spray pyrolysis were catalytically active. A significant improvement of the flame-made ZnO-SiO₂ system could be achieved by depositing the zinc precursor on pre-formed silica particles. Yields >99% at principally 100% selectivity were achieved with 200 mg catalyst and 140 mmol PO at 120 °C in 6 h. This indicates that not single site zinc but rather zinc-clusters play an important role in the catalytic activity of the system, as also evidenced by EXAFS results and STEM.

7.1 Introduction

Immobilized ZnBr₂Py₂-complexes exhibited high turnover rates that are nearly as high as those of the homogeneous counterparts (see Chapter 4). However, the synthesis of such functionalized catalysts is time-consuming and quite expensive. Hence the design of a simple and efficient catalyst for the coupling of PO

and CO₂ according to Scheme 7-1 is still required. In this chapter the focus was placed on zinc-based mixed oxide catalysts synthesized by different preparation techniques. Ideally, these catalysts should be easily accessible and toxicological harmless. Emphasis was laid on achieving high yields at solventless conditions with a relatively low amount of catalyst at short reaction times to reduce the use of chemical products and waste to a minimum. For the zinc-based catalysts, both the synthesis of xerogels via the sol-gel route²⁰⁵ and flame-made materials using flame spray pyrolysis²⁰⁶ were chosen as preparation routes. The latter method allows fast and cheap one-step catalyst synthesis without any reaction work-up and minimized effluents. For comparison, zinc hydroxyapatite was tested. It was recently used in the synthesis of higher and thus more reactive cyclic carbonates.¹¹⁴ TBABr was added as base/co-catalyst.



Scheme 7-1: Reaction scheme of CO₂ fixation to PC on Zn-based catalysts.

7.2 Experimental Section

In Table 7-1 to Table 7-6 the compositions of the various catalysts are given together with the corresponding results of catalytic tests. Specific designations were used throughout this chapter, which included the loading, support, and preparation method (gel: sol-gel based synthesis; TEOS: flame-made with tetraethoxysilane (TEOS); disp: flame-made with colloidal silica precursors), as specified in the corresponding tables.

The CO₂ insertion reaction was performed according to paragraph 2.1.2. 140 mmol of PO, 10 mg TBABr, 0.6 mol CO₂, and typically 100 mg catalysts were used, reaction temperature was 100 °C and reaction time 3 h.

7.2.1 Sol-gel based Synthesis of Catalysts with Oxide Support

Oxide supported xerogels containing different weight percentages of Zn have been prepared applying a sol-gel process and subsequent drying according to ref.²⁰⁷ Zinc acetate has been used as Zn precursor and tetraethoxysilane (TEOS) as silica precursor. For non-silica supports, zinc acetylacetonate has been used as zinc precursor, aluminum and titanium isopropyl-ate as precursor for the silica-free supports, and the corresponding acetylaceton-ates for the mixed oxides.

7.2.2 Flame-made Catalysts

Zinc on silica samples were prepared via flame spray pyrolysis (FSP).^{208,209} In the FSP process, the liquid reactant mixture containing soluble metal-precursors is fed through a capillary to a nozzle. At the tip of the capillary, an oxygen flow disperses the liquid, resulting in a fine spray. This spray is ignited by a supporting methane/oxygen flame around the capillary. The powders were collected on a cooled glass-fibre filter located 50 cm above the burner plate. Zinc acetylacetonate or corresponding metal complexes and TEOS were dissolved in 40 ml of 50/50 vol% methanol/acetic acid. These precursor solutions were fed through the capillary to the flame with 5 ml min^{-1} and dispersed with $5 \text{ l}_n \text{ min}^{-1}$ oxygen. In addition, zinc acetylacetonate was also deposited on SiO_2 using pre-formed silica particles. For this purpose, colloidal silica (Ludox TMA, 34 wt% suspension in water, Sigma-Aldrich) was used. The colloidal silica was sprayed together with the zinc precursor.

7.3 Results

7.3.1 Catalytic Studies

First, a series of 2.5 wt% zinc oxide on different supports was synthesized by the sol-gel method to examine, which support was most suitable for this reaction (Table 7-1). The specific surfaces of the catalysts varied (see Table 7-1), but the nature of the support had a much stronger influence on the reaction rate than the surface area. No leaching of active zinc complexes could be observed. Surprisingly, supports containing aluminum oxide and silica-free titanium oxide showed an even lower yield (conversion) than the blank experiment only containing TBABr. This could be explained by a strong interaction of support and product. Interestingly, mixed Mg/Al oxides were reported to be active as catalysts for the synthesis of PC, but in these studies an additional solvent,¹¹⁰ a much higher catalyst/substrate ratio and/or more drastic conditions were used (80 – 140 bar, 200 °C, 8 h).^{108,111}

Table 7-1: Results of the PC synthesis catalyzed by different sol-gel-derived zinc containing oxides. Note that the selectivity to PC of all the tested catalysts was always ca. 100% so that the yield can directly be used as a measure of conversion (activity).

catalyst	catalyst composition	amount / mg	surface / m ² g ⁻¹	Y / %
2.5Zn/SiO ₂ -gel	2.5wt%ZnO/SiO ₂	100.2	645	10.8
2.5Zn/Al ₂ O ₃ -gel	2.5wt%ZnO/Al ₂ O ₃	100.6	643	0.4
2.5Zn/TiO ₂ -gel	2.5wt%ZnO/TiO ₂	100.3	465	0.4
2.5Zn/AlSi ₅ O _x -gel	2.5wt%ZnO/Al ₂ O ₃ (SiO ₂) ₅	99.7	201	0.4
2.5/TiSi ₅ O _x -gel	2.5wt%ZnO/TiO ₂ (SiO ₂) ₅	100.1	185	7.0
2.5Zn/ZrSi ₅ O _x -gel	2.5wt%ZnO/ZrO ₂ (SiO ₂) ₅	100.1	216	4.3
TBABr	–	10.0 ^{a)}	–	2.0

^{a)} For all other reactions, 10 mg TBABr was used as co-catalyst (see paragraph 7.2).

Table 7-2 shows the catalytic data for PC formation as function of different zinc loading on silica. With increasing zinc loading, more PC was formed. However, the yield did not increase linearly with the zinc content. The average catalytic activity per zinc atom decreased at higher loading, probably due to the growth of larger zinc clusters.

Table 7-2: Influence of zinc content on the synthesis of PC with sol-gel-derived catalysts.

catalyst	catalyst composition	amount / mg	surface / $\text{m}^2 \text{g}^{-1}$	Y / %
0.6Zn/SiO ₂ -gel	0.6wt%ZnO/SiO ₂	99.9	582	3.2
1.3Zn/SiO ₂ -gel	1.3wt%ZnO/SiO ₂	100.2	220	7.1
2.5Zn/SiO ₂ -gel	2.5wt%ZnO/SiO ₂	100.2	645	10.8
6.3Zn/SiO ₂ -gel	6.3wt%ZnO/SiO ₂	100.8	172	16.3
12.5Zn/SiO ₂ -gel	12.5wt%ZnO/SiO ₂	100.6	639	19.2

The flame-made catalysts shown in Table 7-3 were slightly more active than the corresponding catalysts prepared by sol-gel method at a low zinc oxide content of 2.5% (13.4% instead of 10.8%). One reason could be the lower number of free hydroxyl groups on the catalyst surface,²¹⁰ which may result in by-products and blocking of the active sites. Also flame-made silica samples with higher zinc contents were tested. In general, the yields of catalysts with higher Zn loading were not higher than for the 2.5Zn/SiO₂ sample and lower than the yields of the corresponding sol-gel derived silica. Note that the surface areas of the sol-gel catalysts were higher than those of the flame-made materials (generally in the sol-gel series $640 \text{ m}^2 \text{g}^{-1} \pm 20 \text{ m}^2 \text{g}^{-1}$). Another reason for the lower activity of the flame-made catalysts could be the favored incorporation of the zinc into the silica during flame pyrolysis. Furthermore, different precursor concentrations during flame spray pyrolysis resulted only in a slight change of the catalytic activity (Table 7-3, 7.0Zn/SiO₂-TEOS).

Table 7-3: Catalytic results of the PC synthesis on flame-made silica prepared with TEOS.

catalyst	catalyst composition	amount / mg	surface / $\text{m}^2 \text{g}^{-1}$	Y / %
1.3Zn/SiO ₂ -TEOS	1.3wt%ZnO/SiO ₂	100.2	283	11.8
2.5Zn/SiO ₂ -TEOS	2.5wt%ZnO/SiO ₂	100.2	423	13.4
7.0Zn/SiO ₂ -TEOS	7.0wt%ZnO/SiO ₂	100.3	337	12.1
7.0Zn/SiO ₂ -TEOS	7.0wt%ZnO/SiO ₂ ^{a)}	100.5	453	13.3
12.5Zn/SiO ₂ -TEOS	12.5wt%ZnO/SiO ₂	99.7	480	15.5

^{a)} Zn(acac)₂ and TEOS were dissolved in 100 ml instead of 40 ml precursor solution.

Since the highest zinc loadings of sol-gel and flame-made catalysts resulted in the highest yield, zinc oxides without silica as support were catalytically tested (Table 7-4). These zinc oxides were varied by addition of different dopants. Also with these zinc oxides the flame-made materials showed higher yields than commercial zinc oxide, which only gave a conversion of 8.8%. Doping of the zinc oxide by Mg, Ca, and Sr led to an improved activity. Although the additives influenced the surface, still different activities were achieved when the yield was related to the surface area, which could be due to the variation in strength of the basic sites depending on the dopant used.^{110,118}

Table 7-4: Catalytic results of the PC synthesis on different zinc oxides prepared by flame synthesis.

catalyst	catalyst composition	surface / $\text{m}^2 \text{g}^{-1}$	Y / %	Y / 100 $\text{m}^2 \text{g}^{-1}$ / %
ZnO	ZnO	59.6	16.6	27.9
Li ₂ O/ZnO	0.3wt%Li/ZnO	67.6	16.4	24.3
MgO/ZnO	1.5wt%Mg/ZnO	67.2	20.9	31.1
CaO/ZnO	2.5wt%Ca/ZnO	58.3	18.8	32.2
SrO/ZnO	5.5wt%Sr/ZnO	41.5	15.8	38.1
BaO/ZnO	8.6wt%Ba/ZnO	80.6	20.3	25.2

Encouraged by the results of the doped zinc oxides, a series of different doped catalysts was prepared (Table 7-5). Again, as observed when comparing sol-gel and flame-derived catalysts, only at low zinc loadings a beneficial effect of Mg doped material was observed, catalyst 2.5ZnMg/SiO₂-TEOS showed a slightly higher catalytic activity than the undoped catalyst 2.5Zn/SiO₂-TEOS. Since it was reported that zinc hydroxyapatite was quite active in the synthesis of other cyclic carbonates,¹¹⁴ also a hydroxyapatite catalyst 2.5-HAp was tested in the synthesis of PC (Table 7-5). The yield of PC obtained with hydroxyapatite was lower per zinc loading than the yield of both silica catalysts 2.5Zn/SiO₂-gel and 2.5Zn/SiO₂-TEOS. Also no beneficial effect of doping the flame-made catalysts with phosphate or calcium was evident.

Table 7-5: Catalytic results of the PC synthesis over doped flame synthesized materials.

catalyst	catalyst composition	surface / m ² g ⁻¹	Y / %
2.5-HAp	2.5wt%Zn/HAp ^{a)}	64	11.2
1.0ZnPO ₄ /SiO ₂ -TEOS	1.0wt%ZnO,4.0wt%PO ₄ /SiO ₂	360	9.6
2.5ZnMg/SiO ₂ -TEOS	1.0wt%Mg,2.5wt%ZnO/SiO ₂	359	14.9
12.5ZnMg/SiO ₂ -TEOS	5.5wt%Mg,12.5wt%ZnO/SiO ₂	445	12.7
12.5ZnSr/SiO ₂ -TEOS	6.1wt%Sr,12.5wt%ZnO/SiO ₂	419	15.3
12.5ZnSr/MgO-TEOS	2.7wt%Sr,12.5wt%ZnO/MgO	232	13.3
1.0ZnPO ₄ /SiO ₂ -disp	1.0wt%ZnO,4.0wt%PO ₄ /SiO ₂	60	11.9
1.0ZnCaPO ₄ /SiO ₂ -disp	0.7wt%Ca,1.0wt%ZnO, 4.0wt%PO ₄ /SiO ₂	55	11.8

^{a)} The hydroxyapatite was prepared by a sol-gel process and afterwards ion exchanged. Note: the pure zinc content is given and not the content of zinc oxide.

With all tested catalytic materials increasing the zinc loading led after a maximum to a decrease in the yield (activity) per zinc atom. Possible explanations for this behavior are a higher amount of zinc incorporated into the silica lattice or a larger particle size of the zinc oxide clusters on the silica surface. To avoid

incorporation of the zinc an additional series of flame-made zinc-containing silica catalysts was synthesized. In this series, instead of TEOS a dispersion of silica was used. Thus, the zinc particles had to be preferentially deposited on the silica surface. In fact, the catalytic activity was higher than the activity of the materials synthesized with TEOS (Table 7-6). Note additionally that the surface area was significantly lower than for the Zn-based xerogels (Table 7-2) and the prior series of flame-made materials (Table 7-3). With increasing content of zinc the surface area of the catalysts was slightly decreasing. Nevertheless, the influence of the surface area was rather low compared to the zinc content. The highest conversion was found at a zinc oxide content of 5%. Possibly, lower zinc content led to a decrease of the number of active zinc particles. Higher zinc content afforded predominantly larger particles and not a higher amount of accessible active centers. The use of colloidal silica during synthesis greatly enhanced the catalytic activity of zinc/silica (7.0Zn/SiO₂-disp of Table 7-6, compared to 7.0Zn/SiO₂-TEOS of Table 7-3).

Table 7-6: Catalytic results of the PC synthesis over flame synthesized materials using pre-formed silica particles.

catalyst	catalyst composition	amount / %	surface / m ² g ⁻¹	Y / %
1.0Zn/SiO ₂ -disp	1.3wt%ZnO/SiO ₂	100.2	81.2	14.8
2.5Zn/SiO ₂ -disp	2.5wt%ZnO/SiO ₂	100.3	46.6	20.1
5.0Zn/SiO ₂ -disp	5.0wt%ZnO/SiO ₂	100.0	54.4	28.1
7.0Zn/SiO ₂ -disp	7.0wt%ZnO/SiO ₂	100.0	46.5	26.8
9.0Zn/SiO ₂ -disp	9.0wt%ZnO/SiO ₂	100.1	49.6	20.7
12.5Zn/SiO ₂ -disp	12.5wt%ZnO/SiO ₂	100.2	42.4	21.3
17.0Zn/SiO ₂ -disp	17.0wt%ZnO/SiO ₂	99.6	47.3	23.0
5.0Zn/SiO ₂ -disp	5.0wt%ZnO/SiO ₂ ^{a)}	200.1	54.4	84.7
7.0Zn/SiO ₂ -disp	7.0wt%ZnO/SiO ₂ ^{b)}	200.1	46.5	100.0

^{a)} reaction conditions: temperature 120 °C, time 5 h, 20 mg TBABr. ^{b)} reaction conditions: temperature 120 °C, time 6 h, 20 mg TBABr.

All the test reactions in Table 7-1 to Table 7-6 were performed at differential conversion to demonstrate the difference in the catalytic activity. Yet, at modified conditions (120 °C; 6 h; 45 bar; 200 mg catalysts; 20 mg TBABr; 10 ml/140 mmol PO) the flame-made catalyst showed 100% yield in reasonable reaction time and at moderate temperature (Table 7-6, last entry). The selectivity was always >99% even at a conversion of 100%.

7.3.2 Further Characterization of Selected Samples

To clarify the difference in activity of the flame-made catalysts prepared from TEOS and from colloidal silica solutions, XAS spectra were recorded. The XANES region was very similar, but significant differences were found in the EXAFS region. The Fourier transformed EXAFS spectra are shown in Figure 7-1. The signal at about 1.6 Å can be assigned to the oxygen neighbor and no difference is found between the two catalysts. The curve-fitting analysis resulted in an interatomic Zn–O distance of 1.95 Å, which is in accordance to the Zn–O distances observed in a silica matrix.²¹¹ This is shorter than the Zn–O distance of 1.97 Å in silica-free zinc oxide. At higher *R*-values significant differences were found. Whereas the flame-made catalyst using a solution of TEOS had only small contributions at higher *R*-values, the catalyst resulting from the dispersed silica solution featured a signal at 2.8 Å (not corrected for phase shift), which can be assigned to Zn–O–Zn species. This contribution is significantly higher than that of the TEOS derived flame-made catalysts. In addition, *in situ* spectroscopic studies were performed with a batch reactor cell that can measure both the solid and liquid phase (experiments performed analogously to that of Chapter 5). No significant changes of the solid catalyst could be observed, probably because only a fraction of the zinc atoms was involved in the reaction. Moreover, the investigation of the liquid phase proved no leaching of zinc into the liquid phase during and after reaction. Bromide was detected both on the solid catalyst and in the solution.

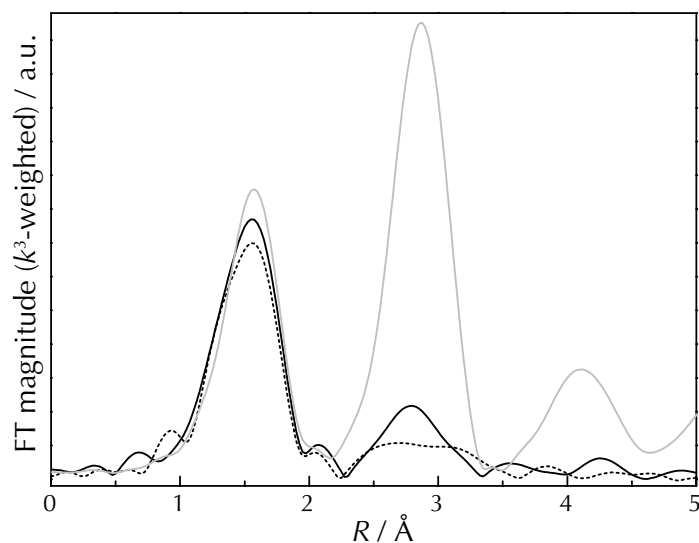


Figure 7-1: Fourier transformed EXAFS spectra. Fourier transformed $k^3 \chi(k)$ function ($k = 2.2 - 14 \text{ \AA}^{-1}$) of catalyst 7.0Zn/SiO₂-disp (solid line) and catalyst 7.0Zn/SiO₂-TEOS (dotted line). As reference the spectrum of ZnO is given (grey line).

STEM measurements coupled with energy dispersive X-ray analysis (EDX) were performed to investigate the different dispersion of zinc oxide on the catalyst 6.3Zn/SiO₂-gel, 7.0Zn/SiO₂-TEOS and 7.0Zn/SiO₂-disp. Rather large zinc containing particles were found on the sol-gel derived catalysts 6.3Zn/SiO₂-gel, typically between 30 and 100 nm. In contrast, an extremely high dispersion was observed for the flame-made catalyst using a solution of 7.0Zn/SiO₂-TEOS (see Figure 7-2 a). The average silica particle size was 7 nm and hardly any zinc oxide particle could be detected by transmission electron microscope (TEM) measurements. Further-more, EDX spectra of different positions showed a constant but low zinc signal over the whole sample. This is consistent with the EXAFS measurements, where only a small Zn–O–Zn contribution at higher R -values was found. The zinc oxide particle size of the catalyst resulting from dispersed silica solution 7.0Zn/SiO₂-disp ranged from 5 to 10 nm (see Figure 7-2 b). This observation is corresponding to the signal found at the Fourier transformed EXAFS spectrum at 2.8 Å, which also showed the formation of Zn–O–Zn clusters.

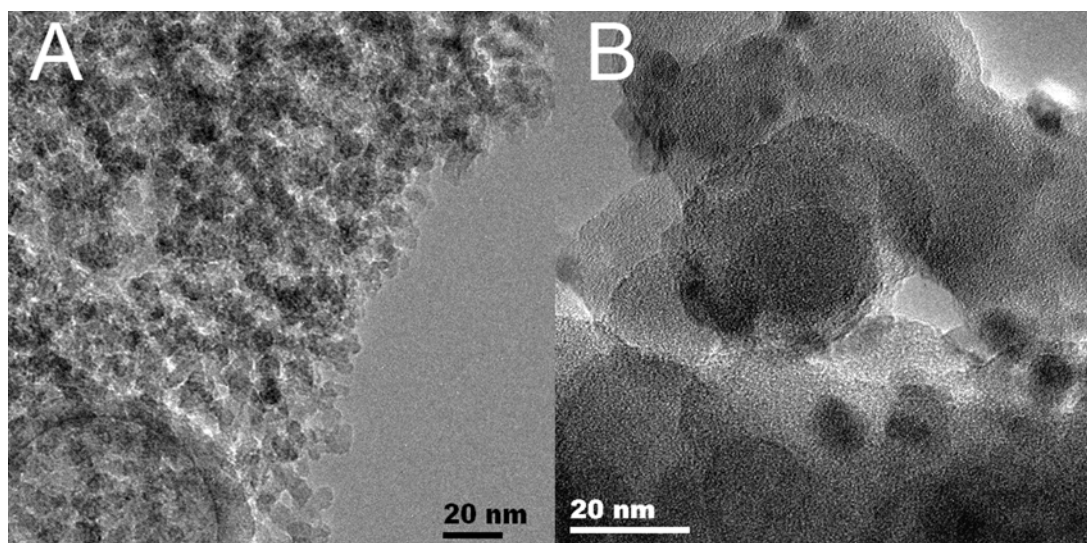


Figure 7-2: TEM pictures of a) 7.0Zn/SiO₂-TEOS and b) 7.0Zn/SiO₂-disp made by flame synthesis.

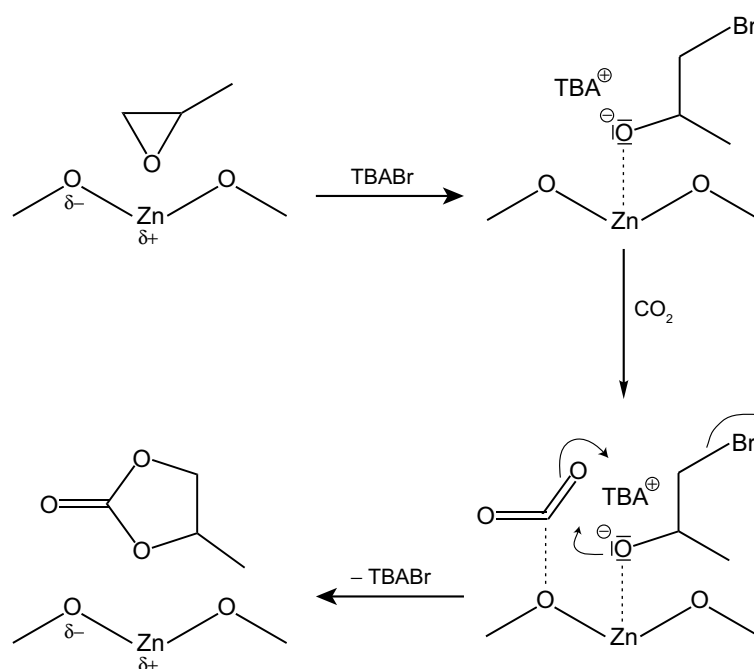
7.4 Discussion

The results show that Zn-based xerogels and flame-made catalysts are good catalysts for the solventless insertion of CO₂ into PO. As outlined in the introduction, up to now, only homogeneous catalysts^{86,92,94–97,100,112,112,121} or heterogeneous organometallic complexes (see ref.^{120,122,124,125,127,130}, Chapter 3, and Chapter 4) were reported to be efficient catalysts. Simple solid oxide or halide catalysts were found to be much less active and the materials investigated in this chapter of the work seem to be an interesting alternative. Catalysts investigated for the solventless PC formation from PO and CO₂ like Cs-P-Si mixed oxide,¹¹⁶ zeolite based organic-inorganic hybrid catalysts,¹¹⁹ as well as polymer-supported nanogold¹³⁰ required a higher catalyst/substrate ratio, higher temperatures and/or longer reaction times. Furthermore, the synthesis of flame-made catalysts is simple and fast. The reactants were dissolved and afterwards sprayed into the flame without any work-up. The highest yields were achieved with catalysts where zinc is decorating the silica particles and, surpris-

ingly, the undoped and doped ZnO materials turned out to be fairly good catalysts as well.

In general, Zn–O–Zn entities seemed to be advantageous for the catalytic activity. With higher loading the catalytic activity increased to a maximum and deposition of zinc on the silica support in the flame synthesis procedure led to a higher catalytic activity although the surface area was smaller (Table 7-6). Notably, small zinc oxide particles in the range of 5 to 10 nm were beneficial for the catalytic activity. The incorporation of Zn in the silica matrix led to a lower catalytic activity and also Zn-exchanged hydroxyapatite was significantly less active. Particularly, the high activity of the ZnO supports the assumption that ZnO-clusters are beneficial for the catalytic activity.

These observations are significantly different from that reported in the literature. Mori et al.¹¹⁴ reported that single-site zinc hydroxyapatite would be an efficient catalyst for the synthesis of other cyclic carbonates like styrene carbonate. In the present study, it appears both from the catalytic results and the EXAFS data that for the PC formation from PO and CO₂ the appearance of Zn–O–Zn entities is beneficial. In the most efficient systems we could evidence Zn–O–Zn interactions by spectroscopy. Since the catalysts are hardly active in the absence of TBABr, the reaction mechanism shown in Scheme 7-2 is proposed. This mechanism is based on the earlier suggested mechanisms reported in ref.¹¹⁵ for the CO₂ absorption on zinc oxides during cycloaddition, and on ref.¹¹³ where the epoxide ring opening by tetrabutyl ammonium halide is described. In studies of immobilized zinc pyridine catalysts TBABr was found to be a co-catalyst for the PC synthesis (see Chapter 5). According to the herein made proposal the reaction is initiated by coordination of the PO on zinc as a Lewis acidic site. Secondly, a bromide attacks the less hindered carbon atom of the coordinated PO followed by ring opening. In parallel CO₂ is activated by the Lewis basic site (O²⁻) of the ZnO/SiO₂. Here Zn–O–Zn species may be beneficial compared to Zn–O–Si species. Finally, the oxygen of the activated CO₂ attacks nucleophilic the carbon atom bonding with bromide, and the PO oxygen attacks the



Scheme 7-2: Reaction mechanism proposed for cycloaddition of CO₂ to PO on a zinc oxide surface with TBABr as co-catalyst.

CO₂ carbon atom to close the PC ring. This reaction mechanism can explain the requirement of a halide co-catalyst and the influence of the Lewis acid and basic site strength.

7.5 Conclusions

Zinc-silicon-oxide materials are effective catalysts for the solventless PC synthesis in dense CO₂ using TBABr as co-catalyst. Both xerogel synthesis and one-step flame spray pyrolysis, which could be performed without any work-up procedure, turned out to be well-suited synthesis methods resulting in high surface area materials. Strikingly, the selective deposition of zinc oxide on silica by using colloidal dispersion of silica in flame synthesis resulted in a significant improvement of the catalyst performance. In general, this approach may be interesting

to avoid substantial incorporation of the catalytically active transition metal into the support matrix during flame synthesis. Both from the catalytic results and the spectroscopic studies, the conclusion can be drawn that not single site zinc but rather zinc oxide clusters are important for the title reaction.

Final Remarks and Outlook

Immobilization of transition metal complexes onto an inert support is a possible path to ‘heterogeneize’ well proven homogeneous catalysts even under the reaction conditions of dense CO₂. However, simple coordinatively bound complexes are not stable enough under these conditions. Only covalently bound complexes showed no leaching of the grafted ligand itself and the metal center.

The remaining catalyst deactivation is mainly due to the loss of the halide, which is beneficial for the activation of the epoxide ring. This finding was the direct result of *in situ* XAS measurements. Such measurements are a well-suited technique for monitoring the structure of a catalyst under real conditions, even under high pressure at elevated temperature. The advantage of *in situ* techniques is obvious compared to other *ex situ* measurements, which were reported in literature and did not discover the important role of the halide. The use of bromide as co-catalyst maintained the catalytic activity of the catalyst system.

The in this thesis reported batch reactor cells for XAS measurements allow *in situ* monitoring of a high pressure reaction at the zinc K-edge and even down to the low energies of the nickel K-edge. Measurements at lower energies are still challenging. However, the know-how gained by the construction and use of these two batch reactor cells, led to a next generation cell by further modification, which makes even measurements at the chromium K-edge possible—simultaneously with UV/Vis spectroscopy. This cell have been tested shortly before this thesis was submitted, and it will be the task of other people to present the results. But this is only the first step of improvement. Even spectroscopic

batch cells for fluorescence XAS measurements or for XAS in combination with IR are imaginable.

Phase behavior measurements are also important for a better comprehension of reactions made in dense gaseous-like mixtures. In this work, it was shown that not the 'supercritical' single-phase region, but a so-called expanded liquid exhibits the highest reaction rates for the synthesis of PC in and with dense CO₂. This reaction is an example that not always single-phase conditions are the most suitable ones for reactions. The complex interaction of many parameters makes it difficult to predict the best reaction conditions. Hence phase behavior measurements can provide useful information about process optimization.

The stability of zinc on silica as well as the finding that bromide plays an important role in the synthesis of PC and can be used as co-catalyst, resulted in the application of zinc silica mixed oxides as catalyst. New catalysts made by flame spray pyrolysis with colloidal silica as precursor, achieved high rates. Not single site zinc was advantageous for this reaction, but small zinc clusters. These catalysts can be simply produced and need no reaction work-up. Maybe, such materials are also beneficial for other reactions.

The very next step in the development of solid catalysts for the synthesis of PC should be the grafting of a halide donating complex onto the zinc silica mixed oxide's surface, to avoid the presence of a co-catalyst. The activity of the herein reported catalysts is in a range, that it is worth testing a continuous flow of the reactants. A long-term objective can be the direct synthesis of cyclic carbonates from olefins/oxygen and CO₂ or the subsequent synthesis of dimethyl carbonate by a carbonate interchange reaction.

Abbreviations

Typical abbreviations and physico-chemical symbols used in this work are collected in this appendix.

Chemical Compounds

DMAP	4-dimethylaminopyridine, <i>N,N</i> -dimethyl-4-pyridinamine
Me	methyl
PC	propylene carbonate, 4-methyl-1,3-dioxolane-2-one
PEEK	polyetheretherketon
PO	propylene oxide, methyloxirane
Py	pyridine
silica-Cl	silica modified with 3-chloropropyltriethoxysilane
silica-NH ₂	silica modified with 3-aminopropyltriethoxysilane
TBABr	tetrabutyl ammonium bromide
TEOS	tetraethyl ortho silicate, tetraethoxysilane

Spectroscopic Techniques and Other Abbreviations

ANKA	Angströmquelle Karlsruhe
ATR-IR	attenuated total reflection infrared spectroscopy
BET	nitrogen physisorption using the theory of Brunauer, Emmett, and Teller
DESY	Deutsches Elektronen-Synchrotron
DRIFTS	diffuse reflectance infrared Fourier transform spectroscopy
EA	elemental analysis

Appendix A Abbreviations

EDX	energy-dispersive X-ray spectroscopy
ESRF	European synchrotron radiation facility
EXAFS	extended X-ray absorption fine structure
FSP	flame spray pyrolysis
HASYLAB	Hamburger Synchrotronstrahlungslabor
ICP-OES	inductively coupled plasma optical emission spectrometry
IR	infrared spectroscopy
IRE	internal reflection element
NMR	nuclear magnetic resonance
STEM	scanning transmission electron microscopy
TA	thermal analysis
TEM	transmission electron microscopy
UV-Vis	ultraviolet-visible spectroscopy
VOC	volatile organic compounds
XANES	X-ray absorption near-edge structure
XAS	X-ray absorption spectroscopy

Physico-chemical Symbols and Variables

A	absorber
B	backscatterer
d_p	penetration depth
δ	density
ΔE_0	shift of the energy threshold
E	energy
h	Planck's constant
k	wavenumber of the photo electron
λ	wavelength
m	mass
n	amount of substance, refractive index
N	coordination number

ν	frequency
p	pressure
r	distance
R	vector in the Cartesian coordinate system
S	selectivity
σ	Debye–Waller factor
t	time, reaction time
T	temperature
θ	angle
TOF	turnover frequency
TON	turnover number
x	mole fraction
X	conversion
Y	yield

Twelve Green Chemistry Principles

The twelve green chemistry principles of Anastas and Warner,^{7,8} as summarized from Winterton.⁹

1. It is better to prevent waste formation than to treat it after it is formed.
2. Design synthetic methods to maximize incorporation of all material used in the process into the final product.
3. Synthetic methods should, where practicable, use or generate materials of low human toxicity and environmental impact.
4. Chemical product design should aim to preserve efficacy whilst reducing toxicity.
5. Auxiliary materials (solvents, extractants etc.) should be avoided if possible or otherwise made innocuous.
6. Energy requirements should be minimized: syntheses should be conducted at ambient temperature/pressure.
7. A raw material should, where practicable, be renewable.
8. Unnecessary derivatisation (such as protection/deprotection) should be avoided, where possible.
9. Selectively catalyzed processes are superior to stoichiometric processes.
10. Chemical products should be designed to be degradable to innocuous products when disposed of and not be environmentally persistent.

11. Process monitoring should be used to avoid excursions leading to the formation of hazardous materials.
12. Materials used in a chemical process should be chosen to minimize hazard and risk.

Additional Analytical Data

C.1 Results of NMR Analysis

C.1.1 Data of Catalyst Precursors

3-Allylsalicylaldehyde

$^1\text{H-NMR}$ (500 MHz, CDCl_3 , TMS, 300 K): δ = 3.4 (d, 2H, $\text{CH}_2\text{CH}=\text{CH}_2$), 5.15 (m, 2H, $\text{CH}=\text{CH}_2$), 5.90 – 6.15 (m, 1H, $\text{CH}=\text{CH}_2$), 6.90 – 7.00 (m, 1H, ArH), 7.38 – 7.48 (m, 2H, ArH), 9.85 (s, 1H, CHO), 11.32 (s, 1H, OH);
 $^{13}\text{C-NMR}$ (500 MHz, CDCl_3 , 300 K): δ = 33.0, 116.5, 119.8, 131.2, 136.0, 137.5, 196.6.

Ligand of Catalyst 38, 39

$^1\text{H-NMR}$ (500 MHz, CDCl_3 , TMS, 300 K): δ = 0.96 (t, $^3\text{J}(\text{H,H}) = 7.4$ Hz, 3H, CH_3), 1.40 (m, 2H, $\text{CH}_3\text{-CH}_2$), 1.70 (m, 2H, $\text{NCH}_2\text{-CH}_2$), 3.66 (dt, $^2\text{J}(\text{H,H}) = 1.2$ Hz, $^3\text{J}(\text{H,H}) = 6.9$ Hz, 2H, N-CH_2), 7.58 (d, $^3\text{J}(\text{H,H}) = 4.4$ Hz, 2H, 3,5-pyridyl), 8.26 (s, 1H, $\text{CH}=\text{N}$), 8.68 (d, $^3\text{J}(\text{H,H}) = 4.4$ Hz, 2H, 2,6-pyridyl).

Ligand of Catalyst 40, 41

$^1\text{H-NMR}$ (500 MHz, CDCl_3 , TMS, 300 K): δ = 0.68 (t, $^3\text{J}(\text{H,H}) = 8.4$ Hz, 2H, $\text{CH}_2\text{-Si}$), 1.23 (t, $^3\text{J}(\text{H,H}) = 7.0$ Hz, 9H, CH_3), 1.85 (tt, $^3\text{J}(\text{H,H}) = 6.9$ Hz, $^3\text{J}(\text{H,H}) = 8.4$ Hz, 2H, $\text{NCH}_2\text{-CH}_2$), 3.67 (dt, $^2\text{J}(\text{H,H}) = 1.3$ Hz, $^3\text{J}(\text{H,H}) = 6.9$ Hz, 2H, N-CH_2), 3.83 (q, $^3\text{J}(\text{H,H}) = 7.0$ Hz, 6H, O-CH_2),

7.59 (d, $^3J(\text{H,H}) = 4.4$ Hz, 2H, 2,6-pyridyl), 8.26 (s, 1H, $\text{CH}=\text{N}$), 8.67 (d, $^3J(\text{H,H}) = 4.4$ Hz, 2H, 3,5-pyridyl).

C.1.2 NMR Data of Catalysts

Catalyst 34

^1H -NMR (500 MHz, $[\text{D}_6]$ DMSO, 300 K): $\delta = 7.44$ (m, 4H, 3,5-pyridyl), 7.84 (m, 2H, 4-pyridyl), 8.59 (m, 4H, 2,6-pyridyl).

^{13}C -NMR (500 MHz, $[\text{D}_6]$ DMSO, 300 K): $\delta = 124.7$ (4C, 3,5-pyridyl), 138.1 (2C, 4-pyridyl), 148.9 (4C, 2,6-pyridyl).

Catalyst 35

^1H -NMR (500 MHz, $[\text{D}_6]$ DMSO, 300 K): $\delta = 1.80$ (s, 6H, CH_3), 7.40 (m, 4H, 3,5-pyridyl), 7.80 (m, 2H, 4-pyridyl), 8.58 (m, 4H, 2,6-pyridyl).

^{13}C -NMR (500 MHz, $[\text{D}_6]$ DMSO, 300 K): $\delta = 22.4$ (2C, CH_3), 124.7 (4C, 3,5-pyridyl), 138.4 (2C, 4-pyridyl), 149.1 (4C, 2,6-pyridyl), 177.1 (2C, COO).

Catalyst 36

^1H -NMR (500 MHz, $[\text{D}_6]$ DMSO, 300 K): $\delta = 7.82$ (d, $^3J(\text{H,H}) = 5.9$ Hz, 4H, 3,5-pyridyl), 8.89 (d, $^3J(\text{H,H}) = 5.9$ Hz, 4H, 2,6-pyridyl), 10.10 (s, 2H, CHO).

^{13}C -NMR (500 MHz, $[\text{D}_6]$ DMSO, 300 K): $\delta = 122.4$ (4C, 3,5-pyridyl), 141.6 (2C, 4-pyridyl), 150.8 (4C, 2,6-pyridyl), 193.1 (2C, CHO).

Catalyst 37

^1H -NMR (500 MHz, $[\text{D}_6]$ DMSO, 300 K): $\delta = 1.83$ (s, 6H, CH_3), 7.87 (d, $^3J(\text{H,H}) = 4.4$ Hz, 4H, 3,5-pyridyl), 8.89 (d, $^3J(\text{H,H}) = 4.4$ Hz, 4H, 2,6-pyridyl), 10.11 (s, 2H, CHO).

^{13}C -NMR (500 MHz, $[\text{D}_6]$ DMSO, 300 K): $\delta = 22.4$ (2C, CH_3), 122.4 (4C, 3,5-pyridyl), 141.6 (2C, 4-pyridyl), 150.9 (4C, 2,6-pyridyl), 177.0 (2C, COO), 193.1 (2C, CHO).

Catalyst 38

$^1\text{H-NMR}$ (500 MHz, $[\text{D}_6]$ DMSO, 300 K): $\delta=0.92$ (t, $^3\text{J}(\text{H,H}) = 7.5$ Hz, 6H, $\text{CH}_2\text{-CH}_3$), 1.35 (tq, 4H, $\text{CH}_3\text{-CH}_2$), 1.62 (tt, 4H, $\text{N-CH}_2\text{-CH}_2$), 3.64 (t, $^3\text{J}(\text{H,H}) = 6.9$ Hz, 4H, N-CH_2), 7.77 (d, $^3\text{J}(\text{H,H}) = 6.0$ Hz, 4H, 3,5-pyridyl), 8.42 (s, 2H, CHN), 8.71 (d, $^3\text{J}(\text{H,H}) = 6.0$ Hz, 4H, 2,6-pyridyl).

$^{13}\text{C-NMR}$ (500 MHz, $[\text{D}_6]$ DMSO, 300 K): $\delta=13.7$ (2C, $\text{CH}_2\text{-CH}_3$), 19.8 (2C, $\text{CH}_3\text{-CH}_2$), 32.2 (2C, $\text{N-CH}_2\text{-CH}_2$), 60.2 (2C, N-CH_2), 122.1 (4C, 3,5-pyridyl), 143.5 (2C, 4-pyridyl), 149.9 (4C, 2,6-pyridyl), 159.0 (2C, CHN).

Catalyst 39

$^1\text{H-NMR}$ (500 MHz, $[\text{D}_6]$ DMSO, 300 K): $\delta=0.91$ (t, $^3\text{J}(\text{H,H}) = 7.5$ Hz, 6H, $\text{CH}_2\text{-CH}_3$), 1.34 (tq, 4H, $\text{CH}_3\text{-CH}_2$), 1.62 (tt, 4H, $\text{N-CH}_2\text{-CH}_2$), 1.83 (s, 6H, COOCH_3), 3.63 (t, $^3\text{J}(\text{H,H}) = 6.9$ Hz, 4H, N-CH_2), 7.72 (d, $^3\text{J}(\text{H,H}) = 4.5$ Hz, 4H, 3,5-pyridyl), 8.40 (s, 2H, CHN), 8.68 (d, $^3\text{J}(\text{H,H}) = 4.5$ Hz, 4H, 2,6-pyridyl).

$^{13}\text{C-NMR}$ (500 MHz, $[\text{D}_6]$ DMSO, 300 K): $\delta=13.7$ (2C, $\text{CH}_2\text{-CH}_3$), 20.0 (2C, $\text{CH}_3\text{-CH}_2$), 22.4 (2C, COO-CH_3), 32.4 (2C, $\text{N-CH}_2\text{-CH}_2$), 60.4 (2C, N-CH_2), 122.3 (4C, 3,5-pyridyl), 143.9 (2C, 4-pyridyl), 150.0 (4C, 2,6-pyridyl), 159.0 (2C, CHN), 177.4 (2C, COO).

Catalyst 40

$^1\text{H-NMR}$ (500 MHz, $[\text{D}_6]$ DMSO, 300 K): $\delta=0.61$ (t, $^3\text{J}(\text{H,H}) = 8.3$ Hz, 4H, $\text{CH}_2\text{-Si}$), 1.15 (t, $^3\text{J}(\text{H,H}) = 7.0$ Hz, 18H, CH_3), 1.72 (tt, 4H, $\text{CH}_2\text{-CH}_2\text{-Si}$), 3.63 (t, $^3\text{J}(\text{H,H}) = 6.4$ Hz, 4H, N-CH_2), 3.76 (q, $^3\text{J}(\text{H,H}) = 7.0$ Hz, 12H, O-CH_2), 7.76 (d, $^3\text{J}(\text{H,H}) = 6.0$ Hz, 4H, 3,5-pyridyl), 8.40 (s, 2H, CHN), 8.70 (d, $^3\text{J}(\text{H,H}) = 6.0$ Hz, 4H, 2,6-pyridyl).

$^{13}\text{C-NMR}$ (500 MHz, $[\text{D}_6]$ DMSO, 300 K): $\delta=7.5$ (2C, $\text{CH}_2\text{-Si}$), 18.2 (6C, CH_3), 23.8 (2C, $\text{CH}_2\text{-CH}_2\text{-Si}$), 57.6 (6C, O-CH_2), 63.0 (2C, N-CH_2), 122.0 (4C, 3,5-pyridyl), 143.3 (2C, 4-pyridyl), 150.0 (4C, 2,6-pyridyl), 159.3 (2C, CHN).

Catalyst 41

$^1\text{H-NMR}$ (500 MHz, $[\text{D}_6]\text{DMSO}$, 300 K): $\delta=0.62$ (t, $^3\text{J}(\text{H,H}) = 8.4$ Hz, 4H, $\text{CH}_2\text{-Si}$), 1.17 (t, $^3\text{J}(\text{H,H}) = 7.0$ Hz, 18H, $\text{CH}_2\text{-CH}_3$), 1.74 (tt, 4H, $\text{CH}_2\text{-CH}_2\text{-Si}$), 1.87 (s, 6H, COO-CH_3), 3.63 (t, $^3\text{J}(\text{H,H}) = 6.4$ Hz, 4H, N-CH_2), 3.77 (q, $^3\text{J}(\text{H,H}) = 7.0$ Hz, 12H, O-CH_2), 7.77 (d, $^3\text{J}(\text{H,H}) = 6.1$ Hz, 4H, 3,5-pyridyl), 8.41 (s, 2H, CHN), 8.71 (d, $^3\text{J}(\text{H,H}) = 6.1$ Hz, 4H, 2,6-pyridyl).

$^{13}\text{C-NMR}$ (500 MHz, $[\text{D}_6]\text{DMSO}$, 300 K): $\delta=7.6$ (2C, $\text{CH}_2\text{-Si}$), 18.2 (6C, CH_3), 22.4 (2C, COO-CH_3), 23.9 (2C, $\text{CH}_2\text{-CH}_2\text{-Si}$), 57.7 (6C, O-CH_2), 63.2 (2C, N-CH_2), 122.1 (4C, 3,5-pyridyl), 143.6 (2C, 4-pyridyl), 150.1 (4C, 2,6-pyridyl), 159.3 (2C, CHN), 177.1 (2C, COO).

C.2 Results of the Elemental Analysis

Catalyst 34

theoretical values ($\text{C}_{10}\text{H}_{10}\text{Br}_2\text{N}_2\text{Zn}$) C 31.33%, H 2.63%, N 7.31%;
obtained C 31.41%, H 2.59%, N 7.28%.

Catalyst 36

theoretical values ($\text{C}_{12}\text{H}_{10}\text{Br}_2\text{N}_2\text{O}_2\text{Zn}$) C 32.80%, H 2.29%, N 6.38%;
obtained C 32.79%, H 2.29%, N 6.36%.

Catalyst 38

theoretical values ($\text{C}_{20}\text{H}_{28}\text{Br}_2\text{N}_4\text{Zn}$) C 43.70%, H 5.13%, N 10.19%;
obtained C 43.77%, H 5.02%, N 10.08%.

Catalyst 40

theoretical values ($\text{C}_{30}\text{H}_{52}\text{Br}_2\text{N}_4\text{O}_6\text{Si}_2\text{Zn}$) C 42.59%, H 6.19%, N 6.62%;
obtained C 42.83%, H 6.11%, N 6.91%.

References

1. I. C. Prentice, G. D. Farquhar, M. J. R. Fasham, M. L. Goulden, M. Heimann, V. J. Jaramillo, H. S. Kheshgi, C. Le Quéré, R. J. Scholes, D. W. R. Wallace, in: J. Houghton, Y. Ding, D. J. Griggs, M. Noguer, P. J. van der Linden, X. Dai, K. Maskell, C. A. Johnson (Eds.), *Climate Change 2001: The Scientific Basis*, Cambridge University Press: Cambridge, 2001, pp. 183–237.
2. B. Clark, R. York, *Theory Society* 34 (2005) 391.
3. I. C. Prentice, M. Heimann, S. Sitch, *Ecol. Appl.* 10 (2000) 1553.
4. N. W. Arnell, M. G. R. Cannell, M. Hulme, R. S. Kovats, J. F. B. Mitchell, R. J. Nicholls, M. L. Parry, M. T. J. Livermore, A. White, *Clim. Change* 53 (2002) 413.
5. M. L. Khandekar, T. S. Murty, P. Chittibabu, *Pure Appl. Geophys.* 162 (2005) 1557.
6. *Kyoto Protocol to the United Nations Framework Convention on Climate Change*, Kyoto, 1997.
7. P. T. Anastas, T. C. Williamson, in: P. T. Anastas, T. C. Williamson (Eds.), *Green Chemistry: Frontiers in Benign Chemical Synthesis and Processes*, Oxford University Press: Oxford, 1998, pp. 1–27.
8. P. T. Anastas, J. C. Warner, *Green Chemistry: Theory and Practice*, Oxford University Press: Oxford, 1998.
9. N. Winterton, *Green Chem.* 3 (2001) G73.
10. H. Arakawa, M. Aresta, J. N. Armor, M. A. Barteau, E. J. Beckman, A. T. Bell, J. E. Bercaw, C. Creutz, E. Dinjus, D. A. Dixon, K. Domen, D. L. DuBois, J. Eckert, E. Fujita, D. H. Gibson, W. A. Goddard, D. W. Goodman, J. Keller, G. J. Kubas, H. H. Kung, J. E. Lyons, L. E. Manzer, T. J. Marks, K. Morokuma, K. M. Nicholas, R. Periana, L. Que, J.

- Rostrup-Nielson, W. M. H. Sachtler, L. D. Schmidt, A. Sen, G. A. Somorjai, P. C. Stair, B. R. Stults, W. Tumas, *Chem. Rev.* 101 (2001) 953.
11. M. Aresta, E. Quaranta, *Chemtech* 27 (1997) 32.
 12. A. Behr, *Angew. Chem., Int. Ed. Engl.* 27 (1988) 661.
 13. R. P. A. Sneed, *Compr. Organomet. Chem.* 2: 1982–1994 8 (1995) 225.
 14. A. A. Clifford, in: E. Kiran, J. M. H. Levelt Sengers (Eds.), *Supercritical Fluids – Fundamentals for Application*, Kluwer Academic Publishers: Dordrecht, 1994, pp. 449–479.
 15. A. Baiker, *Appl. Organomet. Chem.* 14 (2000) 751.
 16. J. D. Grunwaldt, A. Baiker, *Phys. Chem. Chem. Phys.* 7 (2005) 3526.
 17. J. D. Grunwaldt, R. Wandeler, A. Baiker, *Catal. Rev.* 45 (2003) 1.
 18. W. Leitner, *Coord. Chem. Rev.* 153 (1996) 257.
 19. *Carbon and Graphite Fibers to Chlorocarbons and Chlorohydrocarbons*, K. Othmer (Ed.), *Encyclopedia of Chemical Technology*, Vol. 5, 4th Ed., Wiley Interscience: New York, 1993.
 20. J. L. Sarmiento, T. M. C. Hughes, R. J. Stouffer, S. Manabe, *Nature* 393 (1998) 245.
 21. M. Cao, F. I. Woodward, *Nature* 393 (1998) 249.
 22. D. Schimel, *Nature* 393 (1998) 208.
 23. X. D. Xu, J. A. Moulijn, *Energy Fuels* 10 (1996) 305.
 24. D. R. Lide (Ed.), *Handbook of Chemistry and Physics*, 85th Ed., CRC Press: Boca Raton, 2004–2005.
 25. J. M. H. Levelt Sengers, in: E. Kiran, J. M. H. Levelt Sengers (Eds.), *Supercritical Fluids – Fundamentals for Application*, Kluwer Academic Publishers: Dordrecht, 1994, pp. 3–38.
 26. G. M. Schneider, in: E. Kiran, J. M. H. Levelt Sengers (Eds.), *Supercritical Fluids – Fundamentals for Application*, Kluwer Academic Publishers: Dordrecht, 1994, pp. 91–115.
 27. C. J. Peters, in: E. Kiran, J. M. H. Levelt Sengers (Eds.), *Supercritical Fluids – Fundamentals for Application*, Kluwer Academic Publishers: Dordrecht, 1994, pp. 117–145.
 28. R. Wandeler, A. Baiker, *CATTECH* 4 (2000) 128.
 29. W. Leitner, *Appl. Organomet. Chem.* 14 (2000) 809.

30. A. Baiker, *Chem. Rev.* 99 (1999) 453.
31. F. Cansell, C. Aymonier, A. Loppinet-Serani, *Curr. Opin. Solid State Mater. Sci.* 7 (2003) 331.
32. I. J. Barnabas, J. R. Dean, S. P. Owen, *Analyst* 119 (1994) 2381.
33. J. M. Del Valle, J. C. De La Fuente, *Crit. Rev. Food Sci. Nutr.* 46 (2006) 131.
34. M. V. Palmer, S. S. T. Ting, *Food Chem.* 52 (1995) 345.
35. T. W. Randolph, H. W. Blanch, J. M. Prausnitz, C. R. Wilke, *Biotechnol. Lett.* 7 (1985) 325.
36. T. Dumont, D. Barth, M. Perrut, *J. Supercrit. Fluids* 6 (1993) 85.
37. M. Aresta, *Recovery and Utilisation of Carbon Dioxide*, EU-report, 2001.
38. F. Shi, Y. Q. Deng, T. L. SiMa, J. J. Peng, Y. L. Gu, B. T. Qiao, *Angew. Chem., Int. Ed.* 42 (2003) 3257.
39. Y. Kosugi, M. A. Rahim, K. Takahashi, Y. Imaoka, M. Kitayama, *Appl. Organomet. Chem.* 14 (2000) 841.
40. H. Kolbe, E. Lautemann, *Ann. Chem.* 115 (1860) 178.
41. R. Schmitt, *J. Prakt. Chem.* 31 (1885) 397.
42. A. S. Lindsey, H. Jeskey, *Chem. Rev.* 57 (1957) 583.
43. D. J. Darensbourg, J. C. Yarbrough, *J. Am. Chem. Soc.* 124 (2002) 6335.
44. S. Inoue, H. Koinuma, T. Tsuruta, *J. Polym. Sci., Part B: Polym. Lett.* 7 (1969) 287.
45. S. Inoue, H. Koinuma, T. Tsuruta, *Makromol. Chem.* 130 (1969) 210.
46. G. A. Luinstra, G. R. Haas, F. Molnar, V. Bernhart, R. Eberhardt, B. Rieger, *Chem. – Eur. J.* 11 (2005) 6298.
47. D. Chaturvedi, S. Ray, *Monatsh. Chem.* 137 (2006) 127.
48. M. Rohr, C. Geyer, R. Wandeler, M. S. Schneider, E. F. Murphy, A. Baiker, *Green Chem.* 3 (2001) 123.
49. M. Shi, K. M. Nicholas, *J. Am. Chem. Soc.* 119 (1997) 5057.
50. D. X. Shi, Y. Q. Feng, S. H. Zhong, *Catal. Today* 98 (2004) 505.
51. E. M. Wilcox, G. W. Roberts, J. J. Spivey, *Catal. Today* 88 (2003) 83.
52. T. Sakakura, J. C. Choi, Y. Saito, T. Sako, *Polyhedron* 19 (2000) 573.
53. K. Iwakabe, M. Nakaiwa, T. Sakakura, J. C. Choi, H. Yasuda, T. Takahashi, Y. Ooshima, *J. Chem. Eng. Jpn.* 38 (2005) 1020.

References

54. M. Aresta, A. Dibenedetto, E. Fracchiolla, P. Giannoccaro, C. Pastore, I. Papai, G. Schubert, *J. Org. Chem.* 70 (2005) 6177.
55. K. Tomishige, T. Sakaihorii, Y. Ikeda, K. Fujimoto, *Catal. Lett.* 58 (1999) 225.
56. T. Tsuda, K. Maruta, Y. Kitaike, *J. Am. Chem. Soc.* 114 (1992) 1498.
57. A. Behr, M. Heite, *Chem. Eng. Technol.* 23 (2000) 952.
58. P. S. Schulz, O. Walter, E. Dinjus, *Appl. Organomet. Chem.* 19 (2005) 1176.
59. M. Takimoto, M. Mori, *J. Am. Chem. Soc.* 124 (2002) 10008.
60. W. McGhee, D. Riley, K. Christ, Y. Pan, B. Parnas, *J. Org. Chem.* 60 (1995) 2820.
61. B. Ochiai, S. Inoue, T. Endo, *J. Polym. Sci., Part A : Polym. Chem.* 43 (2005) 6613.
62. S. Derien, E. Dunach, J. Perichon, *J. Am. Chem. Soc.* 113 (1991) 8447.
63. K. Shimizu, M. Takimoto, Y. Sato, M. Mori, *Org. Lett.* 7 (2005) 195.
64. D. Ballivet-Tkatchenko, J. C. Folest, J. Tanji, *Appl. Organomet. Chem.* 14 (2000) 847.
65. G. Filardo, S. Gambino, G. Silvestri, A. Gennaro, E. Vianello, *J. Electroanal. Chem.* 177 (1984) 303.
66. D. Y. Hong, J. S. Chang, V. P. Vislovskiy, S. E. Park, Y. H. Park, J. S. Yoo, *Chem. Lett.* 35 (2006) 28.
67. S. B. Wang, Z. H. Zhu, *Energy Fuels* 18 (2004) 1126.
68. C. Amatore, A. Jutand, F. Khalil, M. F. Nielsen, *J. Am. Chem. Soc.* 114 (1992) 7076.
69. J. Bringmann, E. Dinjus, *Appl. Organomet. Chem.* 15 (2001) 135.
70. N. Hoshi, T. Suzuki, Y. Hori, *J. Electroanal. Chem.* 416 (1996) 61.
71. S. Ishimaru, R. Shiratsuchi, G. Nogami, *J. Electrochem. Soc.* 147 (2000) 1864.
72. Y. Hori, A. Murata, R. Takahashi, S. Suzuki, *J. Chem. Soc., Chem. Comm.* (1988) 17.
73. A. A. G. Shaikh, S. Sivaram, *Chem. Rev.* 96 (1996) 951.
74. J. Y. Song, Y. Y. Wang, C. C. Wan, *J. Power Sources* 77 (1999) 183.

75. *Ingredient Report: Propylene Carbonate*, Environmentyl Working Group – Skin Deep, Washington, 2006, www.ewg.org.
76. J. P. Senet, *C. R. Acad. Sci. Sér. 2c : Chim.* 3 (2000) 505.
77. I. J. Drake, K. L. Fajdala, A. T. Bell, T. D. Tilley, *J. Catal.* 230 (2005) 14.
78. B. C. Dunn, C. Guenneau, S. A. Hilton, J. Pahnke, E. M. Eyring, *Energy Fuels* 16 (2002) 177.
79. A. M. Paquin, *Z. Naturforsch.* 1 (1946) 518.
80. Y. Li, X. Q. Zhao, Y. J. Wang, *Appl. Catal., A* 279 (2005) 205.
81. J. S. Tian, J. Q. Wang, J. Y. Chen, J. G. Fan, F. Cai, L. N. He, *Appl. Catal., A* 301 (2006) 215.
82. I. Noriko, Mitsubishi Chem Corp, Patent JP7267944 (1995).
83. N. Kihara, N. Hara, T. Endo, *J. Org. Chem.* 58 (1993) 6198.
84. G. Rokicki, W. Kuran, *Bull. Chem. Soc. Jpn.* 57 (1984) 1662.
85. G. Rokicki, W. Kuran, B. Pogorzelskamarciniak, *Monatsh. Chem.* 115 (1984) 205.
86. A. Baba, T. Nozaki, H. Matsuda, *Bull. Chem. Soc. Jpn.* 60 (1987) 1552.
87. S. A. Lermontov, S. V. Shkavrov, A. S. Lermontov, S. I. Zavorin, *Russ. Chem. Bull.* 47 (1998) 1607.
88. M. Ratzenhofer, H. Kisch, *Angew. Chem., Int. Ed. Engl.* 19 (1980) 317.
89. L. N. He, H. Yasuda, T. Sakakura, *Green Chem.* 5 (2003) 92.
90. D. J. Darensbourg, S. J. Lewis, J. L. Rodgers, J. C. Yarbrough, *Inorg. Chem.* 42 (2003) 581.
91. D. J. Darensbourg, D. R. Billodeaux, *Inorg. Chem.* 44 (2005) 1433.
92. H. S. Kim, J. J. Kim, B. G. Lee, O. S. Jung, H. G. Jang, S. O. Kang, *Angew. Chem., Int. Ed.* 39 (2000) 4096.
93. H. S. Kim, J. J. Kim, S. D. Lee, M. S. Lah, D. Moon, H. G. Jang, *Chem. – Eur. J.* 9 (2003) 678.
94. R. L. Paddock, S. T. Nguyen, *J. Am. Chem. Soc.* 123 (2001) 11498.
95. R. L. Paddock, S. T. Nguyen, *Chem. Commun.* (2004) 1622.
96. X. B. Lu, Y. J. Zhang, B. Liang, X. Li, H. Wang, *J. Mol. Catal. A : Chem.* 210 (2004) 31.
97. X. B. Lu, X. J. Feng, R. He, *Appl. Catal., A* 234 (2002) 25.

References

98. X. B. Lu, B. Liang, Y. J. Zhang, Y. Z. Tian, Y. M. Wang, C. X. Bai, H. Wang, R. Zhang, *J. Am. Chem. Soc.* 126 (2004) 3732.
99. X. B. Lu, Y. J. Zhang, K. Jin, L. M. Luo, H. Wang, *J. Catal.* 227 (2004) 537.
100. F. W. Li, C. G. Xia, L. W. Xu, W. Sun, G. X. Chen, *Chem. Commun.* (2003) 2042.
101. Y. H. Chang, T. Jiang, B. X. Han, Z. M. Liu, W. Z. Wu, L. Gao, J. C. Li, H. X. Gao, G. Y. Zhao, J. Huang, *Appl. Catal., A* 263 (2004) 179.
102. H. Kawanami, A. Sasaki, K. Matsui, Y. Ikushima, *Chem. Commun.* (2003) 896.
103. F. W. Li, L. F. Xiao, C. G. Xia, B. Hu, *Tetrahedron Lett.* 45 (2004) 8307.
104. J. M. Sun, S. Fujita, F. Y. Zhao, M. Arai, *Green Chem.* 6 (2004) 613.
105. J. Palgunadi, O. S. Kwon, H. Lee, J. Y. Bae, B. S. Ahn, N. Y. Min, H. S. Kim, *Catal. Today* 98 (2004) 511.
106. S. Fujita, B. M. Bhanage, Y. Ikushima, M. Shirai, K. Torii, M. Arai, *Catal. Lett.* 79 (2002) 95.
107. B. M. Bhanage, S. Fujita, Y. Ikushima, K. Torii, M. Arai, *Green Chem.* 5 (2003) 71.
108. H. Yasuda, L. N. He, T. Sakakura, *J. Catal.* 209 (2002) 547.
109. H. Kawanami, Y. Ikushima, *Chem. Commun.* (2000) 2089.
110. K. Yamaguchi, K. Ebitani, T. Yoshida, H. Yoshida, K. Kaneda, *J. Am. Chem. Soc.* 121 (1999) 4526.
111. H. Yasuda, L.-N. He, T. Takahashi, T. Sakakura, *Appl. Catal., A* 298 (2006) 177.
112. M. Aresta, A. Dibenedetto, L. Gianfrate, C. Pastore, *Appl. Catal., A* 255 (2003) 5.
113. J. M. Sun, S. I. Fujita, F. Y. Zhao, M. Arai, *Appl. Catal., A* 287 (2005) 221.
114. K. Mori, Y. Mitani, T. Hara, T. Mizugaki, K. Ebitani, K. Kaneda, *Chem. Commun.* (2005) 3331.
115. M. Sankar, N. H. Tarte, P. Manikandan, *Appl. Catal., A* 276 (2004) 217.
116. H. Yasuda, L.-N. He, T. Sakakura, C. Hu, *J. Catal.* 233 (2005) 119.
117. Y. Du, F. Cai, D. L. Kong, L. N. He, *Green Chem.* 7 (2005) 518.
118. M. Tu, R. J. Davis, *J. Catal.* 199 (2001) 85.

119. R. Srivastava, D. Srinivas, P. Ratnasamy, *Appl. Catal., A* 289 (2005) 128.
120. X. B. Lu, H. Wang, R. He, *J. Mol. Catal. A : Chem.* 186 (2002) 33.
121. R. Srivastava, D. Srinivas, P. Ratnasamy, *Catal. Lett.* 89 (2003) 81.
122. A. Barbarini, R. Maggi, A. Mazzacani, G. Mori, G. Sartori, R. Sartorio, *Tetrahedron Lett.* 44 (2003) 2931.
123. R. Srivastava, D. Srinivas, P. Ratnasamy, *J. Catal.* 233 (2005) 1.
124. C. Baleizao, B. Gigante, M. J. Sabater, H. Garcia, A. Corma, *Appl. Catal., A* 228 (2002) 279.
125. M. B. Lu, J. H. Xiu, R. He, K. Jin, L. M. Luo, X. J. Feng, *Appl. Catal., A* 275 (2004) 73.
126. M. Alvaro, C. Baleizao, D. Das, E. Carbonell, H. Garcia, *J. Catal.* 228 (2004) 254.
127. H. S. Kim, J. J. Kim, H. N. Kwon, M. J. Chung, B. G. Lee, H. G. Jang, *J. Catal.* 205 (2002) 226.
128. T. Nishikubo, A. Kameyama, J. Yamashita, M. Tomoi, W. Fukuda, *J. Polym. Sci., Part A : Polym. Chem.* 31 (1993) 939.
129. Y. Du, J. Q. Wang, J. Y. Chen, F. Cai, J. S. Tian, D. L. Kong, L. N. He, *Tetrahedron Lett.* 47 (2006) 1271.
130. F. Shi, Q. H. Zhang, Y. B. Ma, Y. D. He, Y. Q. Deng, *J. Am. Chem. Soc.* 127 (2005) 4182.
131. B. Cornils, W. A. Herrmann, R. Schlögl, C.-H. Wong (Eds.), *Catalysis from A to Z : A Concise Encyclopedia*, 2nd ed., Wiley-VCH: Weinheim, 2003.
132. P. McMorn, G. J. Hutchings, *Chem. Soc. Rev.* 33 (2004) 108.
133. M. H. Valkenberg, W. F. Holderich, *Catal. Rev.* 44 (2002) 321.
134. W. Keim, B. Driessen-Hölscher, in: G. Ertl, H. Knözinger, J. Weitkamp (Eds.), *Handbook of Heterogeneous Catalysis*, Wiley-VCH: Weinheim, 1997, pp. 231–240.
135. T. Mallat, A. Baiker, *Appl. Catal., A* 200 (2000) 3.
136. G. Schulz-Ekloff, S. Ernst, in: G. Ertl, H. Knözinger, J. Weitkamp (Eds.), *Handbook of Heterogeneous Catalysis*, Wiley-VCH: Weinheim, 1997, pp. 374–386.

References

137. C. Louis, M. Che, in: G. Ertl, H. Knözinger, J. Weitkamp (Eds.), *Handbook of Heterogeneous Catalysis*, Wiley-VCH: Weinheim, 1997, pp. 207–216.
138. K. G. Allum, R. D. Hancock, I. V. Howell, S. McKenzie, R. C. Pitkethly, P. J. Robinson, *J. Organomet. Chem.* 87 (1975) 203.
139. D. Brunel, A. Cauvel, F. Fajula, F. DiRenzo, *Stud. Surf. Sci. Catal.* 97 (1995) 173.
140. L. Damoense, M. Datt, M. Green, C. Steenkamp, *Coord. Chem. Rev.* 248 (2004) 2393.
141. N. I. Sakellaros, S. G. Kazarian, *J. Chem. Thermodynamics* 37 (2005) 621.
142. R. Bini, R. Ballerini, G. Pratesi, H. J. Jodl, *Rev. Sci. Instrum.* 68 (1997) 3154.
143. U. Wolf, R. Leiberich, J. Seeba, *Catal. Today* 49 (1999) 411.
144. A. Tolia, T. Wilke, M. J. Weaver, C. G. Takoudis, *Chem. Eng. Sci.* 47 (1992) 2781.
145. D. A. Masten, B. R. Foy, D. M. Harradine, R. B. Dyer, *J. Phys. Chem.* 97 (1993) 8557.
146. J. Lu, B. X. Han, H. K. Yan, *Phys. Chem. Chem. Phys.* 1 (1999) 3269.
147. N. Elvassore, A. Bertucco, V. Di Noto, *J. Chem. Eng. Data* 47 (2002) 223.
148. G. Laurency, M. Faure, L. Vieille-Petit, G. Suss-Fink, T. R. Ward, *Adv. Synth. Catal.* 344 (2002) 1073.
149. M. M. Hoffmann, M. S. Conradi, *J. Supercritical Fluids* 14 (1998) 31.
150. I. T. Horvath, J. M. Millar, *Chem. Rev.* 91 (1991) 1339.
151. J. L. deGrazia, T. W. Randolph, J. A. O'Brien, *J. Phys. Chem. A* 102 (1998) 1674.
152. S. Ganapathy, T. W. Randolph, C. Carlier, J. A. O'Brien, *Int. J. Thermophys.* 17 (1996) 471.
153. K. Takahashi, C. D. Jonah, *Chem. Phys. Lett.* 264 (1997) 297.
154. A. K. Cheetham, A. P. Wilkinson, *Angew. Chem., Int. Ed. Engl.* 31 (1992) 1557.
155. D. Bazin, L. Guzzi, *Appl. Catal., A* 213 (2001) 147.
156. J. D. Grunwaldt, M. Ramin, M. Rohr, A. Michailovski, G. R. Patzke, A. Baiker, *Rev. Sci. Instrum.* 76 (2005) 054104.

157. J. D. Grunwaldt, M. Caravati, M. Ramin, A. Baiker, *Catal. Lett.* 90 (2003) 221.
158. N. J. Harrick, *Internal Reflection Spectroscopy*, Harrick Scientific Corporation: Ossing, 1979.
159. U. P. Fringeli, in: J. C. Lindon, G. E. Tranter, J. L. Holmes (Eds.), *Encyclopedia of Spectroscopy and Spectrometry*, Academic Press: San Diego, 1999, pp. 58–75.
160. G. Margaritondo, *Elements of Synchrotron Light*, Oxford University Press: Oxford, 2002.
161. K. Asakura, in: Y. Iwasawa (Ed.), *Series on Synchrotron Radiation Techniques and Applications*, Vol. 2, World Scientific: Singapore, 1996, pp. 33–58.
162. D. C. Koningsberger, R. Prins, *TrAC Trends Anal. Chem.* 1 (1981) 16.
163. D. C. Koningsberger, R. Prins, *Chemisch Magazine* (1982) 33.
164. R. d. L. Kronig, *Z. Phys.* 75 (1932) 468.
165. R. d. L. Kronig, *Z. Phys.* 70 (1931) 317.
166. D. E. Sayers, E. A. Stern, F. W. Lytle, *Phys. Rev. Lett.* 27 (1971) 1204.
167. T. Ressler, *J. Synchrotron Radiat.* 5 (1998) 118.
168. S. I. Zabinsky, J. J. Rehr, A. Ankudinov, R. C. Albers, M. J. Eller, *Phys. Rev. B : Condens. Matter Mater. Phys.* 52 (1995) 2995.
169. M. S. Schneider, J. D. Grunwaldt, T. Burgi, A. Baiker, *Rev. Sci. Instrum.* 74 (2003) 4121.
170. M. Schneider, *In situ Phase Behavior and Infrared Studies of Catalytic Reactions in 'Supercritical' Fluids*, Dissertation No. 15424, Swiss Federal Institute of Technology: Zurich, 2004.
171. J. D. Grunwaldt, M. D. Wildberger, T. Mallat, A. Baiker, *J. Catal.* 177 (1998) 53.
172. J. D. Grunwaldt, *Low Temperature CO Oxidation on Gold/Metal Oxide Interfaces*, Dissertation No. 12634, Swiss Federal Institute of Technology: Zurich, 1998.
173. C. D. Wagner, L. E. Davis, M. V. Zeller, J. A. Taylor, R. H. Raymond, L. H. Gale, *Surf. Interface Anal.* 3 (1981) 211.
174. D. J. Darensbourg, R. M. Mackiewicz, J. L. Rodgers, A. L. Phelps, *Inorg. Chem.* 43 (2004) 1831.

References

175. R. G. Konsler, J. Karl, E. N. Jacobsen, *J. Am. Chem. Soc.* 120 (1998) 10780.
176. F. Minutolo, D. Pini, A. Petri, P. Salvadori, *Tetrahedron: Asymmetry* 7 (1996) 2293.
177. S. K. Hwang, A. Juhasz, S. H. Yoon, N. Bodor, *J. Med. Chem.* 43 (2000) 1525.
178. D. J. Darensbourg, R. M. Mackiewicz, J. L. Rodgers, C. C. Fang, D. R. Billodeaux, J. H. Reibenspies, *Inorg. Chem.* 43 (2004) 6024.
179. Y. P. Zhang, J. H. Fei, Y. M. Yu, X. M. Zheng, *Catal. Lett.* 93 (2004) 231.
180. X. G. Zhou, X. Q. Yu, J. S. Huang, S. G. Li, L. S. Li, C. M. Che, *Chem. Commun.* (1999) 1789.
181. B. S. Uphade, T. Akita, T. Nakamura, M. Haruta, *J. Catal.* 209 (2002) 331.
182. I. C. Chisem, J. Rafelt, M. T. Shieh, J. Chisem, J. H. Clark, R. Jachuck, D. Macquarrie, C. Ramshaw, K. Scott, *Chem. Commun.* (1998) 1949.
183. V. Simonet, Y. Calzavara, J. L. Hazemann, R. Argoud, O. Geaymond, D. Raoux, *J. Chem. Phys.* 116 (2002) 2997.
184. A. Hutton, D. Thornton, *Spectrochim. Acta, Part A* 34 (1978) 645.
185. R. A. Sheldon, M. Wallau, I. W. C. E. Arends, U. Schuchardt, *Acc. Chem. Res.* 31 (1998) 485.
186. J. A. Widegren, R. G. Finke, *J. Mol. Catal. A : Chem.* 198 (2003) 317.
187. I. W. C. E. Arends, R. A. Sheldon, *Appl. Catal., A* 212 (2001) 175.
188. R. L. Paddock, Y. Hiyama, J. M. McKay, S. T. Nguyen, *Tetrahedron Lett.* 45 (2004) 2023.
189. H. Bertagnolli, T. Engelhardt, B. Lengeler, *Z. Phys. Chem.* 155 (1987) 79.
190. M. P. Feth, A. Klein, H. Bertagnolli, *Eur. J. Inorg. Chem.* (2003) 839.
191. B. Kerler, R. E. Robinson, A. S. Borovik, B. Subramaniam, *Appl. Catal., B* 49 (2004) 91.
192. M. Wei, G. T. Musie, D. H. Busch, B. Subramaniam, *J. Am. Chem. Soc.* 124 (2002) 2513.
193. J. Ke, B. X. Han, M. W. George, H. K. Yan, M. Poliakoff, *J. Am. Chem. Soc.* 123 (2001) 3661.
194. P. Licence, J. Ke, M. Sokolova, S. K. Ross, M. Poliakoff, *Green Chem.* 5 (2003) 99.

195. R. Wandeler, N. Kunzle, M. S. Schneider, T. Mallat, A. Baiker, *J. Catal.* 200 (2001) 377.
196. O. Rutenberg, S. Shakhova, *Russ. J. Phys. Chem. (Engl. Transl.)* 47 (1973) 124.
197. F. M. Mirabella, *Internal Reflection Spectroscopy: Theory and Application*, Marcel Dekker Journals: Monticello, 1993.
198. M. V. Avdeev, A. N. Konovalov, V. N. Bagratashvili, V. K. Popov, S. I. Tsykina, M. Sokolova, J. Ke, M. Poliakoff, *Phys. Chem. Chem. Phys.* 6 (2004) 1258.
199. N. Ai, J. Chen, W. Y. Fei, *J. Chem. Eng. Data* 50 (2005) 492.
200. F. Murrietaquevara, A. Romeromartinez, A. Trejo, *Fluid Phase Equilib.* 44 (1988) 105.
201. M. S. Schneider, J. D. Grunwaldt, A. Baiker, *Langmuir* 20 (2004) 2890.
202. M. Alvaro, D. Das, H. Garcia, A. Leyva, *Tetrahedron* 60 (2004) 8131.
203. S. Bektesevic, T. Tack, M. R. Mason, M. A. Abraham, *Ind. Eng. Chem. Res.* 44 (2005) 4973.
204. D. Ginosar, B. Subramaniam, *Stud. Surf. Sci. Catal.* 88 (1994) 327.
205. M. Schneider, A. Baiker, *J. Mater. Chem.* 2 (1992) 587.
206. W. J. Stark, S. E. Pratsinis, A. Baiker, *J. Catal.* 203 (2001) 516.
207. X. H. Huang, Z. H. Chen, *J. Cryst. Growth* 271 (2004) 287.
208. L. Madler, H. K. Kammler, R. Mueller, S. E. Pratsinis, *J. Aerosol Sci.* 33 (2002) 369.
209. W. J. Stark, S. E. Pratsinis, A. Baiker, *Chimia* 56 (2002) 485.
210. J. D. Grunwaldt, C. Beck, W. Stark, A. Hagen, A. Baiker, *Phys. Chem. Chem. Phys.* 4 (2002) 3514.
211. O. P. Tkachenko, K. V. Klementiev, E. Loffler, I. Ritzkopf, F. Schuth, M. Bandyopadhyay, S. Grabowski, H. Gies, V. Hagen, M. Muhler, L. H. Lu, R. A. Fischer, W. Grunert, *Phys. Chem. Chem. Phys.* 5 (2003) 4325.

List of Publications

List of Publications Related to the Thesis

“Solventless synthesis of propylene carbonate catalysed by chromium salen complexes: Bridging homogeneous and heterogeneous catalysis”

M. Ramin, F. Jutz, J.-D. Grunwaldt, A. Baiker, *J. Mol. Catal. A : Chem.* 242 (2005) 32.

“Behavior of homogeneous and immobilized zinc-based catalysts in cycloaddition of carbon dioxide to propylene carbonate”

M. Ramin, J.-D. Grunwaldt, A. Baiker, *J. Catal.* 234 (2005) 256.

“High pressure *in situ* X-ray absorption spectroscopy cell for studying simultaneously the liquid phase and the solid/liquid interface”

J.-D. Grunwaldt, M. Ramin, M. Rohr, A. Michailovski, G.R. Patzke, A. Baiker, *Rev. Sci. Instr.* 76 (2005) 054104.

“*In situ* monitoring of Ni catalysts during the synthesis of propylene carbonate by carbon dioxide insertion in propylene oxide”

M. Ramin, S. Reimann, J.-D. Grunwaldt, A. Baiker, *ANKA Annual Report* (2004) 53.

List of Publications

“IR spectroscopy and phase behavior studies of the catalytic synthesis of propylene carbonate: Expanded liquid versus supercritical fluid”

M. Ramin, J.-D. Grunwaldt, A. Baiker, *Appl. Catal.*, A 305 (2006) 46.

“Simple preparation routes towards novel Zn-based catalysts for the solventless synthesis of propylene carbonate using dense carbon dioxide”

M. Ramin, N. van Vegten, J.-D. Grunwaldt, A. Baiker, *J. Mol. Catal. A : Chem.* 258 (2006) 165.

List of Other Publications

“Grüne Chemie: Kohlendioxid – umweltfreundliches Lösungsmittel und Synthesebaustein”

J.-D. Grunwaldt, M. Caravati, M. Ramin, A. Baiker, *ETH Bulletin* 293 (2004) 48.

“Probing active sites during palladium-catalyzed alcohol oxidation in ‘supercritical’ carbon dioxide”

J.-D. Grunwaldt, M. Caravati, M. Ramin, A. Baiker, *Catal. Lett.* 90 (2003) 221.

“Influence of the aluminum content of zeolite H-ZSM-5 on the conversion of methylcyclohexane into a high-quality synthetic steamcracker feedstock”

A. Raichle, M. Ramin, D. Singer, M. Hunger, Y. Traa, J. Weitkamp, *Catal. Commun.* 2 (2001) 69.

List of Annual Reports of Synchrotron Radiation Facilities

“*In situ* measurements of an immobilised zinc based catalyst during carbon dioxide fixation”

M. Ramin, J.-D. Grunwaldt, and A. Baiker, *HASYLAB Annual Report* (2004) 255.

“Probing active sites during palladium-catalysed alcohol oxidation in ‘supercritical’ carbon dioxide”

J.-D. Grunwaldt, M. Caravati, M. Ramin, and A. Baiker, *HASYLAB Annual Report* (2004) 19.

“*In situ* formation of a ruthenium catalyst in the formylation of an amine with ‘supercritical’ CO₂”

M. Rohr, J.-D. Grunwaldt, M. Ramin, and A. Baiker, *HASYLAB Annual Report* (2004) 253.

“An *in situ* EXAFS cell for studying the hydrothermal transformation of MoO₃ · 2 H₂O to MoO₃ nanorods”

J.-D. Grunwaldt, A. Michailovski, G.R. Patzke, M. Caravati, M. Ramin, and A. Baiker, *HASYLAB Annual Report* (2004) 867.

“*In situ* catalyst characterization in ‘supercritical’ CO₂ using X-ray absorption spectroscopy”

M. Caravati, J.-D. Grunwaldt, M. Ramin, A. Baiker, *HASYLAB Annual Report* (2003).

List of Contributions to Conferences

“*In situ* studies on heterogeneous catalysts under demanding conditions”

M. Ramin, J.-D. Grunwaldt, and A. Baiker, *Workshop on X-ray Absorption Spectroscopy and Micro-Spectroscopic Techniques*, PSI Villigen (Switzerland), 20 – 21 February 2006, Book of Abstracts, oral presentation.

“*In situ* monitoring of transition metal catalysts during the synthesis of propylene carbonate in carbon dioxide”

M. Ramin, S. Reimann, J.-D. Grunwaldt, and A. Baiker, *Swiss Chemical Society – Fall Meeting 2005*, Lausanne (Switzerland), 13 October 2005, *Chimia* 9 (2005) 614, poster.

“*In situ* high pressure EXAFS studies of immobilized Zn complexes during carbon dioxide fixation”

M. Ramin, J.-D. Grunwaldt, A. Baiker, *International Conference of Energy Technologies for a Sustainable Future ETSF 5*, PSI Villigen (Switzerland), 9 – 10 June 2005, Book of Abstracts, p. 63, poster.

“*In situ* high pressure XAS studies during the Zn catalysed reaction of propylene oxide and carbon dioxide”

M. Ramin, J.-D. Grunwaldt, A. Baiker, *XXXVIII. Jahrestreffen Deutscher Katalytiker*, Weimar (Germany), 16 – 18 March 2005, Tagungsband, p. 190, poster.

“*In situ* measurements of an immobilised zinc-based catalyst during carbon dioxide fixation”

M. Ramin, J.-D. Grunwaldt, and A. Baiker, *HASYLAB Users Meeting*, DESY Hamburg (Germany), 28 January 2005, poster.

“New heterogeneized chromium salen complexes for carbon dioxide insertion in propylene oxide”

M. Ramin, F. Jutz, J.-D. Grunwaldt, and A. Baiker, *Swiss Chemical Society – Fall Meeting 2004*, Zurich (Switzerland), 7 October 2004, *Chimia* 7/8 (2004) 498, poster.

“Carbon dioxide insertion in propylene oxide with new heterogeneized chromium salen complexes”

M. Ramin, F. Jutz, J.-D. Grunwaldt, and A. Baiker, *Green Solvents for Synthesis*, Bruchsal (Germany), 3 – 6 October 2004, Book of Abstracts, p. 88, poster.

“*In situ* monitoring of nickel catalysts during the synthesis of propylene carbonate by carbon dioxide insertion”

M. Ramin, S. Reimann, J.-D. Grunwaldt, and A. Baiker, *ANKA Users Meeting*, Forschungszentrum Karlsruhe (Germany), 23 September 2004, poster.

“Synthesis of propylene carbonate by carbon dioxide fixation using an immobilized zinc-pyridine-catalyst”

M. Ramin, J.-D. Grunwaldt, and A. Baiker, *XXXVII. Jahrestreffen Deutscher Katalytiker*, Weimar (Germany), 17 – 19 March 2004, Tagungsband, p. 230, poster.

“Immobilized catalysts for carbon dioxide fixation”

M. Ramin, J.-D. Grunwaldt, and A. Baiker, *Swiss Chemical Society – Fall Meeting 2003*, Lausanne (Switzerland), 9 October 2003, *Chimia* 7/8 (2003) 405, poster.

Curriculum Vitae

Name	Michael Olaf Ramin
Date of Birth	17 September 1974
City	Böblingen
Nationality	German

Education

1985 – 1994	Gymnasium Böblingen Graduation with Abitur
1995 – 2000	Chemistry Studies at the Universität Stuttgart Graduation as Dipl.-Chem.
Mar. – June 1999	Studies in Organic Chemistry at the École Supérieure Chimie Physique Électronique de Lyon, “Synthèse des ligands chiraux et applications en catalyse asymétrique”, Supervisor: Prof. D. Sinou.
Mar. – Sept. 2000	Diploma work at the Universität Stuttgart “Ringöffnung von Methylcyclohexan an sauren Zeolithen ZSM-5 mit unterschiedlichem Aluminiumgehalt”, Supervisor: Prof. J. Weitkamp.
2000 – 2006	ETH Zurich, Institute for Chemical and Bioengineering Doctoral Thesis, Supervisor: Prof. A. Baiker.